Photo-physicochemical Characterization and *In Vitro* Photodynamic Therapy Activity of Phthalocyanine-Graphene Quantum Dots Conjugates

A thesis submitted in fulfilment of the requirements for the degree of

MASTER OF SCIENCE

By

LINDOKUHLE CINDY NENE

RHODES UNIVERSITY
Where leaders learn

February 2019

DEDICATION

This work is dedicated to individuals that may be battling with cancer or affected by cancer of a loved one.

ACKNOWLEDGEMENTS

A special thank you to my supervisor, Distinguished Professor Tebello Nyokong, for all the knowledge imparted, encouragement and support through the course of my studies.

Thank you to Ms Gail Cobus for all the administrative work and support.

Rhodes University academic staff for support and valuable lessons, Dr Brendan Wilhelmi, Dr John Mack, Dr Johnathan Britton, Dr David Oluwole, Ms Muthumuni Managa and colleagues, “S22-group”. Thank you.

The National Research Foundation (NRF) for support and funding. Thank you.

Professor Nagao Kobayashi and Mutsumi Kimura, who were hosting me during my stay and study at Shinshu University, Japan. Thank you.

Dr Fethi Bedioui and wonderful supervisor Camille Lescot who hosted me during my stay and study at Chimie ParisTech, France. The good friends I made; Dr Wiliam Caneschi, Menel Ben Frej and Getnet Sewnet Kassahun as well as the UTCBS group. Campus France for funding. Thank You.

Warm thank you to my dad, Mandlenkosi Blessing Nene; siblings, Nozipho, Nosisa and Mlondolozi Nene; friends; Reitumetse Nkhahle, Sivuyisiwe Mapukata, Palesa Motsoai, and mentor, Dr Garth Cambray. Thank You.

And most importantly, my guardian angel, late-mother, Mildred Tilly Nene. Thank You.

ABSTRACT

This thesis reports on the preparation of several differently substituted Zn(II) phthalocyanine (Pc) complexes and their respective graphene quantum dots (GQDs) conjugates. In addition, Pc complexes substituted with biologically active molecules used in cancer therapeutics, namely: benzothiazole and morpholine, were also prepared and conjugated to GQDs. The photo-physicochemical properties were determined for both the complexes and their respective conjugates including the fluorescence/ triplet quantum yields and lifetimes as well as the singlet oxygen generating abilities. Upon conjugation to GQDs, the fluorescence of the Pc complexes decreased (insignificant decrease in some cases), with an increase in the triplet quantum yields. However, the singlet quantum yields of the Pcs in the conjugates did not show an increase with the increase in the triplet quantum yields. This is suspected to be due to the screening effect. The cytotoxicity of the complexes *in vitro* decreased upon conjugation, as a result of reduced actual number of Pc units provided in the conjugate for therapy. An increase in the efficacy upon quaternization was observed, and a relatively better performance was also observed for the cationic complex in combination with the biotin-functionalized GQDs, **7**-GQDs-Biotin. Moreover, the cellular uptake of **7**-GQDs-Biotin over 24 h was relatively high compared to complexes alone and other Pcs-GQDs conjugates.

TABLE OF CONTENTS

Title **Page**

LIST OF SYMBOLS

Symbol	Description
Φ_F	Fluorescence quantum yield
τ_F	Fluorescence lifetime
Φ_T	Triplet quantum yield
τ_T	Triplet lifetime
Φ_Δ	Singlet oxygen quantum yield
α/ R_n	Non-peripheral
β/ R_p	Peripheral
$t_{1/2}$	Half-life
n	number of replicates

LIST OF ABBREVIATIONS

Abbreviation	**Description**
ADMA	Anthracene-9,10-*bis*-methylmalonate
DBU	1,8-Diazabicyclo-[5.4.0]-undec-7-ene
DCC	Dicyclohexylcarbodiimide
DLS	Dynamic light scattering
DMF	Dimethylformamide
DMSO	Dimethyl sulfoxide
DPBF	1,3-Diphenylisobenzofuran
EDX	Energy dispersive X-ray
EPR	Enhanced permeability and retention
FT-IR	Fourier transform infrared
GQDs	Graphene quantum dots
^{1}H NMR	Proton nuclear magnetic resonance
H_2Pcs	Metal-free phthalocyanines
HOMO	Highest occupied molecular orbital
ISC	Intersystem crossing
LCAO	Linear combination of atomic orbitals
LUMO	Lowest unoccupied molecular orbital
MALDI-TOF	Matrix-assisted laser desorption ionization- Time of flight
MCF-7	Michigan Cancer Foundation- 7
MPcs	Metallophthalocyanines
MX	Metal salt
NH_2-GQDs	Amino-functionalized graphene quantum dots
NIR	Near infrared
NPs	Nano-particles
Pcs	Phthalocyanines
PDFA	Difluoromethylene phosphobetaine
PDT	Photodynamic therapy

PSs	Photosensitizers
QPcs	Quaternized phthalocyanines
R-group	Substituents
ROS	Reactive oxygen species
SCF_3	Trifluoromethylthio
TCSPC	Time correlated single photon counting
TEM	Transmission electron microscopy
UV-vis	Ultraviolet-visible

CHAPTER ONE

1. Introduction

Problem statement

Cancer remains one of the leading causative agents for the morbidity and mortality burden globally. Several treatment regimens have been used for cancer with the conventional chemotherapy showing limitations such as lack of selectivity and specificity (invasive) [**1,2**]. Photodynamic therapy (PDT) has been introduced to overcome these limitations [**3**], where phthalocyanines (Pcs) have grown as a promising generation of sensitizers for PDT. However, Pcs generally lack specificity for cancer [**4**,**5**]. Therefore, methods of preparing efficacious and cancer-selective Pcs-sensitizers for PDT is paramount in the study and development of effective cancer treatments.

This thesis reports on the conjugation of Pcs to graphene quantum dots (GQDs), as cancer-selective delivery vectors for Pcs. A selection of known chemical groups used for cancer therapeutics including benzothiazole, morpholine, biotin and cationic moieties were used in the design and synthesis of Pc-GQDs conjugates to potentially improve the therapeutic efficacy in terms of solubility in aqueous media, cancer specificity and uptake.

Preface

A summary of the aims of this work is outlined in **Fig. 1.1**.

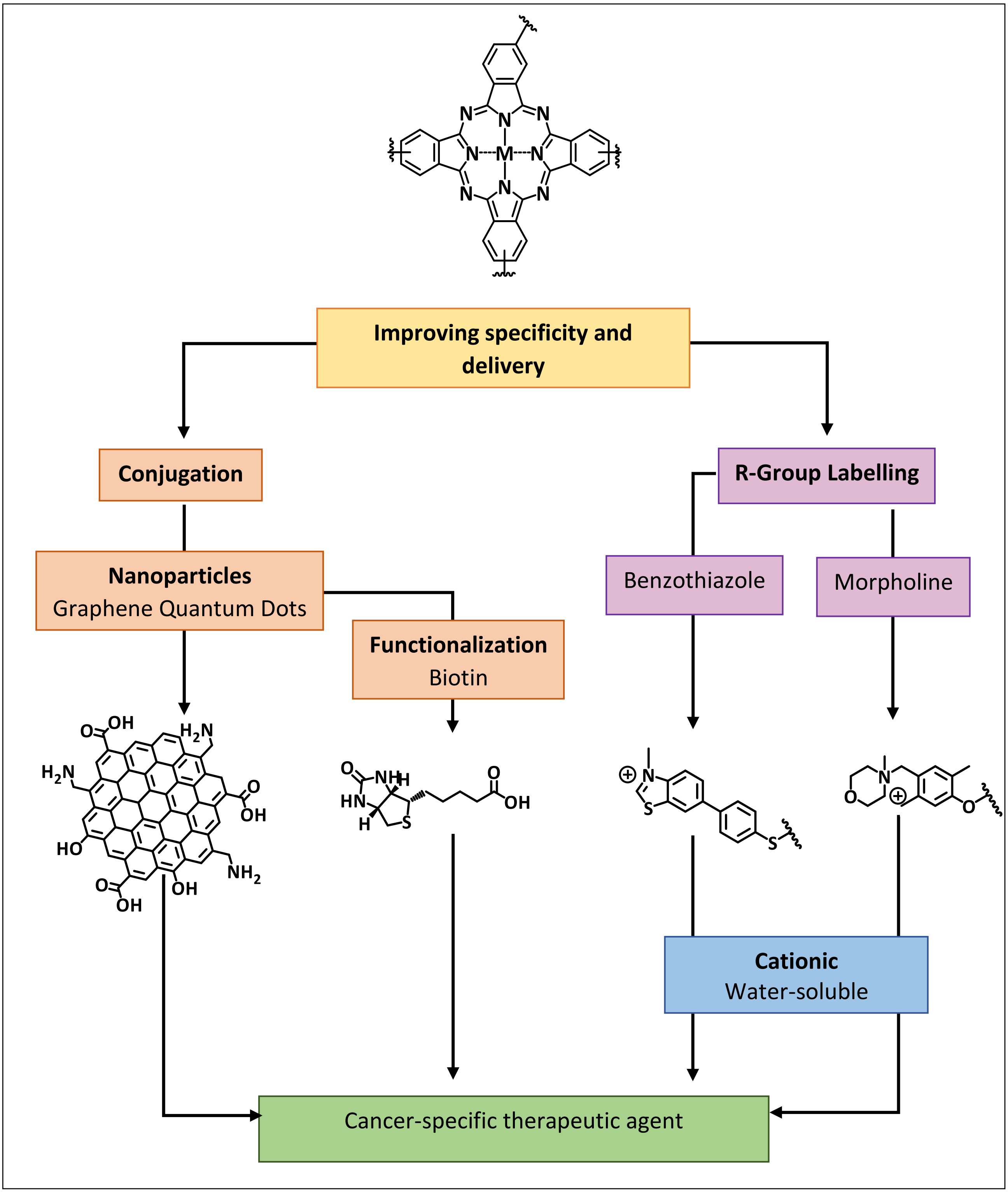

Figure 1.1. Summary of the methods used for modifying phthalocyanines for potential cancer specificity and uptake used in this work.

1.1. Brief background on photodynamic therapy

Photodynamic therapy (PDT) has immerged as a non-invasive/ selective technique developed as an alternative or supplementary to the conventional chemotherapy or radiation therapy for cancer treatment [**3**,**6**,**7**]. PDT is relatively cheaper and gentler, with minimal toxicity to non-malignant somatic cells [**8**]. PDT uses light-responsive-chemical compounds known as photosensitizers (PSs), synergistically with light of specific wavelength (activator) and molecular oxygen (O_2) to initiate cytotoxicity through the generation of reactive oxygen species (ROS) [**9-11**]. The PSs form key components and are required to possess a set of specific properties for potential applications in PDT [**12**-**15**].

The prerequisite properties of PSs for PDT include, in addition to ROS generation upon exposure to light, low to no dark toxicity; chemical and physical stability at storage/ physiological conditions; specificity and selectivity to cancer; rapid accumulation at cancer site; and maximum absorbance of light of wavelength in the near-infrared region (NIR) of the electromagnetic spectrum [**13,16-19**]. Wavelengths in the NIR have relatively better tissue penetrability and can therefore reach deeper-seated cancer cells during PDT [**7**].

A plethora of PSs have been designed and studied for PDT both *in vitro* and *in vivo*. These PSs can be summarised in one of the major groups, namely: pophyrins, chlorins, bacteriochlorins, phenothezium, xanthene, distyryl boron dipyrromethene and phthalocyanines [**20,21**]. Of these, phthalocyanines are regarded as promising PSs for PDT [**22-24**] and are a subject of this thesis.

1.2. Phthalocyanines

Phthalocyanines (Pcs) are a group of brilliant blue or green and sometimes brown coloured organic dyes. The discovery of Pcs dates to the 1900s, where the first Pcs were obtained accidentally as a by-product during the preparation of 2-cyanobenzamide [**25**]. The word phthalo-cyanine is derived from two terms; where "phthalo-" is from the precursor for Pcs, phthalic acid, and "-cyanine", the Greek term for the colour blue.

1.2.1. General structure

Structurally, Pcs are macro-cyclic compounds with a tetrapyrrolic core. These aromatic compounds comprise a characteristic 18 π-electron-system which affords them impressive electronic and optical properties [**26,27**]. The structure of Pcs may vary, depending on the nature and positions of substituents and nature of the central metals**, Fig. 1.2**.

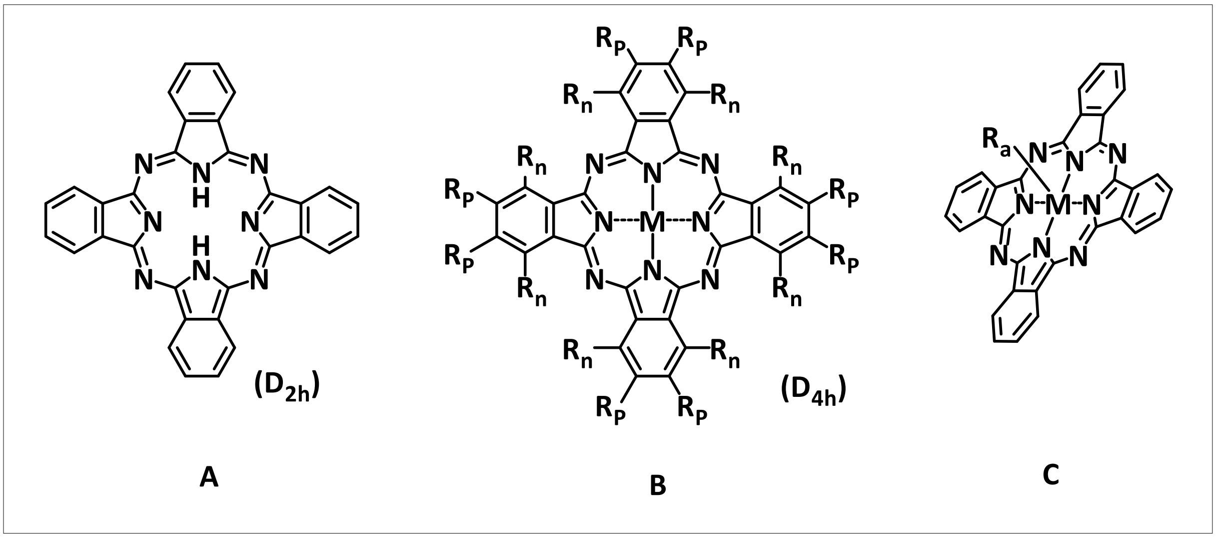

Figure 1.2. The generalised structural formulae of **A**) metal-free and non-substituted Pcs; **B**) metallated and substituted Pcs and **C**) metallated Pcs with axial ligand. Rp: peripheral (β) substituent, Rn: non-peripheral (α) substituent, M: metal, R_a: axial substituent.

Metal-free Pcs (H_2Pcs) are of D_{2h} symmetry **Fig. 1.2A**, and the metallated Pcs (MPcs) are of D_{4h} symmetry **Fig. 1.2B** [**28**]. Depending on the oxidation state of the metal, axial substituents can be incorporated on MPcs through direct linkage to the metal as shown in **Fig. 1.2C**. Additionally, the structural features of Pcs can vary by attachments of substituents on the alpha (α, Rn) and/ or beta (β, Rp) positions respectively, **Fig. 1.2B** [**29**].

1.2.2. Synthesis

The Pcs are synthesized from smaller simpler precursors. The synthesis of Pcs generally involves a single step where the precursors: phthalic anhydride, phthalimide or phthalonitrile, *etc.*, are used along with a metal salt in a cyclotetramerization reaction to form MPcs, or H_2Pcs in the case where a metal is not added in the reaction **Scheme 1.1** [**30,31**].

Alternatively, MPcs may be formed in a two-step reaction, where the H_2Pcs are first synthesized and subsequently metallated instead of the direct interaction of the precursors with the desired metal as shown in **Scheme 1.1** [**32**]. Depending on the application and production scales, specific precursors may be used in the preparation of Pcs, for example, large industrial scale would utilize phthalic anhydride, where in a small laboratory scale, the phthalonitriles would normally be used [**33-36**].

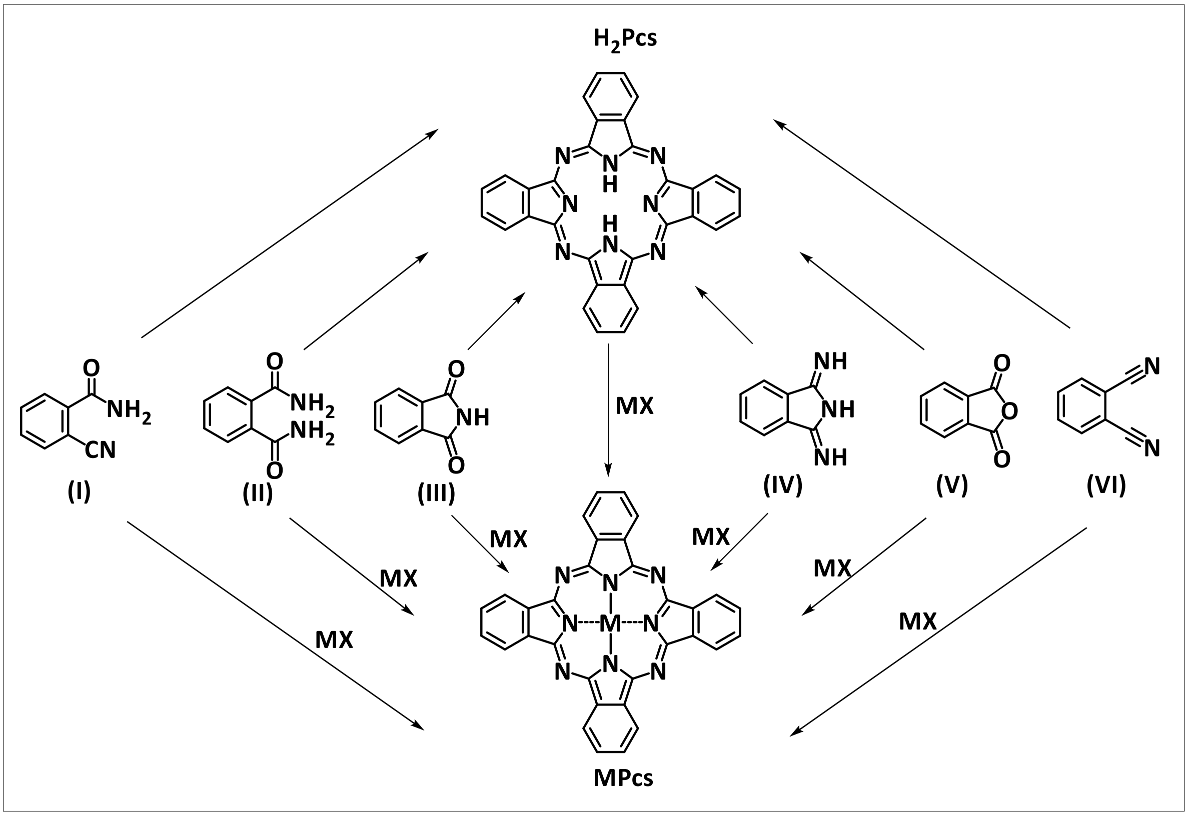

Scheme 1.1. A selection of Pcs precursors for preparing H_2Pcs and MPcs, namely: (I) o-cyanobenzamide, (II) phthalamide, (III) phthalimide, (IV) 1,3-diiminoisoindoline, (V) phthalic anhydride, (VI) phthalonitrile.

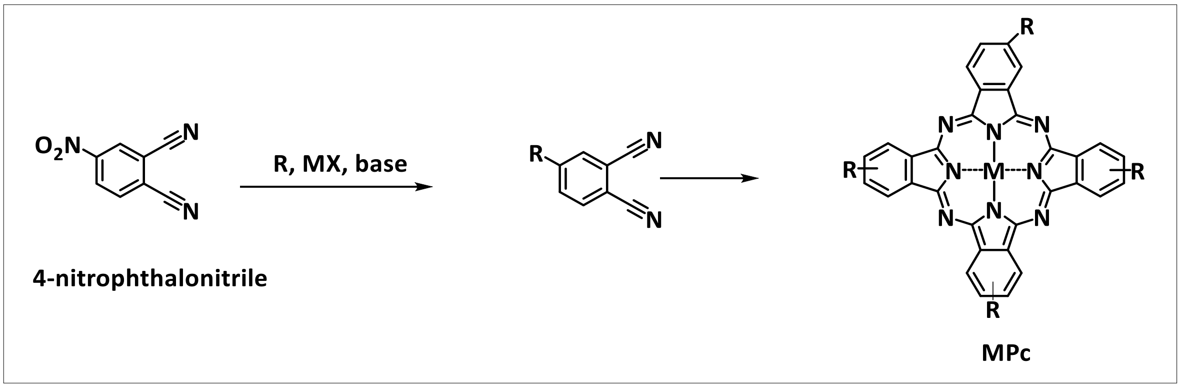

Scheme 1.2. The preparation of tetra-β-substituted Pcs using phthalonitrile precursor. R: substituent, MX: metal-salt, M: metal.

This thesis reports on the peripherally tetra-substituted MPcs. To achieve Pcs with substituents (R-groups), the phthalonitrile precursors bearing the desired R-groups at specific positions are usually used. Commonly, the 4-nitrophthalonitrile is used, where the nitro-group is displaced by the electrophilic-end of the R-group **Scheme 1.2** [**37-39**].

1.2.3. Electronic absorption behaviour

The typical UV-vis absorption spectra of Pcs are characterised by two prominent absorbance peaks that are due to π-π*transitions, namely; the Q and B bands which appear in the NIR and the blue-region, respectively, **Fig. 1.3A** [**40,41**]. The origin of the Q and the B bands can be explained by the Gourteman model of linear combination of atomic orbitals (LCAO) as a function of transitions occurring between the highest occupied molecular orbital (HOMO) and the lowest unoccupied molecular orbital (LUMO) [**42**]. In the case of MPcs, the Q-band appears as one intense peak, which arises from the transitions from the a_{1u} of the HOMO to the e_g of the LUMO. The B-band arises from the transitions from the a_{2u} and b_{2u} of the HOMO to the e_g of the LUMO, **Fig. 1.3B**, [**42-44**]. The absorption spectra of Pcs are mostly dependant on the structural properties, such as the type and size of central metal; the size, nature and position of substituents among other properties [**45-48**].

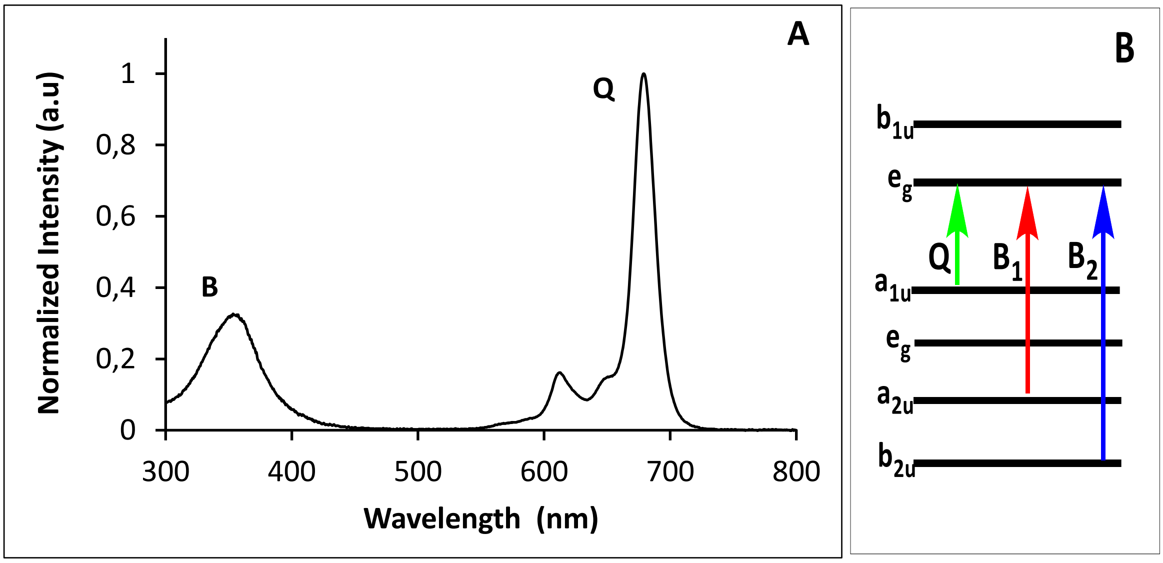

Figure 1.3. The illustration of a typical (**A**) UV-vis absorption spectrum and (**B**) electronic energy levels showing the origin of the Q and B bands of MPcs.

1.2.4. Photo-physicochemical parameters

The photo-physicochemical properties of Pcs are important in determining their potential applicability as PSs for PDT. The PDT mechanism of action is illustrated in **Fig. 1.4**.

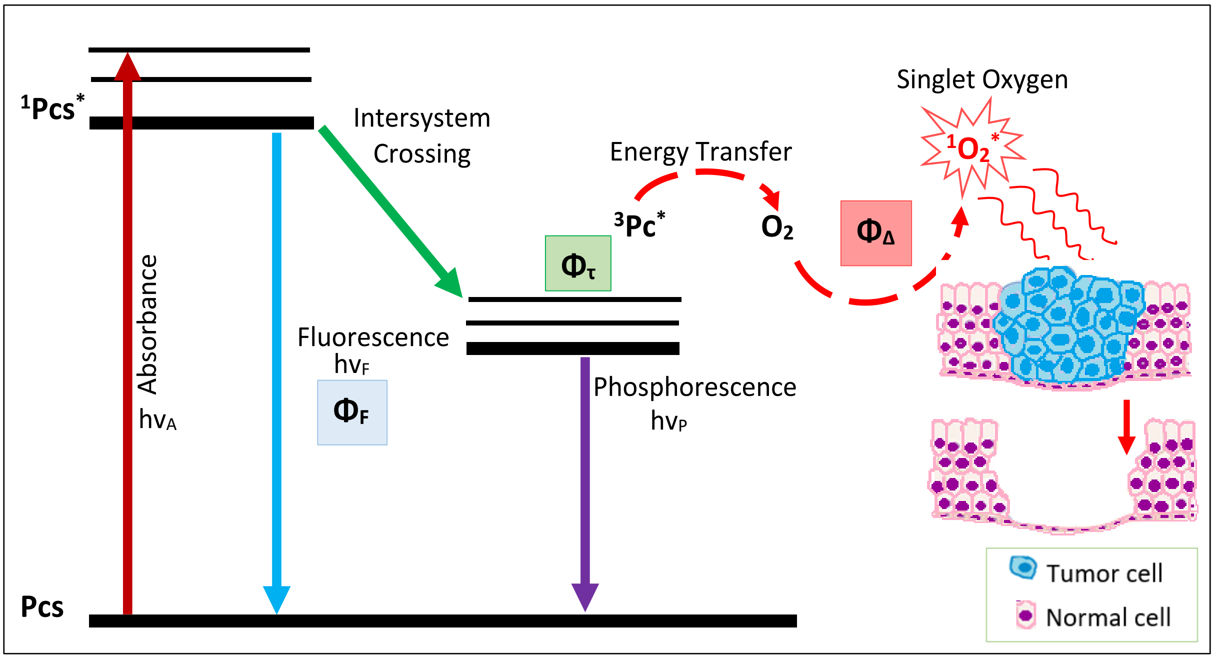

Figure 1.4. Jablonski diagram illustrating the initiation of cytotoxicity by light activated photosensitizer during photodynamic therapy.

Upon irradiation, Pcs in the ground state absorb energy from the light source ($h\nu_A$) to occupy the first excited state,$^1Pc^*$ [**49**]. The excited $^1Pc^*$ eventually relaxes and may undergo fluorescence back to the ground state by emitting light of a different wavelength ($h\nu_F$) or may undergo intersystem crossing (ISC) to occupy the excited triplet state, $^3Pc^*$ [**49**]. Molecules in the triplet state may interact with molecular oxygen (O_2,) to generate singlet oxygen, or will instead undergo phosphorescence, releasing energy ($h\nu_P$) back to the ground state [**15,49,50**]. The photo-physicochemical parameters derived from the Jablonski diagram include the fluorescence, triplet and singlet oxygen quantum yields and they are discussed in the following sections [**51-53**].

1.2.4.1. Fluorescence quantum yield and lifetime

The fluorescence quantum yield (Φ_F) quantifiy the amount of excited molecules, $^1Pc^*$, that will relax back to the ground state, Pc, through fluorescence [**54**] **Fig 1.4**, this value is determined using previously repoted comparitive methods [**52**,**54,55**] using **Equation 1.1**.

$$\boldsymbol{\Phi}_{F(Sample)} = \boldsymbol{\Phi}_{F(Standard)} \frac{F_{(Sample)}.A_{(Standard)}.n^2_{(Sample)}}{F_{(Standard)}.A_{(Sample)}.n^2_{(Standard)}} \qquad \textbf{(Equation 1.1)}$$

Where the $\boldsymbol{\Phi}_{F(Sample)}$ and $\boldsymbol{\Phi}_{F(Standard)}$ are the Φ_F of the sample and standard respectively, $F_{(Sample)}$ and $F_{(Standard)}$ are the areas under the fluorescence curve for the sample and standard, respectively. The $A_{(Sample)}$ and $A_{(Standard)}$ are the absorbance values at the excitation wavelength for the sample and standard, respectively. The $n_{(Sample)}$ and $n_{(Standard)}$ are the solvent refractive indices for the sample and standard, respectively.

The fluorescence lifetimes (τ_F) determine the time it takes the excited photons to relax back to the ground state through fluorescence. The τ_F are directly proportional to the Φ_F for a specific molecule. There are several methods that can be used to determine the τ_F [**56,57**]. The τ_F were determined using time-correlated single photon counting method in this thesis [**58-60**].

1.2.4.2. Triplet quantum yield and lifetime

The excited molecules that will instead occupy the triplet state, $^3Pc^*$, are quantified by the triplet quantum yield (Φ_T) **Fig 1.4** [**61,62**]. The Φ_T can be determined using previosly reported comparitive methods [**51, 63**] using **Equation 1.2**.

$$\boldsymbol{\Phi}_{T(sample)} = \boldsymbol{\Phi}_{T(Standard)} \frac{\Delta A_{T(Sample)}.\varepsilon_{T(Standard)}.}{\Delta A_{T(Standard)}.\varepsilon_{T(Sample)}.} \qquad \textbf{(Equation 1.2)}$$

Where the $\boldsymbol{\Phi}_{T\ (Sample)}$ and $\boldsymbol{\Phi}_{T\ (Standard)}$ are the Φ_T of the sample and standard, respectively, $\boldsymbol{\Delta A}_{T(Sample)}$ and $\boldsymbol{\Delta A}_{T(Standard)}$ are the changes in the triplet state absorbances for the sample and standard, respectively, and the $\boldsymbol{\varepsilon}_{T(Sample)}$ and $\boldsymbol{\varepsilon}_{T(Standard)}$ are the extinction coefficients at the triplet state for the sample and standard, respectively. The $\boldsymbol{\varepsilon}$ values for both the samples and standards may be calculated using **Equation 1.3.**

$$\varepsilon_T = \varepsilon_S \frac{\Delta A_T}{\Delta A_{S.}} \qquad \textbf{(Equation 1.3)}$$

Where $\boldsymbol{\varepsilon}_S$ is the excinction coefficient and $\boldsymbol{A}_S$ is the change in absorbances at the ground singlet state respectively.

The triplet lifetimes (τ_T) determine the amount of time the excited molecules, $^3Pc^*$ will exist in the triplet excited state. In this work, to obtain τ_T the kinetic curves were exponentially fitted on ORIGIN® 8 Professional software [**62**].

1.2.4.3. Singlet oxygen quantum yield

The efficiency of singlet oxygen generation from O_2 mediated by the $^3Pc^*$ can be quantified as the singlet oxygen quantum yield (Φ_Δ) [**64, 65**]. The calculation of the Φ_Δ can be done using methods described in literature [**64-66**]. In this work, the Φ_Δ were determined spectroscopically, by monitoring the photodegradation of the singlet oxygen quencher as described in literature [**67**]. The Φ_Δ values were calculated using the **Equation 1.4**.

$$\boldsymbol{\Phi}_{\Delta(sample)} = \boldsymbol{\Phi}_{\Delta(Standard)} \frac{R_{(Sample).}I_{Abs(Standard).}}{R_{(Standard).}I_{Abs(Sample).}} \qquad \textbf{(Equation 1.4)}$$

Where the $\boldsymbol{\Phi}_{\Delta(Sample)}$ and $\boldsymbol{\Phi}_{\Delta(Standard)}$ are the Φ_Δ of the sample and standard, respectively. The $\boldsymbol{R}_{(Sample)}$ and $\boldsymbol{R}_{(Standard)}$ are the rates of photodegradation of the quencher mediated by the sample and the standard, respectively, and $I_{Abs(Sample)}$ and $I_{Abs(Standard)}$ are the rate at which light is absorbed by the sample and standard, respectively. Where I can be determined using **Equation 1.5**.

$$I_{Abs} = \frac{\alpha.A.I}{N_A} \quad \text{(Equation 1.5)}$$

Where $\alpha = 1\text{-}10^{-A(\lambda)}$, **A** (**λ**) is the absorbance of the Pcs at the irradiation wavelength, A is the irradiated area (2.5 cm^2), I is the intensity of the light used (photons/ cm^2) and N_A is the Avogadro's constant.

1.2.5. Methods of improving photo-activity and therapeutic efficacy

The advantage of working with Pcs is that they are relatively easy to modify to improve their properties for different applications including PDT [**68-72**]. Several structural modifications have been employed with the aim of improving the optical behaviour, photo-physicochemical properties and cancer specificity of the Pcs [**73-75**].

1.2.5.1. Central metal and substituents

The use of heavy atoms as central metals may improve the photo-physicochemical properties and PDT activity through the heavy-atom effect [**76-78**]. Heavy metals may also assist the red-shifting of the Q-band to the NIR, which is essential for therapy [**79**]. Aggregation in Pcs affect their photo-activity and therefore cause challenges in the study and applications of Pcs [**80,81**]. To overcome these, Pcs substituents are carefully designed. Bulky substituents are used to enhance solubility and reduce aggregation in organic solvents through steric hindrances [**82-85**]. A series of differently substituted Pcs, ranging from simple substituents such as the *tert*-butyl and phenylthiol and bulkier substituents such as benzothiazole and morpholine groups were synthesized and studied in this work.

1.2.5.2. Quaternization

Nitrogen-bearing functional groups, usually 2° and 3° amines, are used to form cationic-quaternary amines on the substituent of the Pcs to afford water soluble quaternized Pcs, (QPcs) [**86-88**]. In addition to water-solubility, which is ideal for biological applications such as cancer treatment, cationic drug molecules have been shown to have affinity to cancer cells through electrostatic attraction, owing to the oppositely charged anionic cell membrane [**89-92**], and enter cells through the clathrin-mediated endocytosis pathway [**93**]. Furthermore, Matshitse *et al.* have reported on the improvement of cellular uptake of Pcs upon increase in the number of cations conferred [**94**]. This serves as an advantage since, in addition to promising photo-physicochemical properties for PDT, Pcs also need to be designed/ modified to target cancer as they generally lack specificity.

In this work, benzothiazole and morpholine-substituted Pcs were used to allow for the preparation of quaternary amines. Moreover, these groups are targeted as anti-cancer entities in cancer drug development [**95-97**].

1.2.5.3. Conjugation to nanocarriers

Furthermore, cancer selectivity and delivery of Pcs can be achieved by tagging with specialised carriers [**98-100**]. Nanoparticles (NPs) for drug delivery are attractive due to their versatility, biocompatibility, improved drug loading and targeting [**101-103**]. The NPs-drug conjugates are likely to target the cancer microenvironment due to the leaky vasculature around the cancer site, allowing easier entrance, accumulation and retention at cancer target sites, this is known as the enhanced retention factor (EPR) [**104,105**]. Some of the nanocarriers that have been designed and studied for Pcs' cancer-specificity and delivery include Au-NPs, polyacrylamide nanoparticles and liposomes to mention a few [**106-109**].

Other drug nano-carriers of interest in medicine include graphene quantum dots, which are a subject of this thesis [**110,111**]. In addition to cancer targeting, NPs have been demonstrated to improve the PDT activity of Pcs in Pcs-NPs conjugates through the heavy-atom effect [**78, 112**].

1.3. Graphene quantum dots

Graphene quantum dots (GQDs) are fluorescent, aromatic nanomaterials structurally appearing as flat carbon sheets and may comprise of carboxyl, hydroxyl and amine functional groups on their edges. GQDs have earned a great deal of interest in biology owing to their high biocompatibility and low cytotoxicity [**110**]. Additionally, GQDs have also shown good aqueous dispersity; chemical inertness; pH stability and photostability and have been applied as PDT agents or fluorescent imaging probes in oncology and other diseases [**110-113**].

1.3.1. Syntheses

There are two main approaches for preparing GQDs; the top-down and the bottom-up approach **Fig. 1.5** [**114**]. The top-down approach involves the fragmentation of bigger molecules such as graphite, graphene oxide, carbo-nanotubes *etc.* [**115-117**]. Various methods such as laser ablation, hydrothermal or solvothermal cutting processes *etc.* may be used to form GQDs in the top-down approach [**118**].

The bottom-up approach utilises smaller precursor molecules such as citric acid, glucose, and other aromatic molecules **Fig. 1.5** [**119,120**]. The assembly of these molecules to form GQDs may be assisted by various processes including ultrasonication, hydrothermal treatments, microwave pyrolysis (carbonization) *etc*. [**118**]. The bottom up-approach affords better control in the size and shape of GQDs with fewer defect, unlike the top-down approach [**121**].

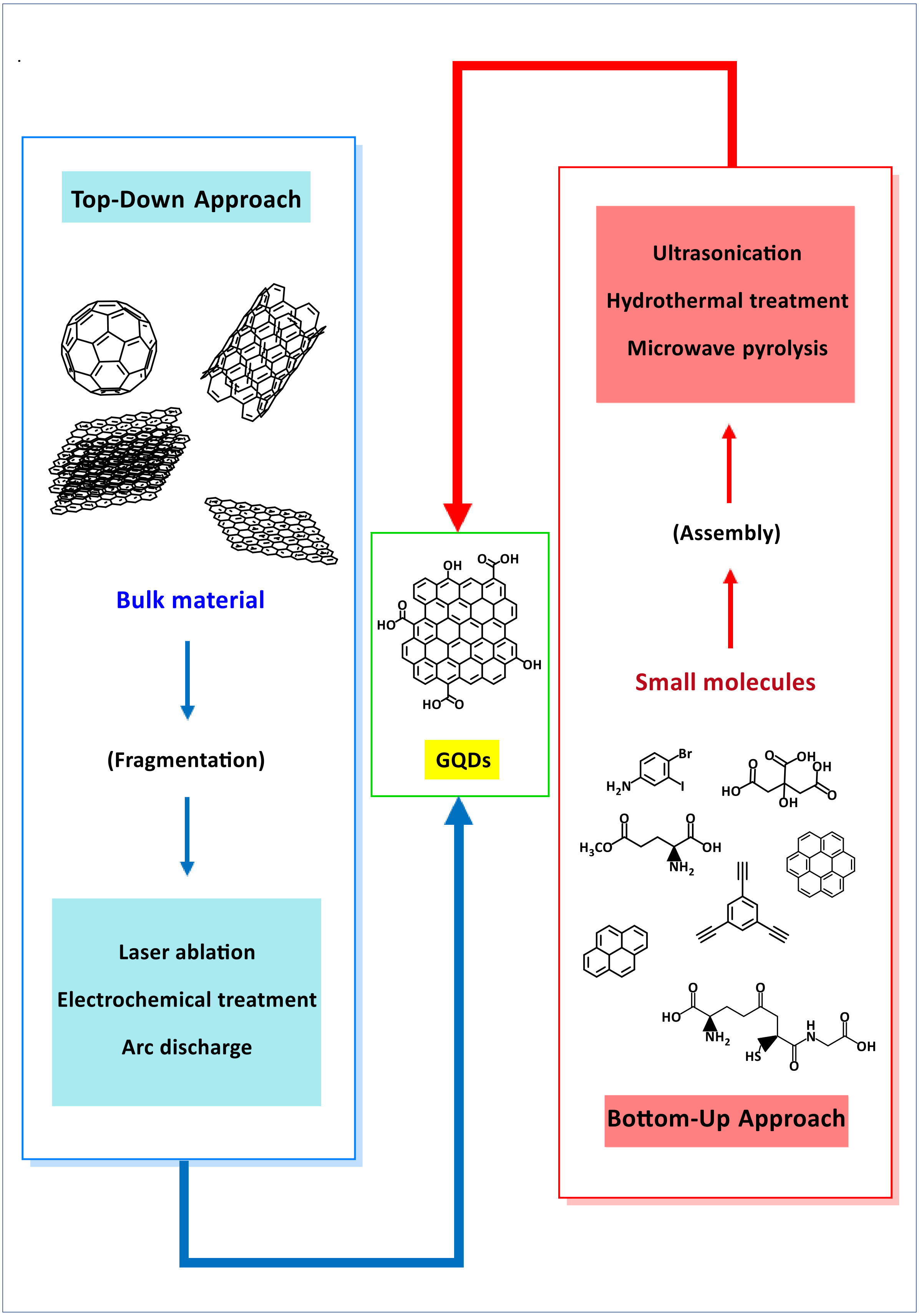

Figure 1.5. Summary of the top-down and bottom-up approaches for the preparation of GQDs.

In this work, the bottom-up approach, using the precursor citric acid, in the presence of polyethyleneimine by hydrothermal treatment was used to afford the NH_2-GQDs. The simplified structure of the NH_2-GQDs is represented in **Fig. 1.6**.

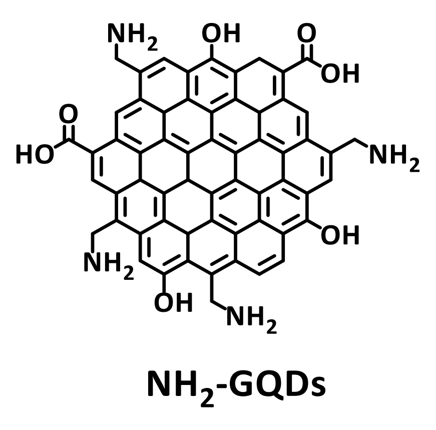

Figure 1.6. Simplified structure of NH_2-GQDs used in this work

1.3.2. Conjugation of Pcs to GQDs

The conjugation of Pcs to GQDs is achievable through the formation of both covalent and non-covalent bonds [**122**]. For covalent conjugation, the functional groups on the edges of the GQDs are used to form bonds directly, or indirectly through a linker to the Pcs with appropriate functional groups. In the case of non-covalent conjugation, the Pcs are loaded on to the flat surface of the GQDs through π-π interactions [**122**]. The large flat surface of GQDs allows for the loading and delivery of multiple drug (Pcs) units.

The Pcs and GQDs conjugates have been prepared and studied for various applications such as in non-linear optics, electrochemistry and fluorescence sensing in our group [**123-125**]. Some of the Pcs-GQDs π-π conjugates that have been prepared are summarized in **Table 1.1**, [**65,124-131**].

Table 1.1. Examples of reported tetra-β- substituted MPcs π-π conjugated to GQDs.

Phthalocyanine	Pcs (R-Group)	Studies done	Ref
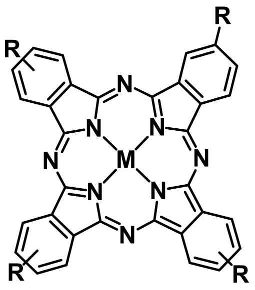	No R-group **M**: Zn(II)	Structural characterisation, Photo-physicochemical characterisation (Φ_F, Φ_Δ, Φ_T, τ_T), Photocatalysis of 4-chlorophenol.	[**126**]
	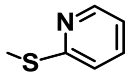 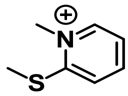 **M**: Zn(II), Al(III)	Structural characterisation, Photo-physicochemical characterisation (Φ_F, Φ_Δ, Φ_T, τ_T), Fluorescence sensing of Hg^{2+}.	[**127**]
	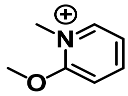 **M**: Zn(II)	Structural characterisation, Photo-physicochemical characterisation (Φ_F, Φ_Δ, Φ_T, τ_T).	[**128**]
	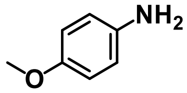 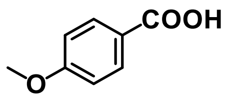 **M**: Co(II)	Structural characterisation, Electrocatalysis.	[**124**]
	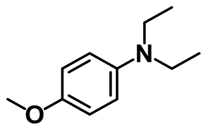 **M**: Zn(II)	Structural characterisation, Photo-physicochemical characterisation (Φ_F, Φ_Δ, Φ_T, τ_T).	[**129**]
	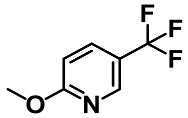 **M**: Zn(II)	Structural characterisation, Photo-physicochemical characterisation (Φ_F, Φ_Δ, Φ_T, τ_T).	[**130**]
	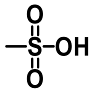 **M**: Al(III)	Structural characterisation, Photo-physicochemical characterisation (Φ_F, Φ_Δ, Φ_T, τ_T).	[**65**]
	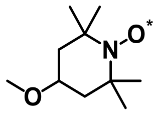 **M**: Zn(II)	Structural characterisation, Photo-physicochemical characterisation (Φ_F, Φ_Δ, Φ_T, τ_T), Fluorescence sensing of Ascorbic acid.	[**131**]

1.3.3. GQDs bio-functionalization

To afford enhanced cancer specificity and uptake of GQDs-drug complexes, biologically active molecules are usually tagged onto GQDs. Some of the commonly used biomolecules for GQDs-mediated drug transport that have been used are listed in **Table 1.2** [**132-137**].

Table 1.2. Examples of biomolecules used to functionalize GQDs for cancer therapeutics.

Biomolecule *(Drug carried)*	Structure	Application	Ref.
Folic acid *(Doxorubicin)*	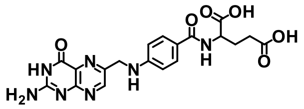	Theranostic for Cervical Cancer (He-La cells)	[**132**]
Biotin *(Doxorubicin)*	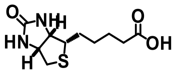	Delivery to adenocarcinoma (A549 cells)	[**110**]
Cyanine5.5 *(Doxorubicin)*	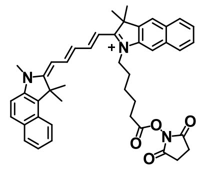	Theranostic for mammary gland derived breast cancer (4T1 cells)	[**133**]
Arginine-glycine-aspartic acid peptide *(Doxorubicin)*	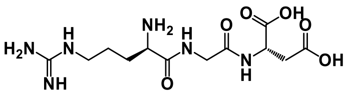	Theranostic for human prostate cancer (DU-145 and PC-3 cells)	[**134**]
Herceptin antibody *(Doxorubicin)*	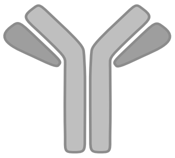	Theranostic for breast cancer (MCF-7 cells)	[**135**]
scFv-B10 antibody *(Cisplatin)*		Theranostic for breast cancer (MDA-MB-231 cells)	[**136**]
Hyaluronic acid-f *(Gemcitabine)*	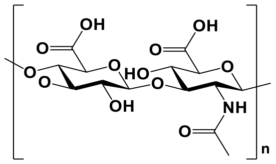	Delivery to pancreatic cancer (Panc-1 cells)	[**137**]

Although the Pcs-GQDs conjugates have not been studied for PDT, the conjugate of Pcs to a biofunctionalized, GQDs-GSH-folic acid have been reported [**65**]. In this thesis, however, the GQDs were functionalized using biotin.

Biotin is widely used as a targeting probe for cancer which allows for the internalization of the drug molecules to which it is coupled [**110,138,139**]. Biotin is a growth promoter, and the biotin uptake system is overexpressed on cancer cells to maintain their rapid proliferation and metastasis [**140**]. Therefore, linking cancer therapeutics to biotin is one way to improve the drug specificity. Moreover, the expression of biotin receptors, in comparison to folic acid receptors is higher in cancer cells [**141**]. The functionalization of GQDs with biotin creates a delivery vector that targets cancer sites through the EPR effect and internalization of the Pcs loaded on the surfaces via the receptor mediated endocytosis.

To maintain the binding ability of biotin to the receptor, the ring-end which fits to the binding cavity of the biotin receptor [**141**] such as Avidin and its derivatives must be left untampered with. Previously, GQDs have been linked to biotin through a linker which affords the NH_2 groups to which biotin may be bound [**110**]. In this work, the NH_2-GQDs were used, where the GQDs were covalently linked to the biotin through amide bonds involving the carboxylic-terminal of biotin and the amine groups on the edges of GQDs, **Fig. 1.7**.

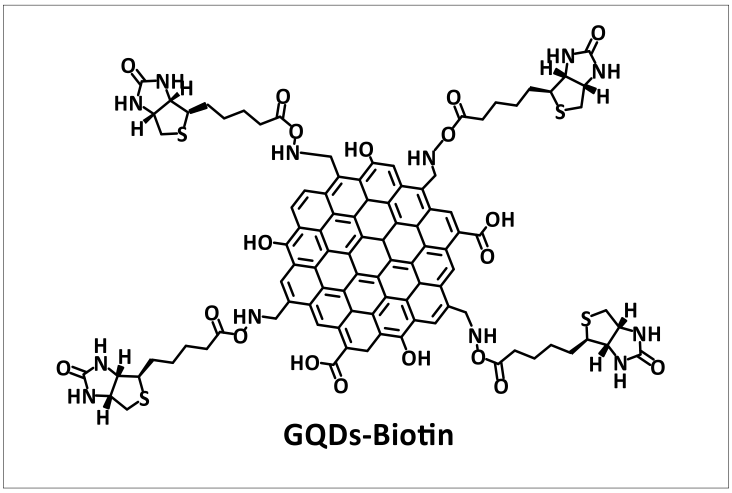

Figure 1.7. Simplified structure of biotinylated NH_2-GQDs.

A summary of the Pc complexes and their corresponding GQDs and GQDs-biotin conjugates prepared in this work is given in **Table 1.3**.

Table 1.3. The Zn(II)Pcs-GQDs conjugates used in this thesis.

Pcs (complex number); name	ref	NPs	Studies done
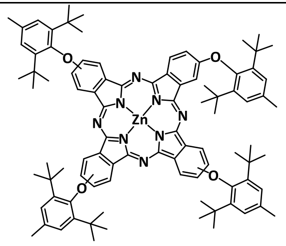 (**1**); di-*tert*-butyl-methyl phenoxy Zn(II)Pc	New	NH_2-GQDs	Structural characterisation, Photo-physicochemical properties (Φ_F, Φ_Δ, Φ_T, τ_T), *In vitro* Photodynamic therapy.
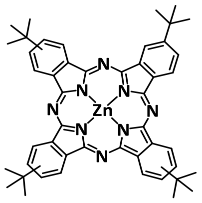 (**2**); *tert*-butyl Zn(II)Pc	[**142**]	NH_2-GQDs	Structural characterisation, Photo-physicochemical properties (Φ_F, Φ_Δ, Φ_T, τ_T), *In vitro* Photodynamic therapy.
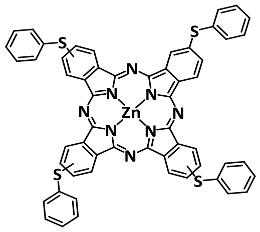 (**3**); phenylthio Zn(II)Pc	[**143**]	NH_2-GQDs	Structural characterisation, Photo-physicochemical properties (Φ_F, Φ_Δ, Φ_T, τ_T), *In vitro* Photodynamic therapy.
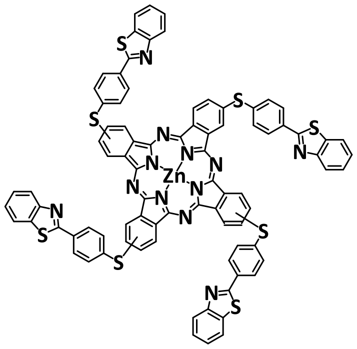 (**4**); -benzo[d]thiazol-2-yl-benzenethiol Zn(II)Pc	[**144**]	NH_2-GQDs	Structural characterisation, Photo-physicochemical properties (Φ_F, Φ_Δ, Φ_T, τ_T), *In vitro* Photodynamic therapy.
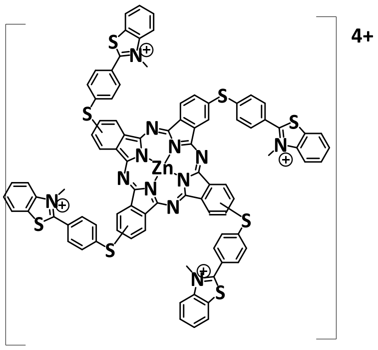 (**5**); cationic benzothiazole-thiophenyl Zn(II)Pc	New	NH_2-GQDs	Structural characterisation, Photo-physicochemical properties (Φ_F, Φ_Δ, Φ_T, τ_T), *In vitro* Photodynamic therapy.

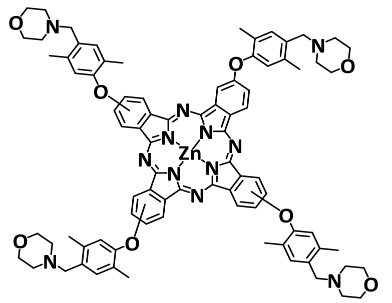 (**6**); 2,5-dimethyl-4-(morpholinomethyl) phenoxy Zn(II)Pc	New	NH_2GQDs	Structural characterisation, Photo-physicochemical properties (Φ_F, Φ_Δ, Φ_T, τ_T), *In vitro* Photodynamic therapy, Cellular uptake studies.
		NH_2-GQDs -biotin	Structural characterisation, Photo-physicochemical properties Φ_F, Φ_Δ, Φ_T, τ_T), *In vitro* Photodynamic therapy, Cellular uptake studies.
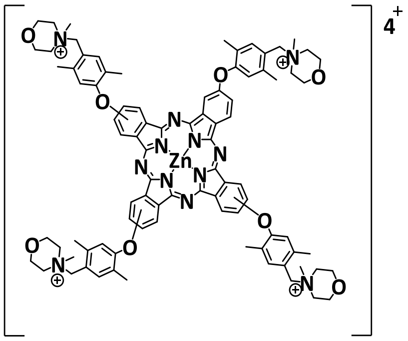 (**7**); cationic 2,5-dimethyl-4-(morpholinomethyl) phenoxy Zn(II)Pc	New	NH_2GQDs	Structural characterisation, Photo-physicochemical properties (Φ_F, Φ_Δ, Φ_T, τ_T), *In vitro* Photodynamic therapy, Cellular uptake studies.
		NH_2-GQDs -biotin	Structural characterisation, Photo-physicochemical properties (Φ_F, Φ_Δ, Φ_T, τ_T), *In vitro* Photodynamic therapy, Cellular uptake studies.

1.4. Novelty statement

The syntheses and structural characteristics of complexes **2-4** have been reported [**142-144**]. Complexes **1** and **5-7** are reported for the first time in this thesis. All the complexes contain Zn(II) as the central metal, to enhances the ISC to the triplet state [**76**].

As shown in **Table 1.1**, there has been no reports on the study of Pcs-GQDs conjugates for PDT, neither *in vivo* nor *in vitro*, hence, the subject of this thesis.

Additionally, Pcs containing biologically active chemical moieties used for cancer therapeutics have not been conjugated to GQDs before. In this thesis, Pc complexes comprising of substituents that have shown anti-cancer properties, such as the benzothiazole (complex **4** and **5**) [**95**] and morpholine (complex **6** and **7**) [**97**] groups, were synthesized and conjugated to GQDs, **Table 1.3**.

The effects of cations conferred on the N atoms of the benzothiazole and morpholine groups were evaluated by comparing complex **4-5** and complex **6-7**, as well as their respective conjugates.

The NH_2-GQDs were used to allow for direct linkage of biotin to the GQDs via the NH_2-groups.

The effects of the cancer specific and uptake-probe, biotin, on the GQDs-biotin was evaluated by comparing complex **6** and **7** to their respective GQDs and GQDs-biotin conjugates.

1.5. Aims and objectives: PDT activity of Pcs-GQDs conjugates

- Aim

The aim of this work was to design Pcs with substituents that will enhance their internalization in cancer cells, MCF-7 and then conjugate them to GQDs, and thereafter study the PDT activity of the prepared complexes on MCF-7 cell lines *in vitro*.

- Objectives

The objectives of this work are outlined in **Scheme 1.3**.

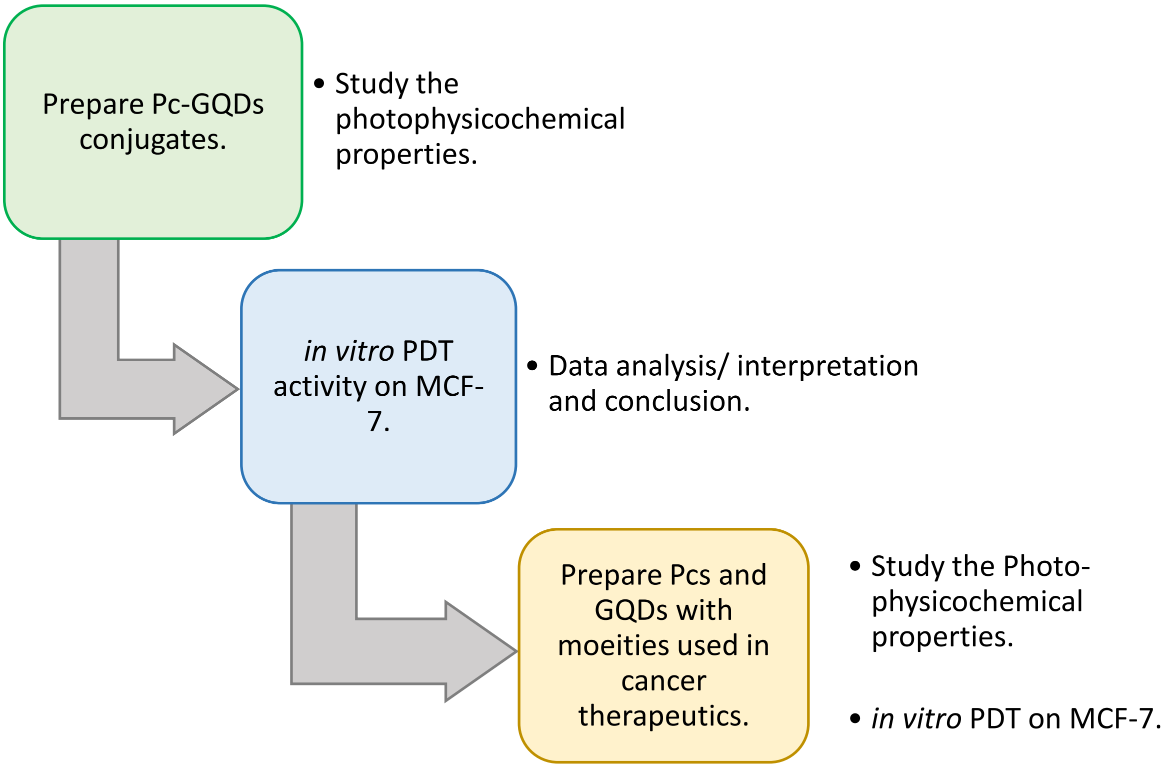

Scheme 1.3. Outline of the objectives for the study of the *in vitro* PDT activity of Pcs-GQDs on the MCF-7 cell line.

A series of analytical techniques were employed to define the structural and photo-physicochemical properties their physico-chemical properties of the newly synthesized complexes and conjugate.

1.6. Side work: Introduction of Flow chemistry for synthesis of probes for positron emission tomography

During my MSc, I spent six months at Chimie ParisTech, France, for training on flow chemistry, and to develop the trifluoromethylthiolation reaction in flow, (a reaction developed for the synthesis of radiotracers). This section introduces the studies that were conducted during the visit.

1.6.1. Radiotracers in cancer imaging

The development of effective bioimaging techniques allowing for early diagnosis of diseases such as cancer is important for ensuring effective treatment [**145**].

Positron emission tomography (PET) is a non-invasive quantitative imaging technique used in the detection and management of various diseases including cancer and Alzheimer disease [**146**]. PET utilises a chemical compound labelled with a positron emitting radionuclide, referred to as radiotracer [**146**]. The radiotracer also comprises of a biologically active molecule (bio-ligand) which functions to direct the radiotracer to specific sites in a biological system **Fig. 1.8**.

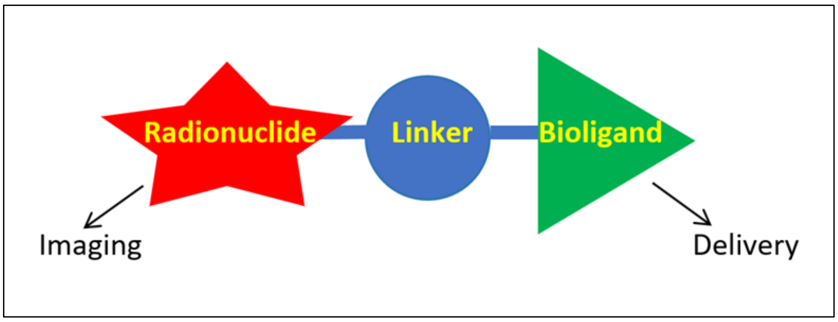

Figure 1.8. Design of a radiotracer comprising the radionuclide and targeting-bioligand.

Several radionuclides have been used for the design and study of PET radiotracers, including: oxygen, ^{15}O ($t_{1/2}$=~2 min); nitrogen, ^{13}N ($t_{1/2}$=~10 min); carbon, ^{11}C ($t_{1/2}$=~20 min); and fluorine,

^{18}F ($t_{1/2}$=~110 min) to mention a few [**147**]. The ^{18}F has gained attention for PET radiotracers owing to its relatively longer half-life ($t_{1/2}$). The [^{18}F]-Fluorodeoxyglucose, ([^{18}F]-FDG), is a commonly used F-based radiotracer for PET which enters cancer cells through the glucose endocytosis system [**147**]. The radiotracer is not for all types of cancer, neither for all diseases. Therefore, a more universal method for efficiently radio-labelling biomolecules for bioimaging is of paramount importance. Noting the inevitable occurrence of radioactive decay, the method of preparing radiotracers must be selected with care to maintain quality radiotracers for imaging.

Additionally, a pharmaceutically valuable moiety, *i.e*. the trifluoromethylthio- group ($-SCF_3$), is of interest in this study for use in radio-labelling chemical compounds. The SCF_3 group is highly electrophilic and has been reported to improve drug transport through the cellular lipid membrane as well as improve the metabolic stability of the drug. [**148**].

1.6.2. Difluorocarbene-derived trifluoromethylthiolation reaction

Zheng and colleagues have described for the first time the one-pot synthesis of SCF_3-functionalised compounds using the difluorocarbene reagent, difluoromethylene phosphobetaine ($Ph_3P^+CF_2CO_2^-$; PDFA) [**149**]. This method allows for the *in-situ* incorporation of a third F atom, which may be radioactive or non-radioactive isotope depending on the application, on the difluoro-bearing carbon derived from the difluorocarbene, **Scheme 1.4**.

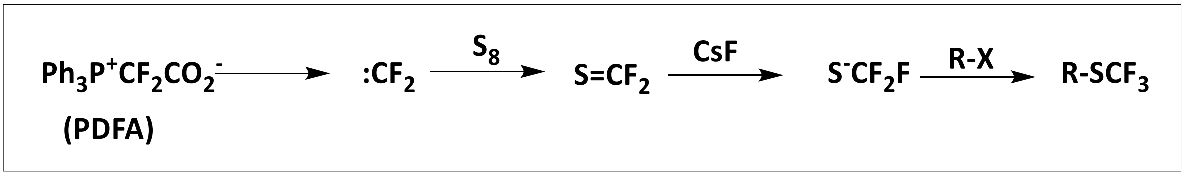

$$\underset{\text{(PDFA)}}{Ph_3P^+CF_2CO_2^-} \longrightarrow :CF_2 \xrightarrow{S_8} S{=}CF_2 \xrightarrow{CsF} S^-CF_2F \xrightarrow{R\text{-}X} R\text{-}SCF_3$$

Scheme 1.4. Trifluoromethylthiolation reaction of aliphatic electrophiles derived from the difluorocarbene PDFA.

Upon heating, the PDFA dissociates to generate a difluorocarbene which readily forms S=CF$_2$ in the presence of S$_8$, **Scheme 1.4**. A third F is subsequently added *in situ* to the S=CF$_2$ carbon to form the SCF$_3$. The SCF$_3$ is thereafter incorporated to the aliphatic group (R) through a nucleophilic substitution mechanism, displacing the electrophile (X) initially bound to it (R-X) to form the desired R-SCF$_3$ compound [**149**].This reaction mechanism is also attractive for PET radiotracer design in that it is time efficient when incorporating the SCF$_3$ on a bioactive-compound, compared to preparing the SCF$_3$ prior to bio-conjugation. The method described by Zheng *et al*. [**149**], was performed in a batch reaction system. The disadvantages following this type of a reaction technique are attributed to the inefficient heat and mass transfer since there is a low volume to surface ratio in the reaction vessel [**150**]. This tends to be even more problematic when upscaling, leading to incomplete reactions and formation of side products [**150**].

In this project, the application of the reaction mechanism as described in **Scheme 1.4** was introduced in a flow system instead of a batch reaction system. The non-radioactive isotope, ^{19}F, was used for safety purposes.

1.6.3. Flow chemistry

Flow chemistry involves the performance of synthetic chemistry in a tube in continuous flow unlike the conventional batch reactions [**151**].

Flow reactors have an increased surface-volume ratio, generally improving the heat and mass transfer in the reaction mixture thus relatively improving the reaction efficiency with reduced side products [**151]**. Therefore, making flow chemistry a promising technique for the synthesis of quality radiotracers.

1.7. Aims and objectives: Development of the trifluoromethylthiolation reaction in flow.

- Aim

The aim of this work was to develop the difluorocarbene-derived difluoromethylthiolation reaction in flow. The trifluoromethylthiolation reaction explored in this project is as described by Zheng and colleagues [**149**]. The reaction as described in literature, is performed and optimized in DMF for batch reactions. The major challenge for applying the reaction directly in flow is due to the poor solubility of some reagents in DMF.

- Objectives

The objectives of this work are outlined in **Scheme 1.5**.

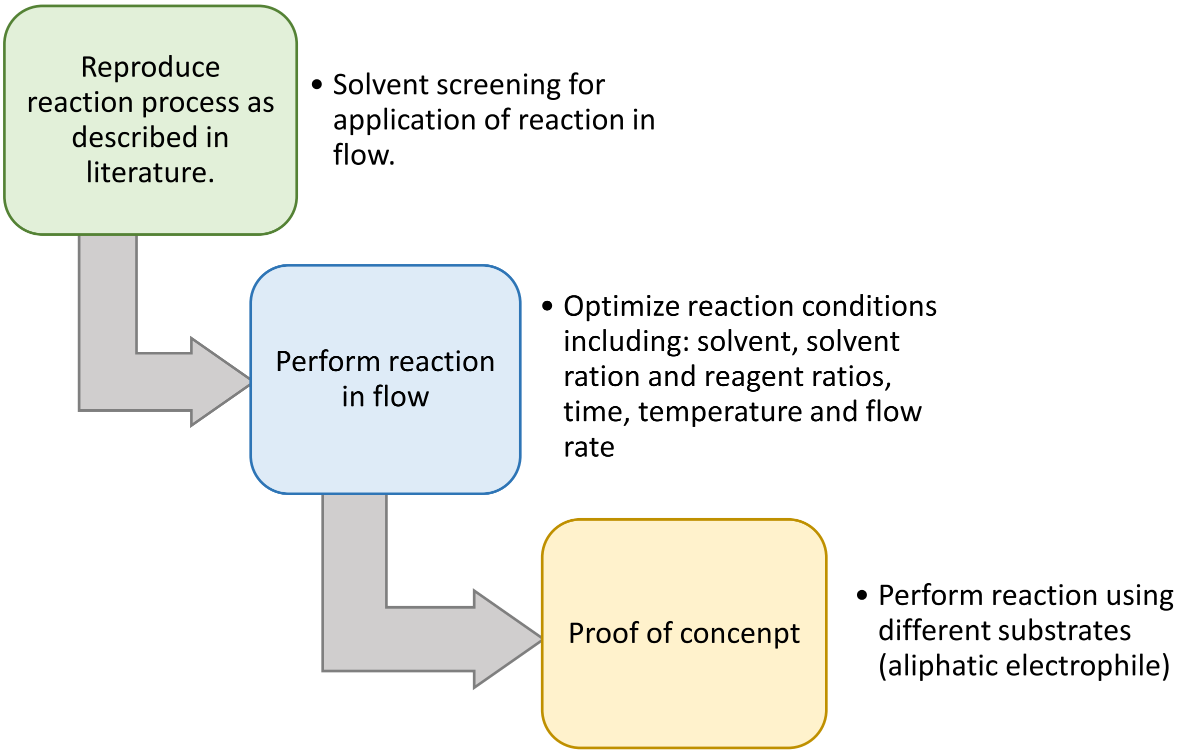

Scheme 1.5. Outline of the objectives for the development of the trifluoromethylthiolation reaction in flow.

The reaction was monitored using ^{1}H and ^{19}F nuclear magnetic resonance.

CHAPTER TWO

2. Experimental

2.1. Materials

2.1.1. Solvents

The *N,N*-dimethylformamide (DMF), dimethyl sulfoxide (DMSO) ethanol, methanol, and tetrahydrofuran (THF) were purchased from Merck®. The 1-pentanol, chloroform, ethyl acetate, diethyl ether, acetone, toluene and hydrochloric acid were all purchased from Sigma-Aldrich®.

2.1.2. Reagents for the synthesis of phthalonitriles, Pcs and Biotin-GQDs

The zinc acetate ($Zn(OAc)_2$, 99%), 1,8-diazabicyclo [5.4.0] undec-7-ene (DBU), 2,5-dimethyl-4-(morpholinomethyl) phenol hydrochloride monohydrate, 2,6-di-*tert*-butyl-4-methylphenol, sodium sulphate, potassium carbonate, dimethyl sulphate (DMS), biotin, N,N'-dicyclohexylcarbodiimide (DCC), 4-dimethylamino)pyridine (DMAP), and aluminium oxide 90 active neutral were purchased from Sigma-Aldrich®. The Millipore water was acquired from a Milli-Q water system (Millipore Corp, Bedford, MA, USA).

2.1.3. Standards and quenchers for photo-physicochemical studies

The anthracene-9,10-*bis*-methylmalonate (ADMA), 1,3-diphenylisobenzofuran (DPBF), unsubstituted Zn(II)Pc, and quinine sulphate (QS) were purchased from Sigma-Aldrich®. AlPcSmix (mixture of sulfonated Pcs derivatives) was prepared as described in literature [**152**]

2.1.4. Previously synthesized materials

Some of the reagents and complexes used in this work were synthesized following methods previously described in literature. These include, 4-nitro-phthalonitrile [**153**], 4-(2,6-di-*tert*-butyl-4-methylphenoxy) phthalonitrile (**Pn 1**, **Scheme 3.1.**) [**154**], tetra-*tert*-butyl Zn(II)Pc (complex **2**) [**142**], tetra-phenylthio Zn(II)Pc (complex **3**) [**143**], and tetra- 4-(benzo[d]thiazol-2-yl)benzenethiol Zn(II)Pc (complex **4**) [**144**], and the NH_2-GQDs [**155**].

2.1.5. Materials for cell studies

The human breast adenocarcinoma Michigan cancer-7 (MCF-7) cell line were purchased from Cellonex®. The Dulbecco phosphate-buffer saline (DPBS), Dulbecco's modified eagle's medium (DMEM) with and without phenyl-red were purchased from Lonza®. The heat-inactivated fetal bovine serum (FBS, 10 % (v/v)) and the 100 μg/ mL-penicillin:100 unit/ mL-streptomycin-amphotericin-B-mixture (PSA) as well as the neutral red cell proliferation reagent (WST) were all purchased from Biowest®.

2.2. Instruments and methods

2.2.1. Structural characterisation

- The Infrared (FT-IR) spectra were recorded using the Burker Alpha model FT-IR spectrometer with universal attenuated total reflectance (ATR) sampling accessory.
- Mass spectra (MS) data were collected on a Bruker AutoFLEX III Smart-beam TOF/TOF mass spectrometer using α-cyano-4-hydrocinnamic acid as the matrix.
- The ^{1}H nuclear magnetic resonance (NMR) spectra were recorded with Bruker Advance II+ 600 MHz (or 400 MHz) NMR spectrometers.
- Elemental analysis was done using a VARIO ELEMENTAR EL III CHNS instrument.
- The Raman spectra were collected using the Burker Vetex 70-Ram II Raman spectrometer, with a 1064 nm Nd:YAG laser and a germanium laser cooled with liquid nitrogen.
- The transmission electron microscope (TEM), ZEISS LIBRA model 120 operated at 90 kV and iTEM software was used for TEM micrographs processing.

- For dynamic light scattering (DLS) measurements, Malvern Zetasier Nanoseries, Nano-ZS90 was employed. Energy dispersive X-ray spectroscopy (EDS) was done in the INCA PENTA FET coupled with the VAGA TESCAM, at 20 kV accelerating voltage.

2.2.2. Photo-physicochemical characterization

- The ultraviolet-visible (UV-Vis) spectra of the complexes were recorded using the Shimadzu 2550 UV-Vis spectrophotometer, in the range of 300-800 nm.
- The fluorescence emission and excitation spectra were recorded using the Varian Eclipse spectrofluorimeter using a 360-1100 nm filter.
- The fluorescence lifetimes were recorded using the time correlated single photon counting (TCSPC) **Fig. 2.1**, (FluoTime 300, Picoquant GmbH). A diode laser (LDH-P-670 driven by PDL 800-B, 670 nm 20 MHz repetition rate, Picoquant GmbH) was employed where Pc absorbs and LDH-P-387 with 10 MHz repetition rate, 88 ps pulse width where GQDs absorb.
- A laser flash photolysis system, **Fig. 2.2**, consisting of a LP980 spectrometer with a PMT-LP detector and an ICCD camera (Andor DH320T-25F03) detector was used to determine triplet quantum yields. The signal from the PMT detector was recorded on a Tektronix TDS3012C digital storage oscilloscope. The excitation pulses were produced using a tuneable laser system consisting of an Nd:YAG laser (355 nm, 135 mJ/4–6 ns) pumping an optical parametric oscillator (OPO, 30 mJ/3–5 ns) with a wavelength range of 420–2300 nm (NT-342B, Ekspla).
- Triplet lifetimes were determined by the exponential fitting of the kinetic curves using the ORIGIN® 8 Professional software.

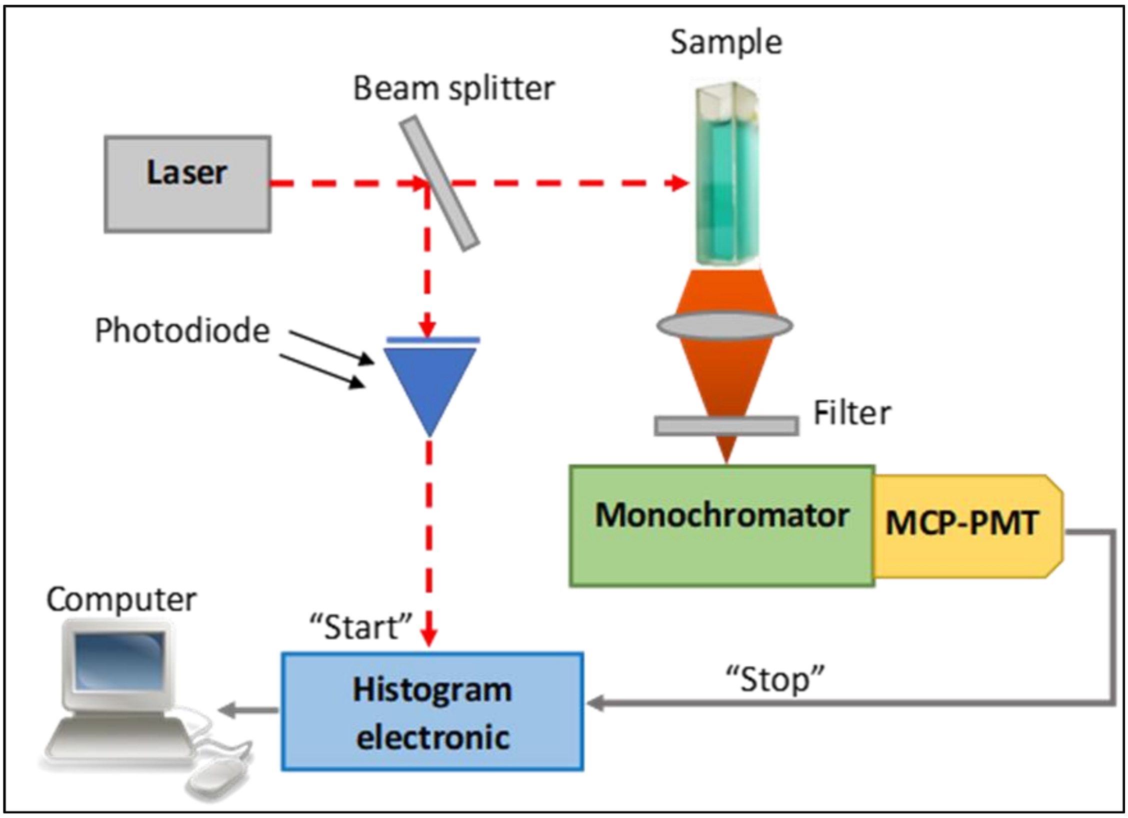

Figure 2.1. Time correlated single photon counting setup for fluorescence lifetimes studies.

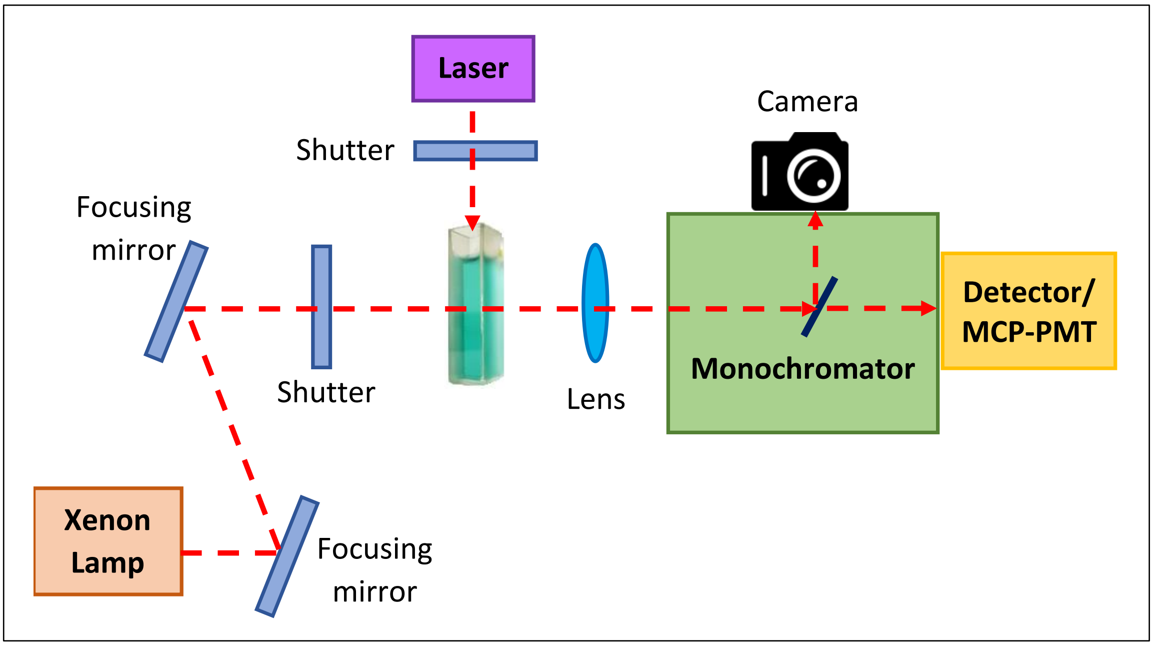

Figure 2.2. Laser flash photolysis system setup for triplet quantum yields and lifetime studies.

- Irradiations for singlet oxygen quantum yields were done using a General Electric quartz projector lamp (300 W). The system has a 600 nm glass (Schott), water filter, cut of filter and A 670 nm interference filter placed in the light path before the sample **Fig. 2.3**. Light intensities were measured with a POWER MAX 5100 (Molelectron® detector incorporated) power meter.

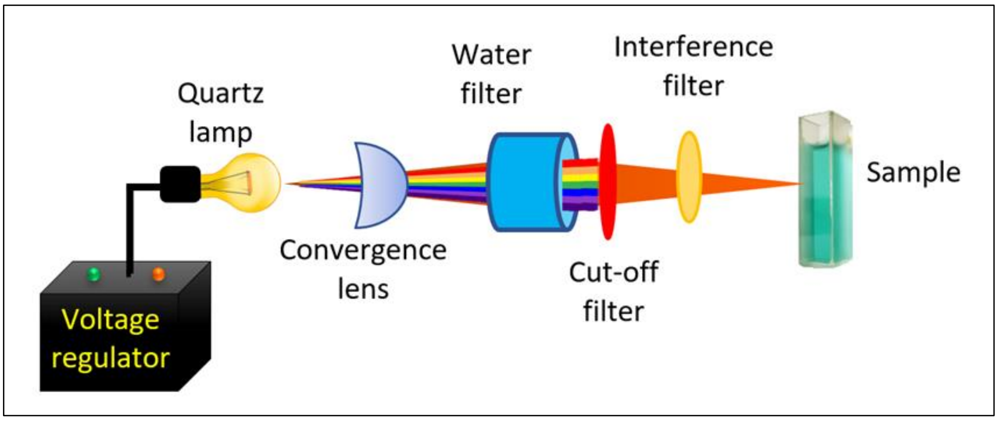

Figure 2.3. Singlet oxygen generation studies set-up.

2.2.3. PDT irradiation

For photodynamic therapy studies, sample irradiations were performed in the Modulight® Medical Laser System 7710-680, with a sample holder, a Turnkey laser system connected to a 2.3 W channel at 680 nm, a hand switch pedal, connectors and safety interlocks, **Fig. 2.4**.

Figure 2.4. The Modulight® Medical Laser System used for PDT studies.

2.3. Syntheses

2.3.1. tetra-(2,6-di-*tert*-butyl-4-methylphenoxy) Zn(II)Pc, complex 1, Scheme 3.1

To obtain the tetra-(2,6-di-*tert*-butyl-4-methylphenoxy) Zn(II)Pc (complex **1**), the metal free tetra-(2,6-di-*tert*-butyl-4-methylphenoxy) Pc (**H_2-1**) was first synthesized as follows: **Pn 1** (1.00 g, 2.89 mmol) was dissolved in 1-pentanol (5 mL) in the presence of DBU (0.3 mL, 1.93 mmol) and refluxed for 6 h under Ar to obtain the **H_2-1**, **Scheme 3.1**. The reaction mixture was cooled and the H_2-**1** was thereafter evaporated to dryness. The product was purified using neutral aluminium oxide 90 active gel column chromatography by gradient eluent using a methanol: $CHCl_3$ solution. **H_2-1**, Yield: 79.1%. UV-vis ($CHCl_3$): λ_{max} 661 nm,697 nm. Anal. Calc. for $C_{92}H_{106}N_8O_4$, expected C, 79.62; H, 7.70; N 8.07%, found: C, 79.27; H, 7.20; N, 8.02%. IR [(ATR) V_{max}/cm^{-1}]: 1650 (C–C), 1457 (C–H), 1380 (C–N), 1239 (C–O–C), 1156 (–C–O). NMR: ^1H NMR (600 MHz, $CDCl_3$), (δ:ppm): 9.51–9.31 (12H, m, Ar-H), 8.04–6.67 (8H, m, Ar-H), 1.63 (12H, m, CH_3-H), 1.45–1.43 (72H, m, CH_3-H), 0.09 (2H, m, NH_2-H). MALDI-TOF (m/z): Calculated: 1386.83, Found: 1387.73 $[M]^+$.

The **H_2-1** (0.2 g; 0.14 mmol) was dissolved in 5 ml of anhydrous DMF in the presence of $Zn(OAc)_2$ (0.04 g; 0.22 mmol) and DBU (0.1 mL; 0.67 mol) and was left to reflux while stirring continuously under Ar overnight to form complex **1**, **Scheme 3.1**. The reaction mixture was cooled to ambient temperature and the product was precipitated out of solution with 1:1 (v/v) methanol and water solution and collected by centrifugation at 3500 rpm for 5 min. The product was dried in an enclosed fume hood. The product was further purified and isolated using neutral alumina packed column with gradient eluents using a hexane: $CHCl_3$ solution. Complex **1**, Yield: 75%. Anal. Calc. for $C_{92}H_{104}N_8O_4Zn$, expected: C, 76.14; H, 7.22; N, 7.2%, found: C, 76,80; H, 7.91; N, 7.15%. IR[(ATR), V_{max}/cm^{-1}]: 2951 (Ar, C-H stretch), 2867 (-C-H), 1645 (Ar, C=C), 1627 (Ar, C=N),1093 (-C-O-C). ^{1}H NMR (600 MHz, $CDCl_3$), (δ, ppm): 9.29 (s, 7H, Ar-H), 7.97 (s, 4H, Ar-H), 7.01 (d, *J = 8.52*, 9H, Ar-H), 2.16 (d, *J* = 11.2 Hz, 12H, CH_3-H), 1.50 – 1.17 (m, 72H, CH_3H). MALDI-TOF-MS (m/z): Calculated: 1451.28, found 1452.35 $[M]^+$. UV/ Vis λ_{max} (nm) (log ε, DMSO): 679 (4.6), 613 (4.0), 356 (4.2).

2.3.2. tetra-(4-(2,5-dimethyl-4-(morpholinomethyl) phenoxy)) Zn(II)Pc, complex 6, Scheme 3.2

The tetra-(4-(2,5-dimethyl-4-(morpholinomethyl) phenoxy)) Zn(II)Pc (complex **6**) was prepared by first synthesizing the corresponding phthalonitrile, 4-(2,5-dimethyl-4-(morpholinomethyl) phenoxy) phthalonitrile (**Pn 2**), **Scheme 3.2**, as follows: 2,5-dimethyl-4-(morpholino-methyl) phenol hydrochloride was first suspended in Millipore H_2O and filtered to remove the HCl dissolved in the H_2O. The solid was thereafter dissolved in $CHCl_3$, Na_2SO_4 was added to the solution to remove residual H_2O and this was followed by filtration. The filtrate was dried under pressure in vacuo. The dry light-brown solid (3 g, 14.5 mmol) and 4-nitro-phthalonitrile (2 g, 11.55 mmol) was dissolved in 15 mL anhydrous DMF, then K_2CO_3 (5 g, 36.18 mmol) was added into the reaction mixture in 1 g portions after 1 h intervals. The reaction mixture was maintained at ambient temperature under Ar with continuous stirring for 48 h. The product was precipitated with ice and collected through vacuum filtration. The product was thereafter dried and recrystalized in acetone. **Pn 2**, Yield: 68%, Anal. Calc. for $C_{21}H_{21}N_3O_2$, expected: C, 72.60; H, 6.09; N 12.10%, found: C, 71.41; H, 6.3; N, 12.0%. IR[(ATR), V_{max}/cm^{-1}]: 2961 (Ar, C-H), 2853 (-C-H), 2233 (-C≡N), 1674 (Ar, C=C), 1600 (Ar, C=N),1093 (-C-O-C). NMR: ^{1}H NMR (400 MHz, $CDCl_3$), (δ:ppm): 8.05 (d, 1H, Ar-H), 7.87 (s, 1H, Ar-H), 7.23 (m, 2H, Ar-H), 6.91 (s, 1H, Ar-H), 3.78-3.76 (m, 4H, CH_2-H), 3.61 (s, 2H, CH_2-H), 2,71 (s, 4H, CH_2-H), 2.29 (s, 3H, CH_3-H), 2.04 (s, 3H, CH_3-H).

The 2,9,16,23-tetrakis-(2,5-dimethyl-4-(morpholinomethyl)) phenoxy Zn(II)Pc (complex **6**) was obtained through cyclo-condensation of **Pn 2** (0.5 g, 1.5 mmol) dissolved in 1–pentanol (3 mL) in the presence of $Zn(OAc)_2$ (0.4 g, 2 mmol) and DBU (0.3 ml), **Scheme 3.2**. The mixture was heated at 140 ^{o}C under Ar atmosphere and left to stir for 24 h. The reaction mixture was thereafter cooled to ambient temperature. The product was precipitated out of solution with 1:1 methanol and water solution (v/v) and centrifuged at 3500 rpm, then finally washed with methanol and then collected by centrifugation. The pelleted product was then air-dried in an enclosed fume hood. The product was further purified using silica gel column, eluted with 1:1 (v/v) $CHCl_3$: THF as the eluting solvent. Complex **6**, Yield: 82.5%. Anal. Calc. for $C_{84}H_{84}N_{12}O_8Zn$, expected: C, 69.34; H, 5.82; N, 11.55%, found: C,69.80; H, 5.70; N, 11.21%. IR[(ATR), V_{max}/cm^{-1}]: 3000 (Ar, C-H stretch), 2817 (-C-H), 1720 (Ar, C=N), 1211 (-C-N), 1000 (-C-O-C). NMR: ^1H NMR (600 MHz, $CDCl_3$), (δ:ppm): 8.07 (d, 2H, Ar-H), 7.75 (m, 4H, Ar-H), 7.0 – 7.25 (m, 6H, Ar-H), 6.6-6.71 (m, 8H, Ar-H), 3.75-4.0 (s, 11H, CH_2-H), 3.70 (s, 3H, CH_2-H), 3.3 (m, 10H, CH_2-H), 2.55-2.25 (m, 16H, CH_2-H), 2.18 (s, 4H, CH_3-H), 1.75 (d, 20H, CH_3-H). MALDI-TOF-MS (m/z): calculated: 1455.02, found: 1455.02 $[M]^+$. UV-vis (DMSO): λ_{max} 684 nm, UV/ Vis λ_{max} (nm) (log ε): 684 (4.87), 615 (4.24), 355 (4.6).

2.3.3. Cationic Zn(II) Pcs, complex 5 and complex 7, Schemes 3.3 and 3.4

To obtain the cationic tetra-4-(benzo[d]thiazol-2-yl) benzenethiol Zn(II)Pc (complex **5**) a solution of complex **4** (0.5 g, 0.32 mmol) in anhydrous DMF and excess DMS was prepared and stirred for 72 h at 70 ^{o}C under Ar, **Scheme 3.3**. The mixture was then cooled to room temperature, the solid product was washed with hot acetone, collected by centrifugation, and thereafter continuously washed with methanol, ethyl acetate, THF and $CHCl_3$, and finally dried with diethyl ether and left to dry further in fume hood. Complex **5,** Yield: 76 %. Anal.

Calc. for $C_{84}H_{44}N_{12}S_8Zn$, expected: C, 65.38; H, 2.87; N, 10.48; S, 16.00%, found: C, 63.46; H, 3.0; N, 10.79; S, 16.4%. IR[(ATR), V_{max}/cm^{-1}]: 3044 (Ar, C-H), 2796 (CH_3, C-H), 1603 (C=N), 1478 (Ar, C=C), 752 (C-S). ^1H NMR (600 MHz, DMSO-D_6), (δ, ppm): 8.59-8.62 (m, 4H, Ar-H), 8.09-8.1 (m, 4H, Ar-H), 7.80-7.82 (m, 6H, Ar-H), 7.72-7.74 (d, 2H, Ar-H), 7.59-7.64 (m, 8H, Ar-H), 7.4-7.5 (d, 16H, Ar-H), 7.42 (d, 4H, Ar-H), 4.03 (s, 12H, CH_3-H). UV/ Vis λ_{max} (nm) (log ε, DMSO): 683 (4.4), 615 (3.8), 355 (4.3).

To obtain the cationic tetra (4-(2,5-dimethyl-4-(morpholinomethyl) phenoxy)) Zn(II)Pcs (complex **7**), a solution of complex **6** (80 mg, 0.055 mmol) in anhydrous DMF was prepared and stirred at 90 ^oC for 30 min under Ar gas. Excess DMS was thereafter added drop-wise and the mixture continued to stir for 72 h, **Scheme 3.4**. The product was purified as described for complex **5** above. Complex **7**, Yield: 67.5%. Anal. Calc. for $C_{88}H_{96}N_{12}O_8Zn$, expected: C, 69.76; H, 6.39; N, 11.09; Found: C, 67.9; H, 6.82; N, 11.2%. IR[(ATR), V_{max}/cm^{-1}]: 2996 (Ar, C-H), 2807 (-C-H), 1611 (Ar, C=N), 1241 (-C-N), 1000 (-C-O-C). NMR: ^1H NMR (600 MHz, $CDCl_3$), (δ:ppm): 8.12 (d, 2H, Ar-H), 7.7 (m, 4H, Ar-H), 7.34-7.4 (m, 2H, Ar-H), 7.08 – 7.25 (m, 4H, Ar-H), 6.82-.7.1 (m, 8H, Ar-H), 4.5 (s, 8H, CH_2-H), 3.72-3.65 (m, 16H, CH_2-H), 3.37-3.48 (m, 16H, CH_2-H), 3.3 (s, 12H, CH_3-H), 2.25 (s, 12H, CH_3-H), 1.97 (s, 12H, CH_3-H)., (log ε): 682 (4.25), 618 (3.73), 357 (4.08).

2.3.4. Synthesis of GQDs-biotin, Scheme 3.5

To prepare the biotin functionalised GQDs, a solution of biotin (0.015 g, 0.06 mmol) in 2.5 mL anhydrous DMF was prepared. To the solution, DCC (0.0083 g, 0.05 mmol) and DMAP (0.01 g, 0.08 mmol) were added, and left to stir at room temperature for 24 h, **Scheme 3.5**. A separate solution of GQDs (0.1 g) in water (1 mL) was prepared and added to the biotin solution. The resulting mixture was stirred at room temperature for 24 h. The Biotin-GQDs were precipitated using ethanol and then collected by centrifugation to remove non-conjugated biotin and GQDs, as well as the soluble DCC and DMAP.

2.3.5. Conjugation of Pc complexes to GQDs and GQDs-biotin, Scheme 3.6

The π-π conjugation of the Pcs onto GQDs was similar for the different Pcs (complexes **1**-**7**). The GQDs (10 mg) were dissolved in 1 mL of Millipore water and each of the Pcs (10 mg) were dissolved in 4 mL anhydrous DMF in separate vials and sonicated for 4 h separately. The GQDs and the Pcs solutions were then mixed and stirred at room temperature for 48 h. The same method was used for conjugation of the complexes to GQDs-Biotin (**6**-GQDs-biotin and **7**-GQDs-biotin). **1**-GQDs, **2**-GQDs, **3**-GQDs, **4**-GQDs and **6**-GQDs conjugates were thereafter washed with ethanol, the cationic conjugates **5**-GQDs, **7**-GQDs and **7**-GQDs-biotin were washed with THF, and then diethyl ether, **6**-GQDs-biotin conjugates were washed with methanol. The conjugates were thereafter collected using a centrifuge at 3500 rpm for 5 min and dried in a closed fume hood overnight.

2.4. Photo-physicochemical parameters

2.4.1. Fluorescence quantum yields and lifetimes

The Φ_F were calculated using **Equation 1.1**, following methods described in literature [**54,55**]. The unsubstituted Zn(II)Pc (Φ_F = 0.20) was used as a standard for Φ_F in DMSO [**62**] when exciting where the Pcs absorb. Quinine sulphate (QS) in 0.05 M H_2SO_4 solution (Φ_F = 0.60) [**156**] was used as the standard when determining the Φ_F at the excitation wavelength of GQDs. The samples and ZnPc standard for Φ_F determination where Pcs absorb were prepared such that the absorbance of the v-band was ~0.05 a.u, and the λ_{exc} (nm) used were at the crossover of the Q-bands of the test samples and the standard. The samples for the determination of the Φ_F of GQDs were prepared such that the absorbance of the GQDs in the and QS are ~0.5 a.u, where the λ_{exc} (nm) used were the cross-over wavelengths between the QS and GQDs in each sample. The τ_F were obtained using TCSPC, **Fig. 2.1**, by exciting where Pcs absorb and where GQDs absorb for GQDs and GQDs-Biotin.

2.4.2. Triplet quantum yields and lifetimes

The Φ_T were calculated using **Equation 1.2**, following methods described in literature [**51,63**]. The unsubstituted Zn(II)Pc (Φ_T = 0.65) was used as standard for Φ_T in DMSO [**157**]. The triplet absorption decay curves were obtained using the instrument illustrated in **Fig. 2.2**. The samples were prepared such that the absorbance intensity at the Q-band was ~1.5 a.u. All the samples for Φ_T studies where deaerated using Ar for 12 min.

2.4.3. Singlet oxygen quantum yields

The Φ_Δ were calculated using **Equation 1.4**, following methods described in literature [**64-66**]. The unsubstituted Zn(II)Pc (Φ_Δ = 0.67) was used as standard for Φ_Δ in DMSO [**158**] and AlPcSmix (Φ_Δ = 0.42) was used as standard for Φ_Δ in water [**159**]. Samples for Φ_Δ studies, using DPBF, were prepared such that the absorbance at the Q-band was ~1.5 a.u for each of the complexes/ conjugates and the ZnPc standard. The DPBF maximum absorbance was ~2 a.u (at λ = 417 nm). For Φ_Δ studies, using ADMA, the absorbances at the Q-band was ~1 a.u for the test complexes/ conjugates and the AlPcSmix, and ~2 a.u for ADMA (at λ = 380 nm). Each of the complexes/ conjugates were mixed at 1:1 v/ v ratio with DPBF or ADMA, in the dark, prior irradiation. For Φ_Δ studies using DPBF in DMSO, the samples were irradiated for 20 s over 2 min, where irradiations for Φ_Δ studies using ADMA were done at 10 min intervals over 50 min. The system used for Φ_Δ studies is shown in **Fig. 2.3**.

2.5. Cell studies

2.5.1. Tissue culture

The human breast cancer MCF7-cells in T75 cm^2 vented flasks containing culture media (DMEM with 4.5 g/ L glucose with $_{L}$-glutamine and phenol red, supplemented with 10% FBS and 5% PSA), were incubated in a 37 ^{0}C, ~5% CO_2 humidified atmosphere incubator from HeatForce®, and were grown to 100 % confluency. The cells were quantified using the haemocytometer. For dark and PDT studies, the cells were inoculated into 96 well plates (10^5 cells/ well) and incubated over 24 h in conditions described earlier.

2.5.2. Dark and PDT toxicity studies

The Pcs and conjugates were inoculated into the 96-well plates at different concentrations: 5, 10, 20, 40, 60, 80 and 100 µg/ mL in culture media with 1% DMSO solution. The cells incubated in the dark for 24 h. The cells were thereafter washed with DPBS, and the DMEM without phenyl-red, was added to the wells.

For PDT studies, the cells were irradiated for 5 min using the Modulight® Medical Laser System, **Fig. 2.4**. The DMEM without phenyl red was thereafter decanted, and the cultured media was added. The cells were re-incubated in growth conditions. For dark toxicity studies, cell samples similar to those prepared for PDT studies were prepared. The cells were however kept in the dark for 24 h. The cell viability assay using WST was performed to quantify viable cells.

Cell viability was measured for both dark and PDT tests after 24 h using the WST assay on a Synergy™ 2 multi-mode microplate reader BioTek at 450 nm, **Equation 2.1**.

$$\boldsymbol{Cell\ viability} = \frac{\boldsymbol{Absorbance\ of\ sample}}{\boldsymbol{Absorbance\ of\ control}} \ .\ \mathbf{100}\% \qquad \textbf{(Equation 2.1)}$$

2.5.3. Cellular drug-uptake studies

To determine the cellular drug uptake in 24 h, cells were grown in 96 well-plate and inoculated with Pc complexes, Pc-GQDs conjugates and GQDs at concentrations 5, 10, 20, 40, 60, 80 and 100 µg/ mL in 1% DMSO in culture media. A control sample containing 1 % DMSO in culture media was prepared. The plates were incubated at 37 ^{0}C under ~5% CO_2 humidified atmosphere for 24 h. The media was then decanted, and the cells were washed with DPBS to remove complexes that have not been absorbed into the cells. The DMEM with no phenyl-red was added and the fluorescence of the samples were obtained at the excitation λ_{max} of Pcs for the Pc complexes and Pcs-GQDs conjugates, and λ_{max} of GQDs for GQDs and GQDs-biotin. To correct the fluorescence of the samples, the average fluorescence of the control sample (MCF-7 cells with no compounds) was subtracted from the average fluorescence of the test samples. The graph of corrected fluorescence intensity against the corresponding concentration for each test compound was plotted. The fluorescence intensities were obtained for each sample, using the SpectraMax® M3, Molecular Devices multi-well-plate reader from Separations using the SoftMax® Pro6.4 programme.

2.6. Side work: Trifluoromethylthiolation reaction in flow

2.6.1. Flow reactor

The flow reactions were performed in the Syrris Asia Syringe Pump 16 mL flow reactor. A simplified diagram alongside the image of the flow reactor used for this study is shown in **Fig. 2.5A** and **B**, respectively.

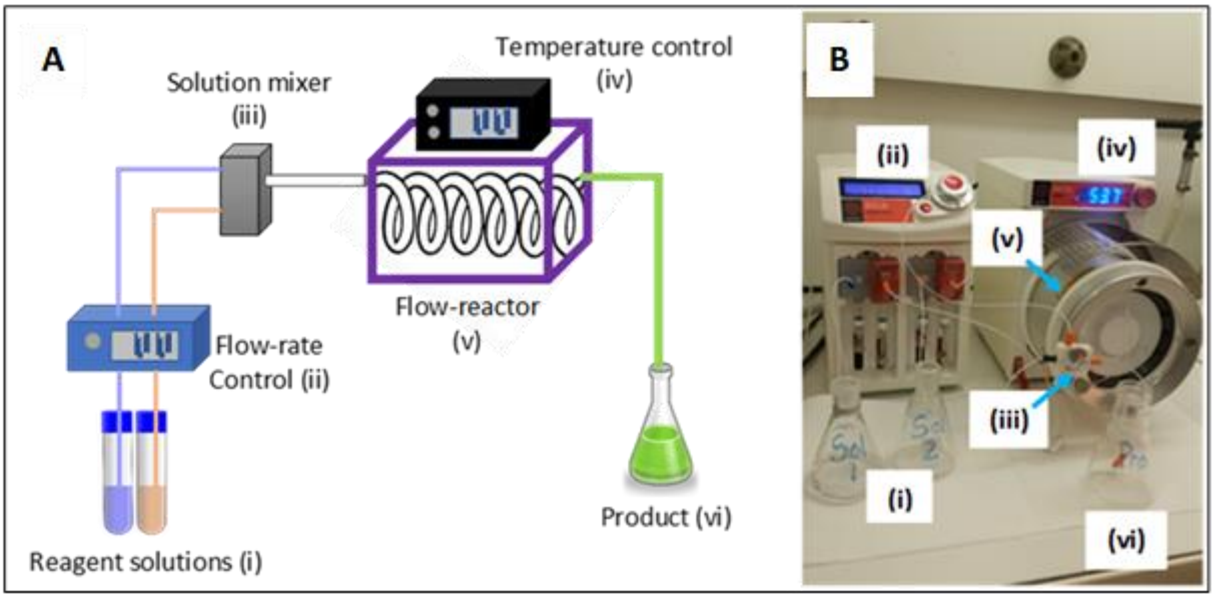

Figure 2.5. Flow reactor, **A**) set-up outline and **B**) instrument image. (**B** is labelled in the same order as **A**).

The features in the flow system include: feed-pumps, through which reagent solutions in a specified flow-rate are introduced in a mixer, the reagent mixtures then enters a temperature-adjustable-reactor, where the chemical reaction will occur for a specified duration and thereafter flow out in to a collecting vessel.

2.6.2. Sample analysis and quantitative NMR

Proton ^1H NMR spectra were recorded on a Bruker AC300 instrument with a carrier frequency of 300 MHz. The chemical shifts are given in part per million (ppm) on the delta scale. The solvent peak was used as a reference value in ^1H NMR, where $CDCl_3$= 7.24 ppm. The ^{19}F NMR spectra were recorded using a Bruker Avance 400 NMR spectrometer at 400.13 MHz.

The product yields in the crude samples were calculated using quantitative ^1H NMR methods, where 1,3,5-trimethoxybenzene was used as an internal standard.

List of publications

The results discussed in this thesis have been presented in the articles as listed below that have been published or submitted for publication in peer-reviewed journals.

1. **Lindokuhle C. Nene,** Muthumuni Managa, David O. Oluwole, Donovan M. Mafukidze, Azole Sindelo, and Tebello Nyokong. The Photo-physicochemical Properties and In Vitro Photodynamic Therapy Activity of Differently Substituted-Zinc (II)-Phthalocyanines and Graphene Quantum Dots Conjugates on MCF7 Breast Cancer Cell Line. *Inorganica Chimica*, **2019**, 488: 304-311.

2. **Lindokuhle C. Nene**, Muthumuni Managa and Tebello Nyokong. Photophysical properties and In Vitro Photodynamic Therapy Activity of Morpholine-Substituted Zinc(II)-Phthalocyanines π-π Stacked onto Biotinylated Graphene Quantum Dots. Submitted to: *Dyes and Pigments*.

Additional

3. David O. Oluwole, Njemuwa Nwaji, **Lindokuhle C. Nene**, Lesedi Mokone, Edith Dube and Tebello Nyokong. Novel nano-dyad of homoleptic sandwich-type phthalocyanines with nitrogen doped graphene quantum dots for nonlinear optics. *New Journal of Chemistry*, **2018**, 42: 10124-10133.

CHAPTER THREE

3. Synthesis and structural characterization

3.1. Phthalocyanines

The structural characteristics in terms of elemental composition, morphology and size of the new Pc complexes, GQDs, GQDs-biotin and the conjugates prepared are reported in this chapter. The values obtained are summarized in **Table 3.1**.

Table 3.1. UV-vis maximum absorbance and size estimations in DMSO, unless stated otherwise. References in square brackets.

Complex	Absorbance λ_{max} (nm) [a]	I_D/I_G ratio	DLS size (d.nm)	Loading (mmol (Pc)/ g (Pc-GQDs))	Ref
1	679	-	-	-	TW
2	678	-	-	-	[**142**]
3	691	-	-	-	[**143**]
4	685	-	-	-	[**160**]
5	683	-	-	-	TW
6	684	-	-	-	TW
7	682 (647)	-	-	-	TW
GQDs	365 (367)	0.08	7.5	-	[**126**]
1-GQDs	677	0.23	24.4	0.68	TW
2-GQDs	676	0.15	26.4	1.23	TW
3-GQDs	690	0.16	32.7	1.42	TW
4-GQDs	680	0.17	36.4	0.80	TW
5-GQDs	681	0.40	28.2	0.70	TW
6-GQDs	680	0.14	22.0	0.61	TW
7-GQDs	680 (647)	0.26	18.7	0.57	TW
GDQs-biotin	367 (372)	0.20	12.0	-	TW
6-GQDs-biotin	683	0.25	31.4	0.56	TW
7-GQDs-biotin	682 (646)	0.32	24.2	0.55	TW

[a] Values in round brackets are in water.

[b] TW, values reported in this work.

3.1.1. Neutral Pc complexes

The complexes used in this work were tetra-β-substituted Z(II)Pc. The synthesis and structural characterization of complexes, **2**, **3** and **4** have been reported [**142**,**143**,**160**]. This section reports on the synthesis and structural characterization of complexes **1** and **6**. The desired substituents were introduced on the phthalonitriles, prior to cyclization. A series of analytical techniques were employed to confirm the structures of the target complexes. The results obtained were in agreement with the expected results.

The metal free **H_2-1** was first synthesized through the cyclization of phthalonitrile **Pn 1** and thereafter metallated with Zn(II) (from the $Zn(OAc)_2$) to obtain complex **1** in the presence of DBU, using 1-pentanol as the solvent, **Scheme 3.1**.

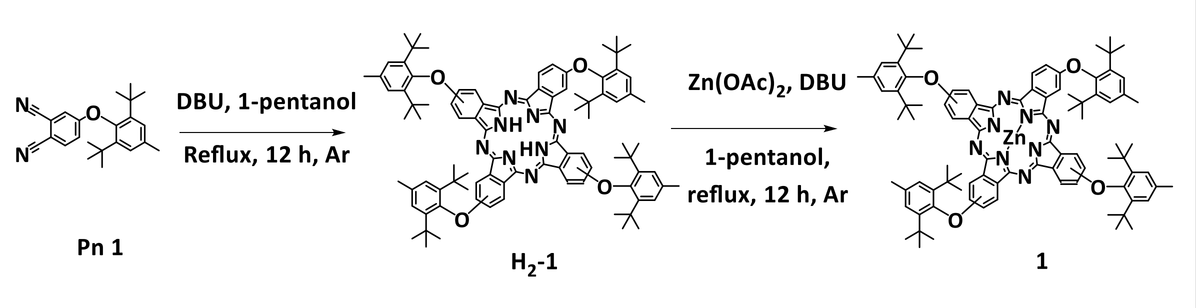

Scheme 3.1. Synthesis of complex **H_2-1** and subsequent metalation to form complex **1**.

The ^1H NMR integration for complex **H_2-1** showed the two central hydrogens at 0.09 ppm, a sum of 84 -CH_3 protons from the substituents and a sum of 20 aromatic protons from both the substituents and Pc ring. The total number of protons are the expected number of protons for complex **H_2-1**. The molecular weight of complex **H_2-1** was obtained using mass spectroscopy where the expected mass was 1386.83 m/z and the mass obtained was 1387.73 m/z. The CHN elemental analysis for complex **H_2-1** gave the expected values. These results confirmed the structure of complex **H_2-1**.

Complex **H_2-1** was metallated using Zn(II) to form complex **1**. The ^{1}H NMR integration for complex **1** showed the absence of the $-NH_2$ protons (from the centre of the Pc ring) and general reduction of the total number of protons by two was suggestive of successful metalation of **H_2-1**. A sum of 20 aromatic protons and 84 $-CH_3$ protons were obtained for complex **1**. The molecular weight for complex **1** was obtained using mass spectroscopy where the expected mass was 1451.28 m/z and the mass obtained was 1452.35 m/z. The CHN elemental analysis for complex **1** gave the expected. These results confirmed the structure of complex **1**.

The phthalonitrile **Pn 2** was prepared through a substitution reaction of the nitro- group on the 4-nitrophthalonitrile by the 2,5-dimethyl-4-(morpholino methyl) phenol, **Scheme 3.2**. Complex **6** was obtained by cyclization of phthalonitrile **Pn 2** with the Zn(II) metal inserted *in situ* in the presence of DBU, using 1-pentanol as the solvent.

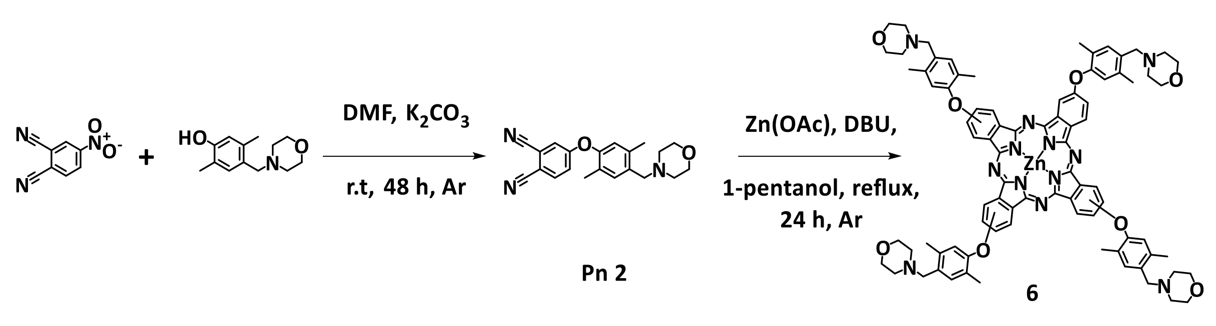

Scheme 3.2. Synthesis of phthalonitrile **Pn 2** and complex **6**.

The ^{1}H NMR integration for complex **6** gave a sum of 20 aromatic protons, 40 $-CH_2$ protons and 24 $-CH_3$ protons confirm complex **6**. The molecular weight for complex **6** was obtained using mass spectroscopy where the expected mass was 1455.02 m/z and the mass obtained was 1455.02 m/z. The CHN elemental analysis for complex **6** gave the expected values. These results confirmed the structure and purity of complex **6**.

The structural compositions of the newly synthesized complexes **1** and **6** along with their corresponding phthalonitriles were further characterized by FT-IR spectroscopy detailing the functional groups comprising the structures, **Fig. 3.1**.

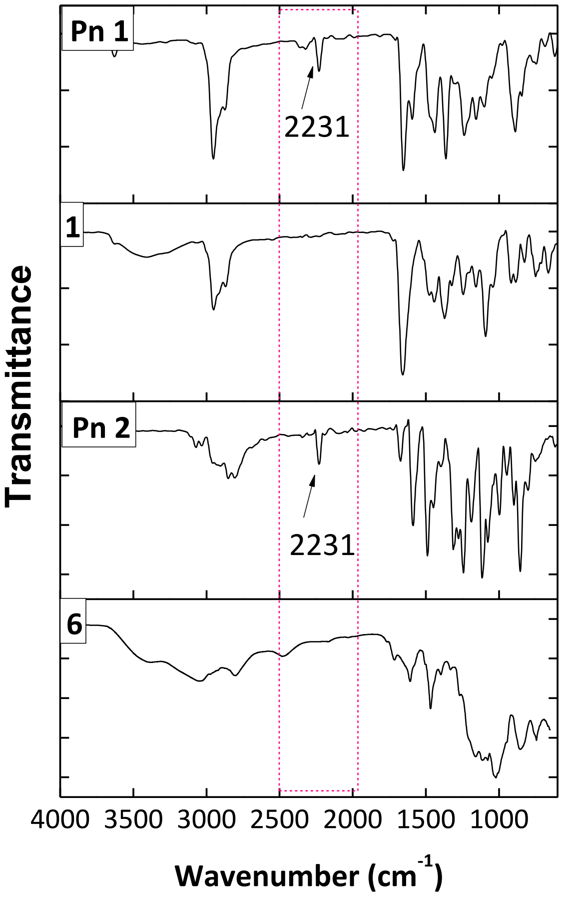

Figure 3.1. FT-IR spectra of the phthalonitriles **Pn 1** and **Pn 2** and the Pc complexes **1** and **6**.

The FT-IR spectra of the phthalonitriles show the presence of the nitrile peaks at shift ~2231 cm^{-1}, as seen for **Pn 1** and **Pn 2**, **Fig. 3.1**. The nitrile peaks disappear upon formation of the complexes since new bonds are formed during cyclo-condensation of the phthalonitriles, as seen for complexes **1** and **6**.

The process of the Zn(II) metal insertion in the core of the **H_2-1** to obtain complex **1** was monitored using UV-vis absorption spectroscopy at λ>600 nm, **Fig. 3.2**.

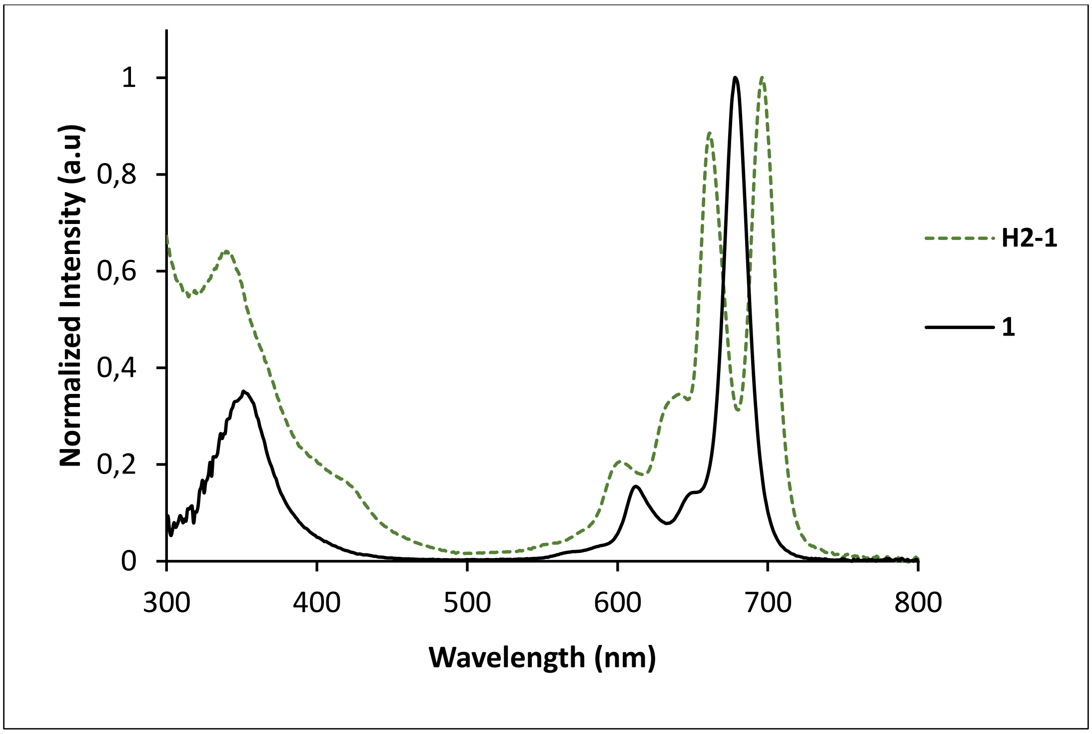

Figure 3.2. The UV-vis absorption spectrum of the metal free complex **H_2-1** and the metallated complex **1** in chloroform. Concentration: complex **H_2-1** mM and **1** at 1.55 x 10^{-5} M.

MPc characteristically show a single Q-band, unlike metal free complex which have a split Q-band, in the near-infrared region of the UV-vis spectrum, **Fig. 3.2**. The split Q-band of the **H_2-1** occur at wavelengths 659 nm and 697 nm in DMSO. Upon metalation, a single Q-band is observed at 679 nm. The UV-vis absorption spectrum of complex **1** is typical of MPc, a similar trend was observed for the MPc reported in this thesis. The Q-band wavelengths (λ_{max}) for the complexes are reported in **Table 3.1** and are compared to the reported complexes **2**-**4** [**142,143,160**].

Complex **3** has a relatively high λ_{max} of 691 nm, followed by complexes **4** and **6**. This may due to the heavy atomic effect by the presence of N, O and S in the structures [**76**-**78,161**]. The λ_{max} is relatively lower for complexes **1** and **2**, with λ_{max} of 679 nm and 678 nm respectively.

3.1.2. Cationic Pc complexes

This section discusses the synthesis and structural characterization of the cationic complexes **5** and **7** obtained from the formation of quaternary amines on the substituents from complex **4** and **6**, respectively, using DMS, **Scheme 3.3** and **Scheme 3.4**.

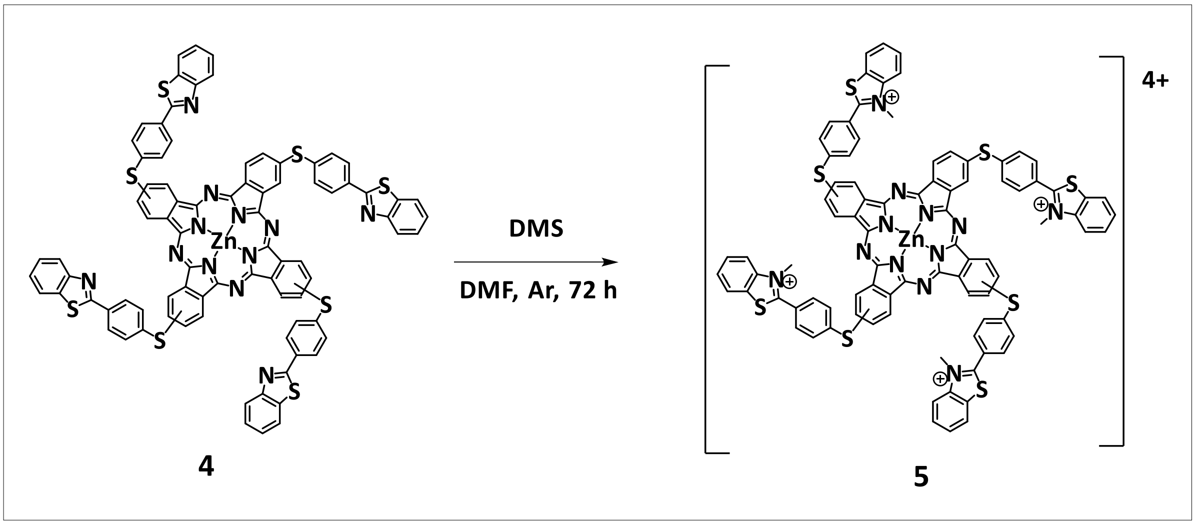

Scheme 3.3. Synthesis of cationic complex **5** through quaternization of complex **4** using DMS in DMF for 72 h.

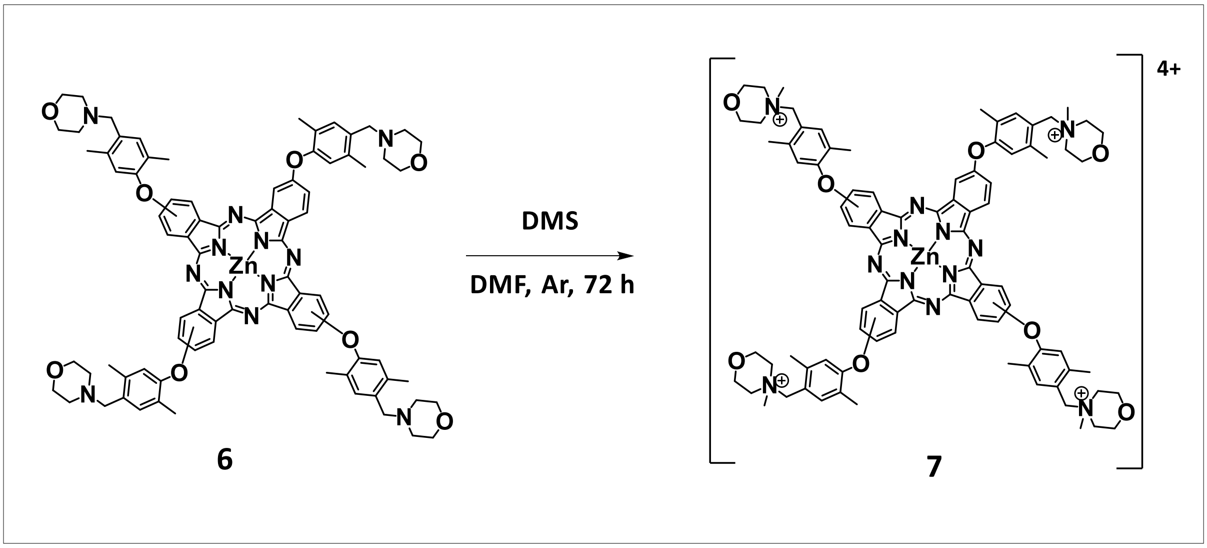

Scheme 3.4. Synthesis of cationic complex **7** through quaternization of complex **6** using DMS in DMF for 72 h.

The ^1H NMR for complex **5** in comparison to the corresponding complex **4** gave a sum of 44 aromatic protons and 12 -CH_3. The presence of aliphatic protons at ~4.03 ppm indicates the introduction of the methyl groups forming quaternary amines since the corresponding complex **4** only comprises of aromatic protons, **Scheme 3.3**. The CHNS elemental analysis for complex **5** gave the expected values. The results obtained confirmed the structure and purity of complex **5**.

The ^1H NMR integration for complex **7** gave a sum of 20 aromatic protons, 40 -CH_2 protons and 36 -CH_3 protons. The sum of the protons obtained corresponds to the sum of the protons calculated from the structure of the complex. The CHN elemental analysis for complex **7** gave the expected values. The agreement of the expected values and the obtained values confirmed the structure and purity of the complex **7**.

The increase in the sum of protons by 12 protons for both complexes **5** and **7** compared to the corresponding complexes **4** and **6**, respectively, indicates the quaternization of all 4 nitrogen atoms at the substituents of each of the complexes (introducing 3 protons on each nitrogen atom). The mass spectra of the cationic complexes **5** and **7** could not be obtained due to the inability of the complexes to ionize. The FT-IR of complex **5** and **7** were similar to the corresponding complexes **4** and **6**, due to similar functional groups of Pc backbone, C=N, C=C, C-H.

The UV-vis spectra of the cationic quaternized complexes were obtained and compared to the non-quaternized parent complexes. Furthermore, the UV-vis spectra of the quaternized complexes in water were obtained and compared to the UV-vis spectra in DMSO. The UV-vis spectra of complexes **4** and **5** are shown in **Fig. 3.3** and complexes **6** and **7** are shown in **Fig. 3.4**.

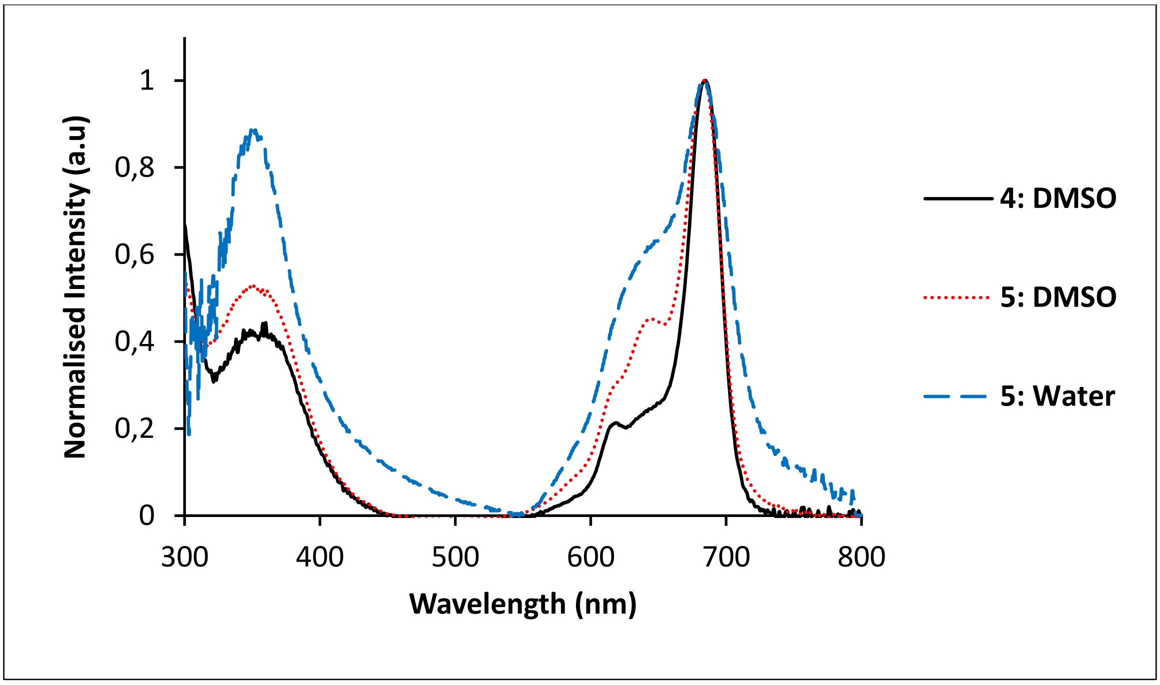

Figure 3.3. UV-vis absorption spectrum of Complex **4** in DMSO and **5** in DMSO and water. Concentration: complex **4** 1.9 x 10^{-5} M at in DMSO and complex **5** at 3.9 x 10^{-5} M in DMSO.

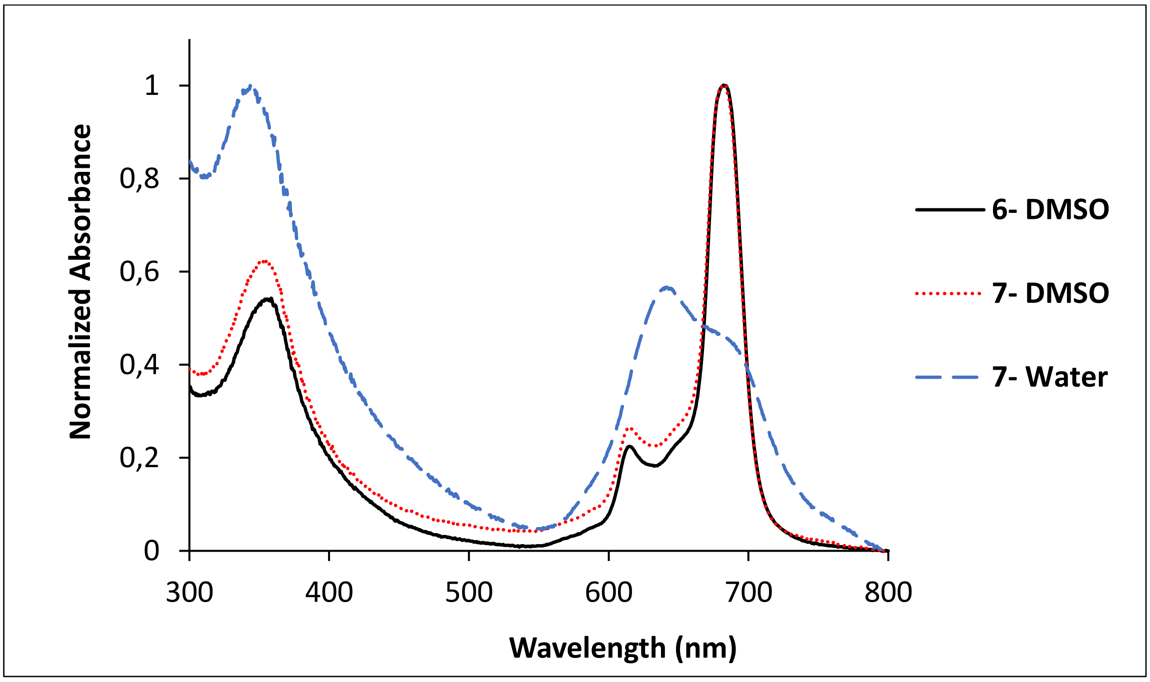

Figure 3.4. UV-vis absorption spectrum of Complex **6** in DMSO and **7** in DMSO and water. Concentrations: complex **6** at 1.35 x 10^{-5} M and complex **7** at 5.5 x 10^{-5} M in DMSO.

The UV-vis absorption spectrum of the cationic complex **5** shows aggregation in DMSO, when compared to the spectrum of complex **4** in DMSO **Fig. 3.3**. Aggregation in water for complex

5 increases compared to DMSO. Aggregation is typical of Pc in aqueous media [**162**]. Aggregation in Pc is judged by the presence of broad or split Q bands, with the low energy band being due to the aggregate and the high energy band due to the monomer [**162**]. In the case of the complex **7**, the spectrum in DMSO is similar to the spectrum of complex **6** with little evidence of aggregation, as seen with a defined Q-band, **Fig. 3.4**. In water, both complexes **5** and **7** are aggregated.

The Lambert – Beer law was observed in DMSO for complexes, showing monomeric behaviour [**163**], complex **7** is shown as an example in **Fig. 3.5**.

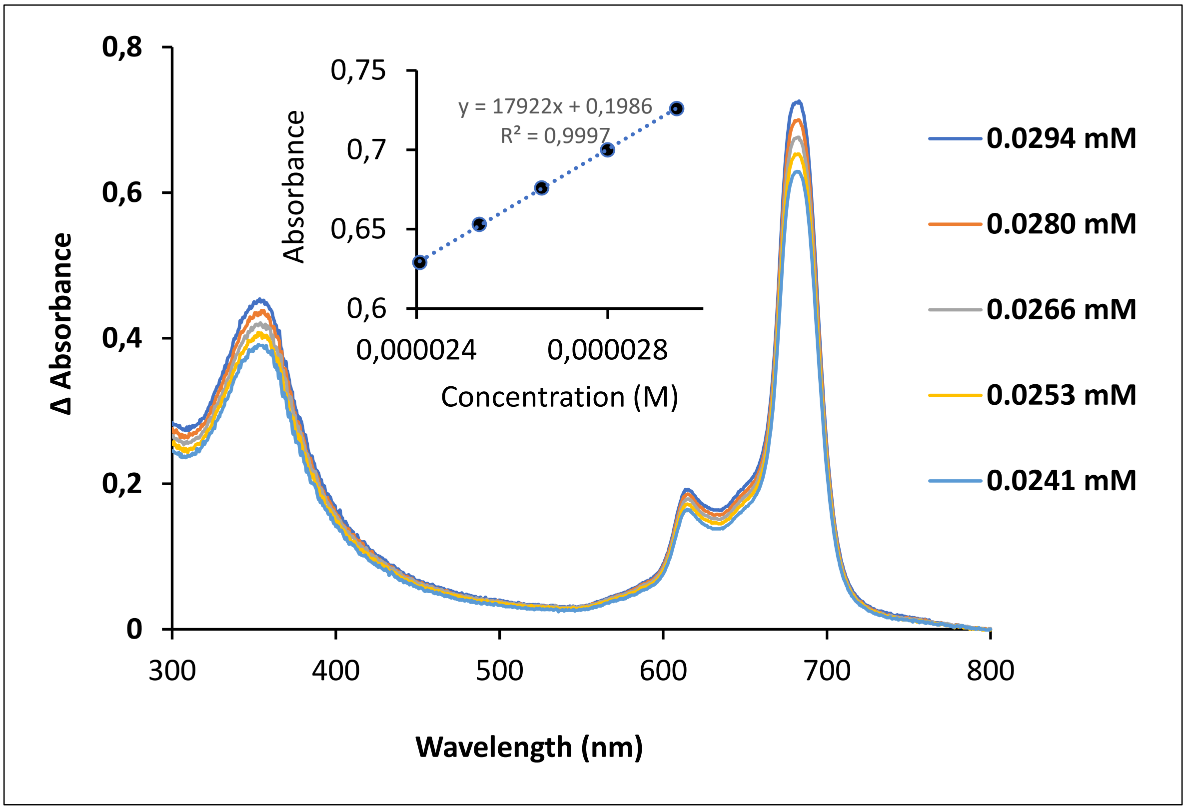

Figure 3.5. Molar absorptivity of complex **7** in DMSO. *Insert*: Concentration vs Δ absorbance graph for complex **7**.

The λ_{max} for the complexes are listed in **Table 3.1**. Upon quaternization, the Q-band of the complexes slightly blue-shifts in DMSO, and more in water. The λ_{max} for complex **4** occurs at

685 nm, where the λ_{max} for complex **5** blue shifts to 683 nm. Similarly, for complex **6**, with an λ_{max} at 684 nm, the λ_{max} blue shifts to 682 nm for complex **7**. The blue shifts for complexes **5** and **7** are due to the lowering of the electron donating ability of the quaternary nitrogen groups [**164**].

The solubility of complexes **5** and **7** in water, unlike complexes **4** and **6**, was one way to monitor the introduction of cationic charges by quaternary amines on the structures. The water-soluble complex **7** and non-water soluble complex **6** are shown on **Fig. 3.6**.

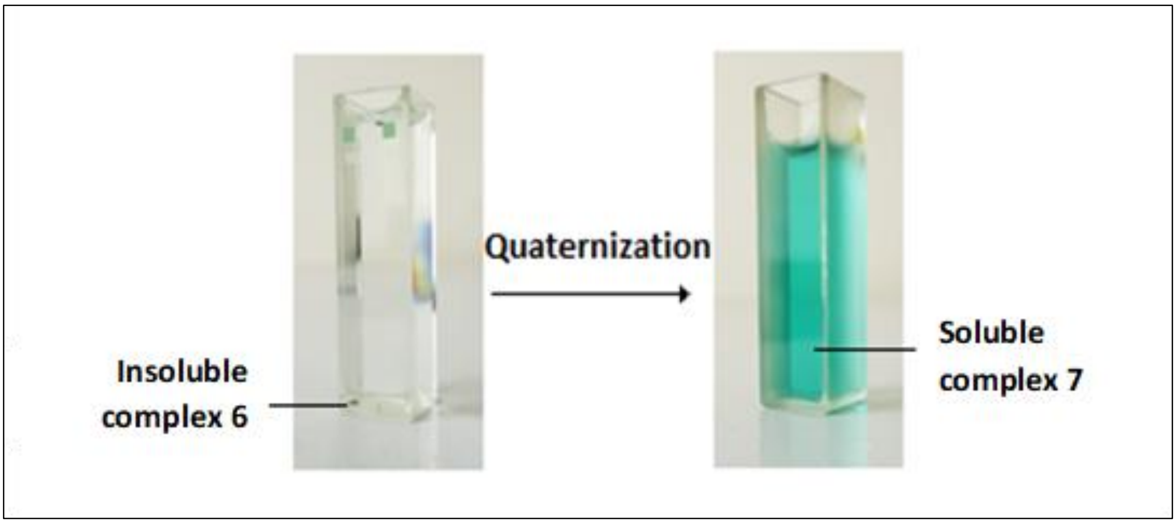

Figure 3.6. Image of complex **6** and the cationic complex **7** in water.

3.2. Biotin-functionalized GQDs

Biotinylation on the edges of the GQDs was achieved through the formation of covalent amide bonds to form GQDs-biotin in the presence of DCC and DMAP, **Scheme 3.5**.

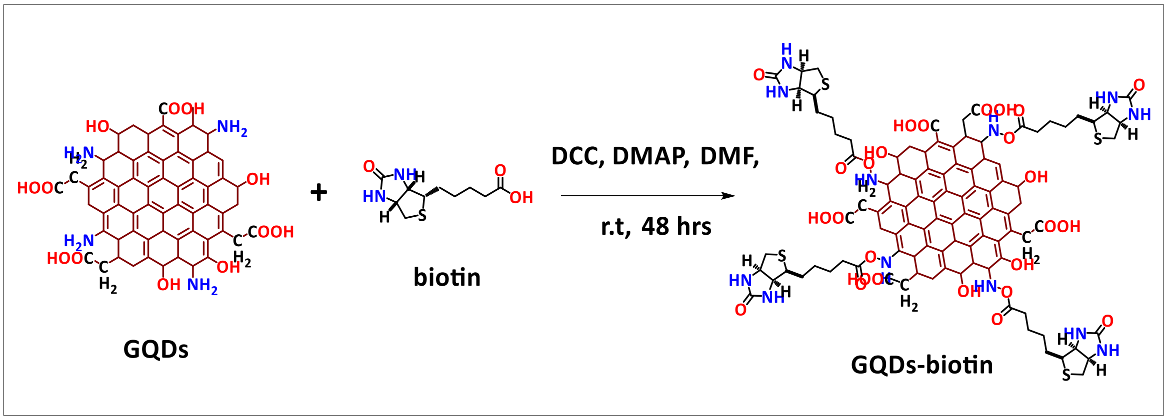

Scheme 3.5. Biotinylation of GQDs to form GQDs-biotin.

To evaluate the chemical composition of the biotin-functionalized GQDs, the FT-IR spectra were obtained for the pristine GQDs, biotin and the GQDs-biotin conjugates, **Fig. 3.7**.

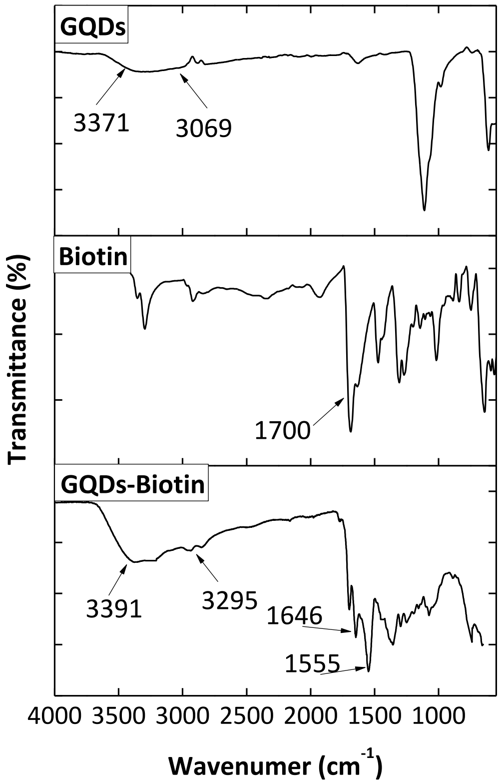

Figure 3.7. The FT-IR spectra of pristine GQDs, biotin and GQDs-biotin.

The covalent linkage of biotin to GQDs was confirmed by the presence of amide bonds. The amide functional group in the GQDs-biotin was shown by the presence of the NH stretches at 3391 cm-^{1} and 1646 cm-^{1}, the C=O stretch at 1555 cm-^{1} and C-H stretch at 3295 cm-^{1} which are characteristic to an amide group combined. A strong C=O stretch at 1700-1668 cm-^{1} is seen in the biotin spectrum, this may be for both the carboxylic end and the carbonyl in the ring of the structure.

Furthermore, EDX spectroscopy was used to determine the elemental composition of the GQDs in comparison to the GQDs-biotin, **Fig. 3.8**.

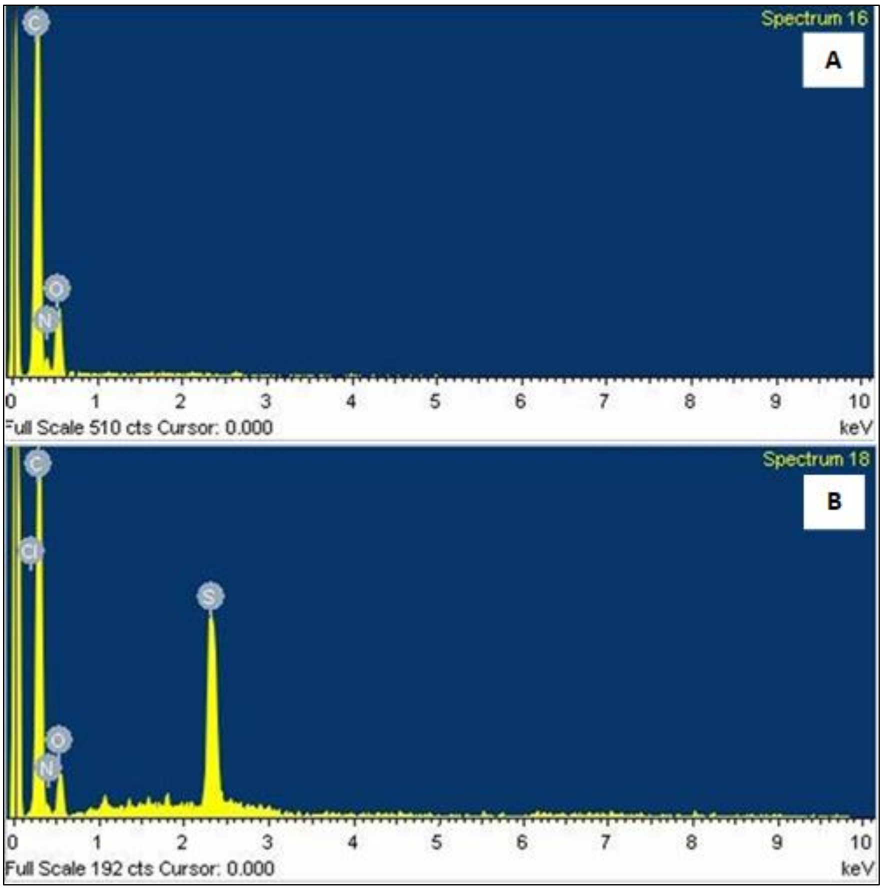

Figure 3.8. The EDX spectra showing the chemical composition of **A**) GQDs and **B**) GQDs-biotin.

The main elements present in both the structures include C at 0.2 keV, N at 0.4 keV and O at 0.6 keV, where the biotin in the GQDs-biotin affords S at 2.3 keV on the structure as shown in **Fig. 3.8**, and absent in the GQDs, **Fig. 3.8A**.

The UV-vis absorption spectra of the GQDs and GQDs-biotin were obtained, **Fig 3.9**.

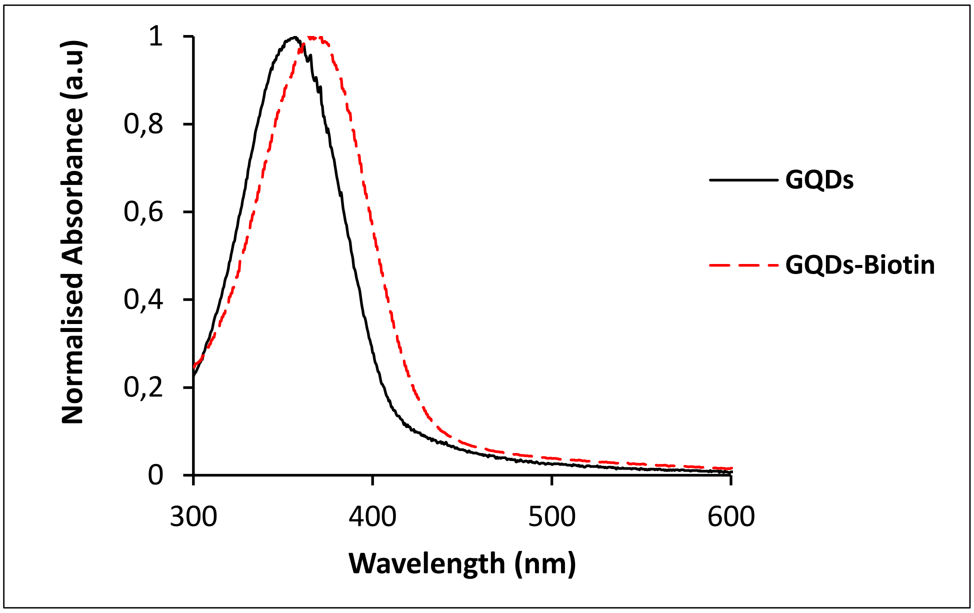

Figure 3.9. The UV-vis absorption spectrum of GQDs and GQDs-biotin in water.

The GQDs absorb in the blue-region, with λ_{max} at 367 nm in water **Fig. 3.9**. The absorbance red-shifts when linked to biotin, with λ_{max} at 372 nm in water. The additional N groups introduced to the GQDs structure from the biotin may hold the same effect as does N groups in N-doped GQDs, which causes the absorption and emission of GQDs to red-shift [**165**]. In DMSO, the λ_{max} is 365 nm for GQDs and 367 nm for GQDs-biotin, **Table 3.1**.

3.3. Conjugation of Pc complexes to GQDs and GQDs-biotin

3.3.1. Syntheses

The Pc complexes were conjugated to GQDs and/ or GQDs-biotin through π-π interactions. Complexes **1-5** were conjugated to the GQDs, and complexes **6** and **7** were conjugated to both the GQDs and GQDs-biotin, **Scheme 3.6**. The conjugates were structurally characterized using various analytical techniques.

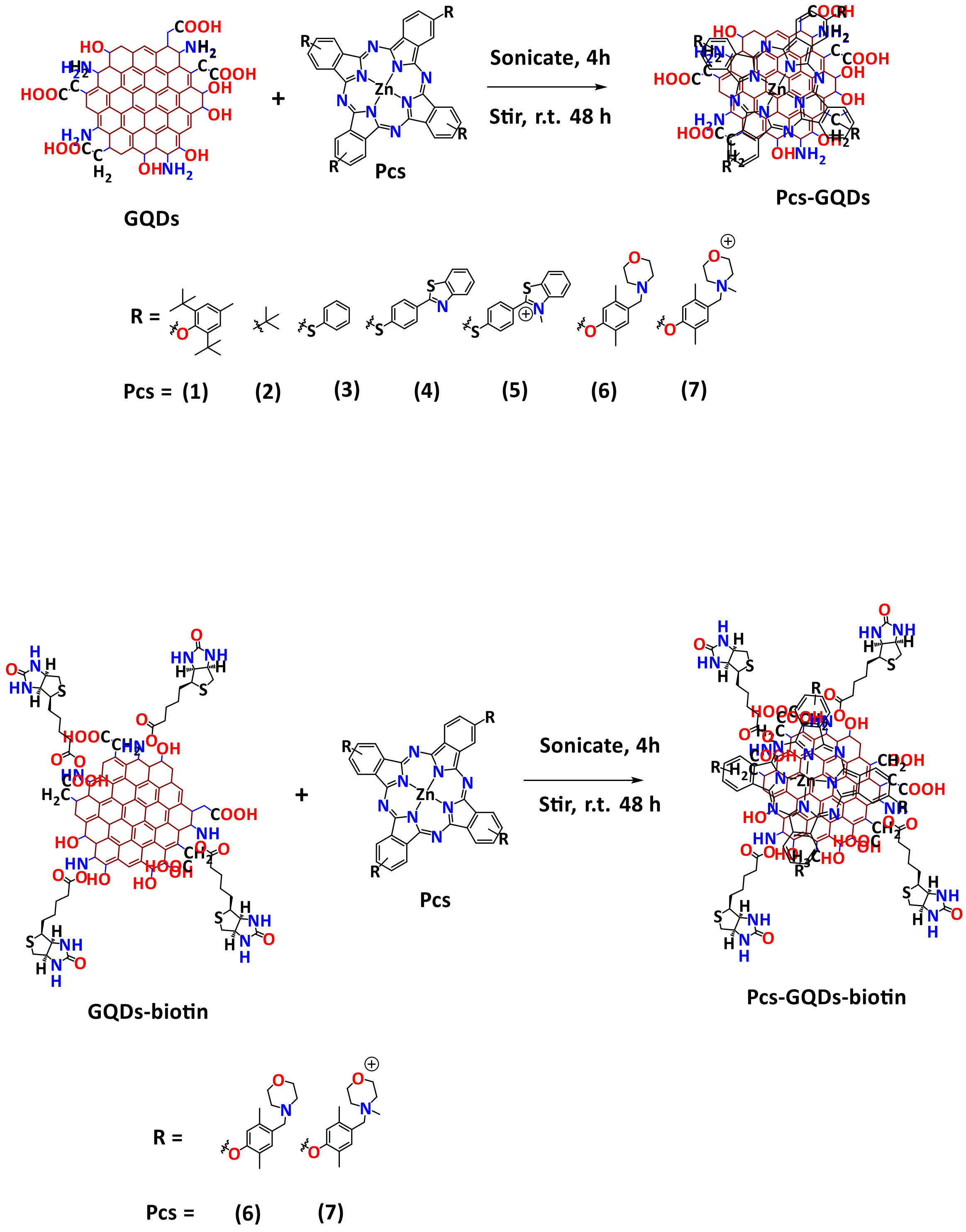

Scheme 3.6. The π-π conjugation of the complexes on to GQDs and or GQDs-biotin.

3.3.2. TEM imaging and DLS

The TEM images of the pristine GQDs/ GQDs-biotin and the conjugates were obtained to evaluate the shape, size distribution and an estimation of the particle sizes. The average sizes were further estimated using DLS (alongside the corresponding TEM images), **Fig. 3.10**.

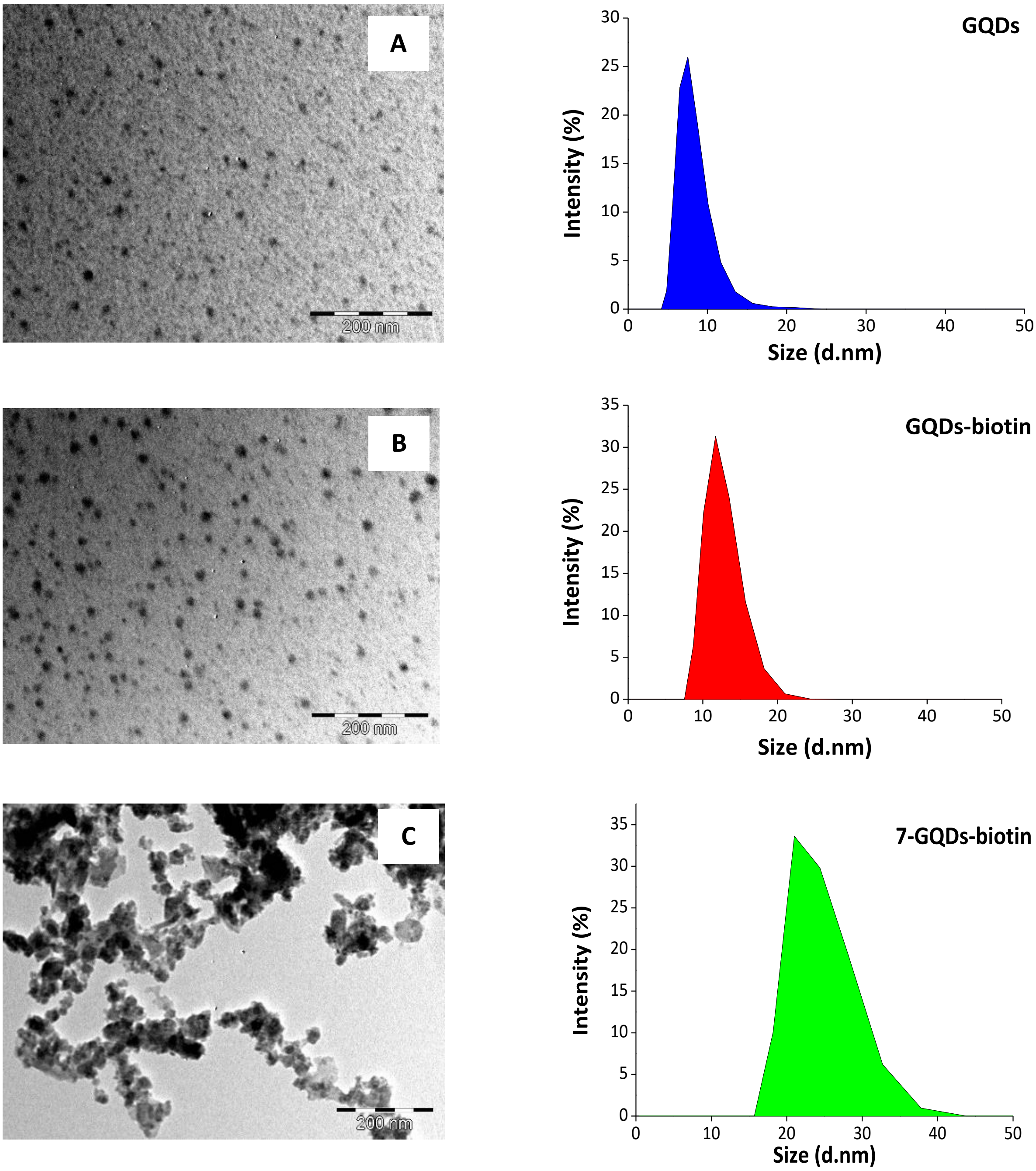

Figure 3.10. The TEM images of **A**) GQDs in ethanol, **B**) GQDs-biotin in methanol and **C**) **7**-GQDs-biotin in ethanol with their respective DLS graphs showing the average dimeter sizes in water.

The solvents were selected based on solubility for sample preparation for both TEM imaging and DLS. The GQDs are circular in shape and are monodispersed as shown in **Fig. 3.10A** and **Fig. 3.10B**. The conjugates (**7**-GQDs-biotin), **Fig. 3.10C,** appear aggregated compared to the pristine and GQDs-biotin. This is likely to be due to interactions between the Pc complexes on adjacent GQDs via π-π stacking since Pc are known for their π-π stacking to form H aggregates [**162**], and size estimation is therefore difficult to ascertain from the TEM images.

The DLS plots were obtained to determine the average particle sizes of the GQDs and GQDs-biotin complexes **Fig. 3.10**. The average diameter for GQDs obtained was 7.5 nm and approximately 12 nm for GQDs-biotin as shown in **Fig 3.10A** and **B**. The average size for the **7**-GQDs-biotin obtained was 24.2 nm. An increase in the size of the GQDs-conjugates as compared to the pristine GQDs observed is due to the stacking of Pc onto the surface of the GQDs. This is observed for all conjugates in **Table 3.1**.

3.3.3. Pc complex loading on GQDs

The Pc loading onto the surface of GQDs was determined using a quantitative method as described previously [**166**]. This involves comparing the spectra of the Pc complexes before and after conjugating to GQDs or GQDs-biotin. The Pc loading on GQDs, (mmol (Pc)/g (Pc-GQDs)), values are summarized in **Table 3.1**

The UV-vis spectra for determination of the Pc loading is shown in **Fig. 3.11**, using complex **7** and **7**-GQDs as an example.

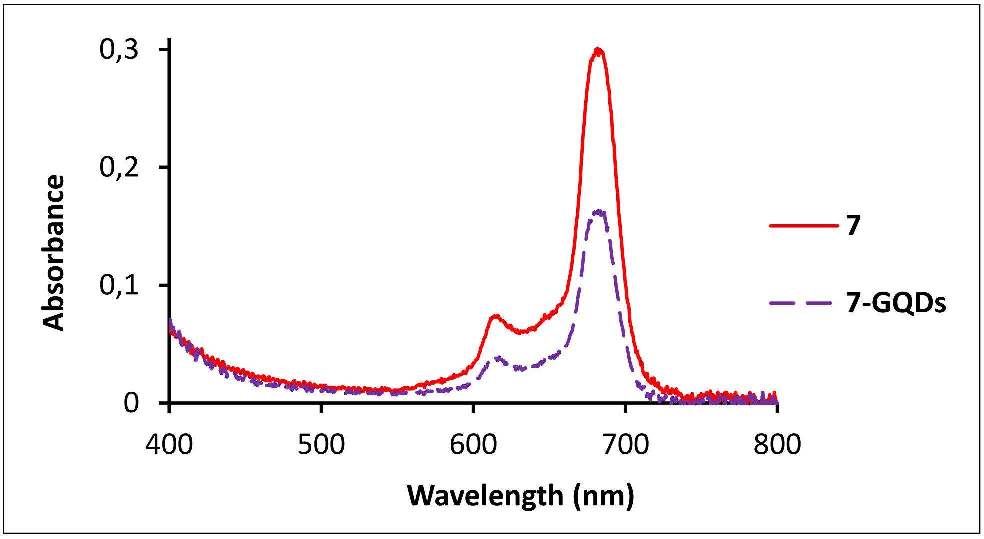

Figure 3.11. UV-vis spectra of complex **7** and **7**-GQDs in DMSO. Concentrations: complex **7** at 1.69 x 10^{-5} M and **7**-GQDs at 9 x 10^{-6} M in DMSO.

The absorbance intensity of the Pc is relatively higher for complex **7** and lower in the conjugates, **7**-GQDs since the mass of the sample is the sum of the Pc and GQDs, **Fig. 3.11**. The loading for complexes **1** and **4**-**7** were generally relatively lower compared to complexes **2** and **3**. This may be due to the bulky substituents covering a larger surface and therefore reducing the loading of the complexes. The loading for complex **2** is however lower compared to complex **3**, the *tert*-butyl substituents' geometric arrangement may also reduce loading through steric hindrance. The loading for the cationic complexes, **5** and **7**, is lower in comparison to the corresponding non-ionic complexes, **4** and **6**, **Table 3.1**. Although the cationic complexes are attracted to the surface of the GQDs by electrostatic attraction, the cations may reduce stacking of Pc on each other through like-charge repulsion, hence the decrease in Pc loading on GQDs upon introduction of cations. The Pc loading further decreases when conjugated on GQDs-biotin, as seen for the conjugates **6**-GQDs-biotin and **7**-GQDs-biotin, compared to **6**-GQDs and **7**-GQDs, respectively. The presence of biotin on the edges of the GQDs may introduce steric hindrances, hence reduced Pc loading compared to non-functionalized GQDs. However, the decrease in the loading of the Pc is relatively low.

3.3.4. Raman spectroscopy

Raman spectroscopy was used to evaluate the quality of the GQDs **Fig. 3.12**. The GQDs are known to display characteristic Raman peaks termed the G-Band (sp^2) tangential mode and the D-(disorder) band (sp^3) breathing mode, **Fig. 3.12**. The G-band is a representation of in-plane vibrations of sp^2 bonded carbon atoms, whereas the D band is due to the out of plane vibrations attributed to the presences of structural defects [**167**]. The D-bands are observed at 1200 cm^{-1} for GQDs, at 1240 cm^{-1} for GQDs-biotin and at 1271 cm^{-1} for **6**-GQDs-biotin, whereas the G bands are observed at 1506 cm^{-1} for GQDs and 1537 cm^{-1} for GQDs-biotin and at 1579 cm^{-1} for the **6**-GQDs-biotin, **Fig. 3.12**. Shifts in the Raman frequencies are often indicative of strong π-electron interactions in hybrid materials [**168**].

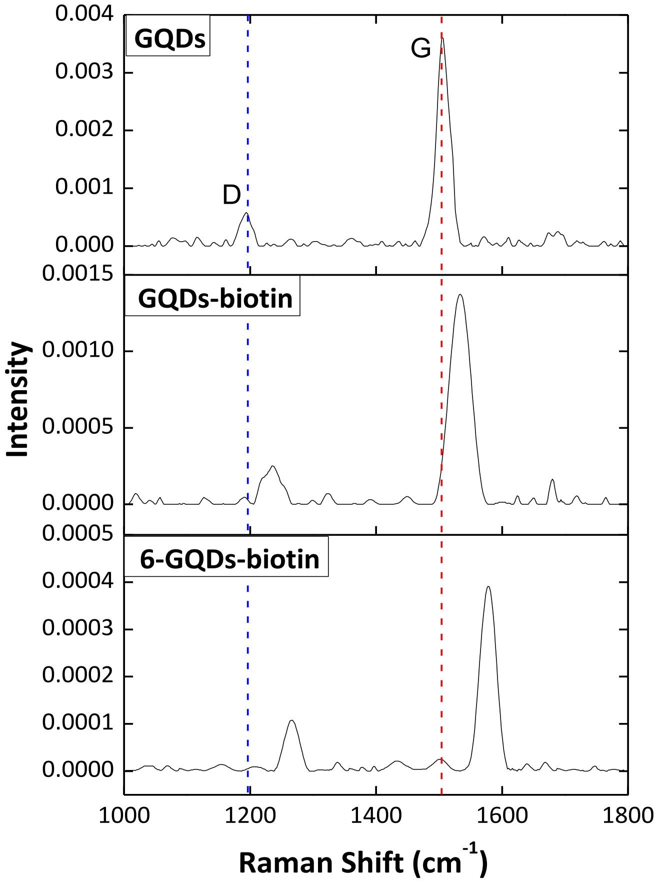

Figure 3.12. The Raman spectra of GQDs, GQDs-biotin and **6**-GQDs-biotin.

The ratio of the D and G intensities, denoted I_D/I_G, is generally considered as a quality parameter to determine the extent of functionalization of the carbon nanomaterials. The I_D/I_G obtained for GQDs is 0.08, **Table 3.1**. The value increases upon the covalent conjugation to biotin, GQDs-biotin. This is due to the introduction of defects. The I_D/I_G is increases upon π-π conjugation to the Pc, where the cationic complexes have higher I_D/I_G ratios compared to the non-ionic conjugates. This is due to additional electrostatic interaction. The I_D/I_G also increases for complexes conjugated to GQDs-biotin, since biotin introduces out of plane functional groups and therefore increasing the D-Band.

3.3.5. UV-vis spectroscopy

The UV-vis absorption spectra of the complexes and their GQDs and GQDs-biotin conjugates were obtained and compared. The UV-vis spectra of complex **7** and the respective conjugates are shown in **Fig. 3.13** as an example.

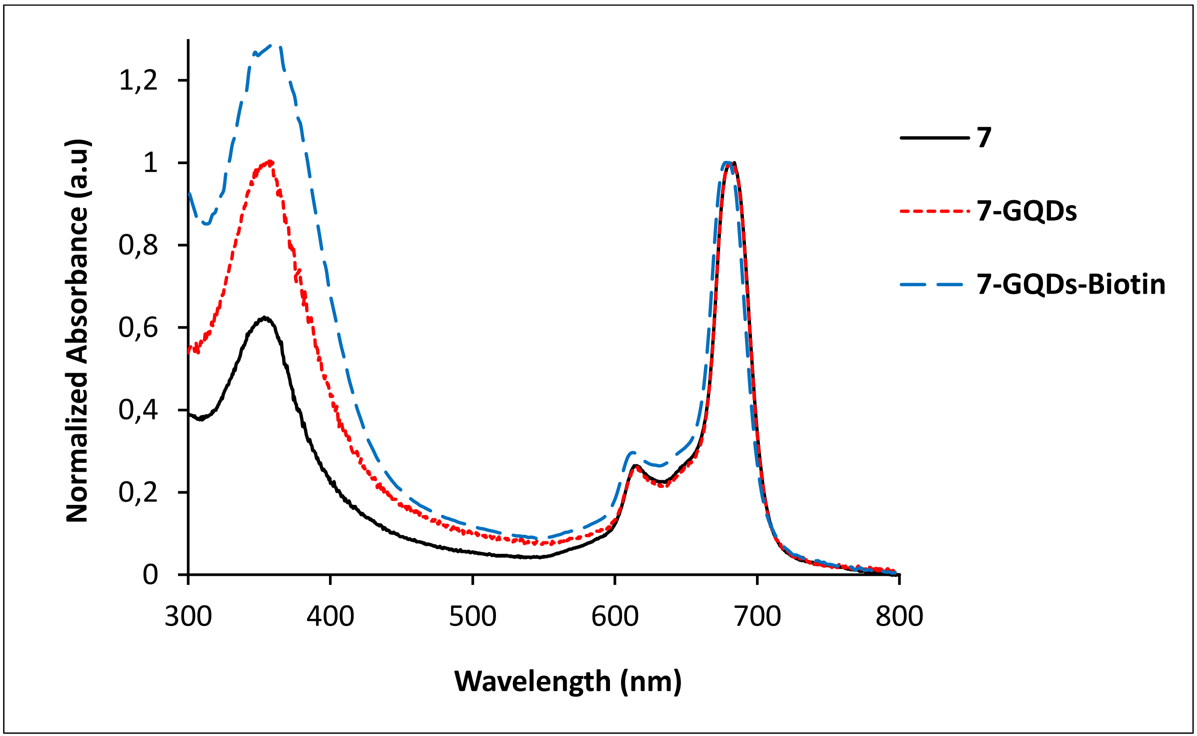

Figure 3.13. The UV-vis absorption spectra of **7** and **7**-GQDs and **7**-GQDs-biotin in DMSO. Concentrations: complex **7** at 5.5 x 10^{-5} M in DMSO.

The Q-band of complex **7** is slightly blue shifted in the presence of GQDs **Fig. 3.13**, but there was no difference in the presence of biotin in GQDs-biotin observed, **Table 1**. The blue shifting of the Q band in the presence of semiconductor QDs has been reported to be dependent on the functionalities on the surface of the QDs [**169**]. The B-band, between 300 nm and 400 nm increases upon conjugation. This is the sum of the absorbance intensities of the GQDs and complex **7** in the conjugates since the GQDs also absorb in the blue-region, with λ_{max} at 365 nm in DMSO, **Fig. 3.9**. This was observed for all the conjugates, however, the increase in the absorbance intensity between 300 nm and 400 nm differed for the complexes, this may be the result of amount of the complex loading on the GQDs/ GQDs-biotin.

3.4. Conclusion of chapter

The synthesis and structural characterization of the novel Pc complexes, GQDs-biotin and Pc-GQDs/ Pc-GQDs-biotin conjugates were presented. The results obtained in ascertaining the structural composition of the complexes were in aggreement with the expected results. Therefore, the structures and purity of the newly synthesized complexes were confirmed.

The λ_{max} of GQDs red-shifts upon conjugation to biotin in GQDs-biotin. Where the λ_{max} of all the complexes blue shifts slightly upon conjugation to GQDs. The quality of the Pc-GQDs conjugates was studied using Raman spectroscopy, where the I_D/I_G ratios represent the degree of structural defects introduced on the GQDs surface upon conjugation. As expected, the I_D/I_G ratio increases for GQDs upon conjugation to biotin in GQDs-biotin due to introduction of out-of-plane functional groups from the biotin. The I_D/I_G ratio also increases upon conjugation to Pc complexes. The number of moles of Pc complexes loaded on the surface of the GQDs/ GQDs-biotin differ dependig on the nature, size and geometry of the substituents. Bulkier substituents showed relatively lower Pc loading values (complex **1** and **4-7**). Where less bulky substituents had relatively higher loading values (complex **2** and **3**). The loading values decrease upon introduction of cations on the substituents, this may be due to like-charge repulsion, which may reduced Pc loading. Loading further decreases for Pc complexes loaded on GQDs-biotin compared to the corresponding Pc-GQDs conjugates. The additional biotin groups on the GQDs may introduce stearic hindrance, and therefore reduce loading.

The morphology of the GQDs and GQDs-biotin appeared monodispersed, and clustered upon conjugation to Pc complexes.

CHAPTER FOUR

4. Photo-physicochemical characterization

4.1. Photophysical properties

The photophysical parameters of the Pc complexes and conjugates including the fluorescence (Φ_F) and triplet (Φ_T) quantum yields were determined for the new complexes and conjugates prepared in this work, **Table 4.1**. Some of the parameters have been reported for the complex **2** [**142**], complex **3** [**143**], complex **4** [**160**] and GQDs [**126**].

4.1.1. Absorption, emission and excitation parameters

The absorption, excitation and emission spectra of complex **6** are shown in **Fig. 4.1** as an example.

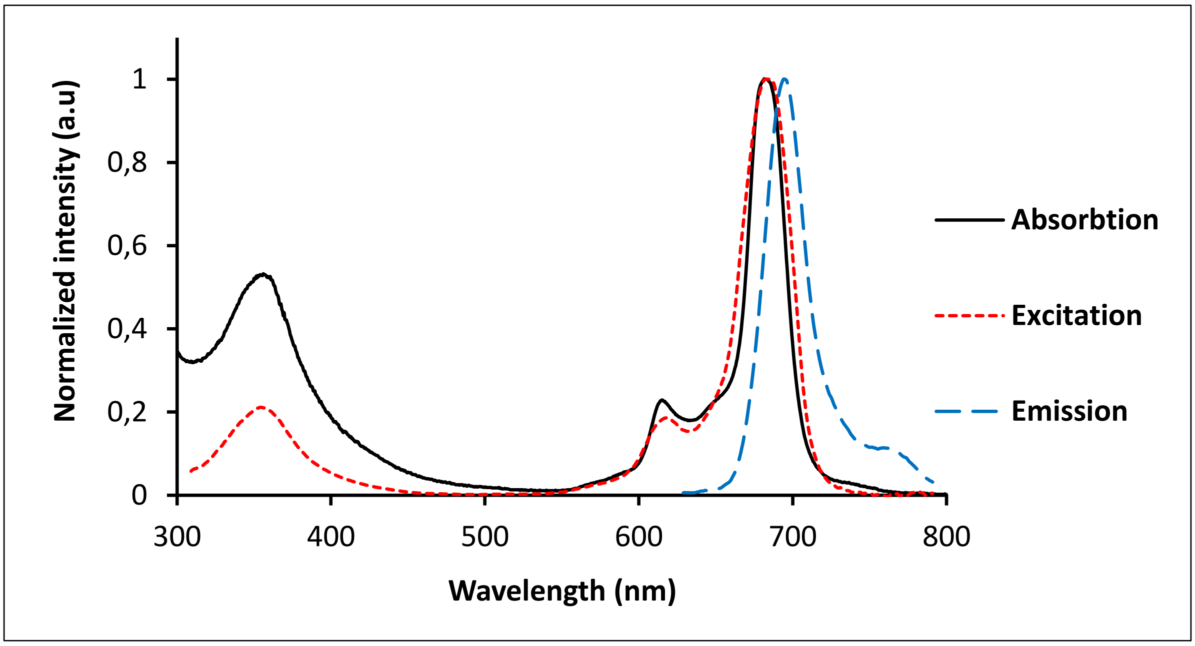

Figure 4.1. The UV-vis absorption, upon excitation at 610 nm and emission spectra complex **6** in DMSO. At excitation wavelength λ_{exc} is 610 nm. Concentrations: 1.35 x 10^{-5} M.

The absorption spectra of the complexes were similar to the excitation spectra and mirror images to their emission spectra, similar to the illustration shown in **Fig. 4.1** for complex **6**. This means that the absorbing molecules are the same as the emitting molecules [**169**].

Table 4.1. The photo-physicochemical parameters of the complexes and conjugates studied in DMSO unless stated otherwise. References in square brackets.

Complex	**Φ_F [a] ± 0.01**	**τ_F (ns) [a] ± 0.01**	**Φ_T ± 0.01**	**τ_T (µs) ± 0.01**	**Φ_Δ ± 0.01**
1	0.16	2.94	0.78	353	0.50
2	0.18 [**142**]	3.2[**142**]	0.77	214	0.49
3	0.14 [**143**]	2.46	0.65 [**143**]	149 [**143**]	0.50
4	0.18 [**160**]	2.73 [**160**]	0.67 [**160**]	148[**160**]	0.54
5	0.10	2.65	0.75	217	0.35 0.19 [b]
6	0.20	2.93	0.68	238	0.67
7	0.20 0.13	2.89 2.88	0.69 -	269 -	0.53 0.11 [b]
GQDs	(0.17) [**126**] (0.20) [b]	(3.65) (4.80) [b]	- -	- -	- -
1-GQDs	0.15 (0.05)	2.86	0.81	367	0.44
2-GQDs	0.17 (0.06)	3.04	0.83	223	0.40
3-GQDs	0.01 (0.09)	2.15	0.67	189	0.45
4-GQDs	0.11 (0.04)	2.59	0.70	159	0.50
5-GQDs	0.09 (0.04)	2.67	0.77	223	0.30 0.10 [b]
6-GQDs	0.15 (0.1)	2.95	0.72	234	0.60
7-GQDs	0.14 (0.07) 0.10 (0.08) [b]	2.92 2.34 [b]	0.74 -	267 -	0.58 0.08 [b]
GDQs-biotin	(0.24) (0.25) [b]	(3.92) (3.98) [b]	- -	- -	- -
6-GQDs-biotin	0.16 (0.09)	2.21	0.72	274	0.47
7-GQDs-biotin	0.14 (0.05) 0.12 (0.08) [b]	2.36 2.2 [b]	0.70 -	274 -	0.54 0.08 [b]

[a] Values in round brackets are where GQDs absorb.

[b] Values in water.

The emission spectra of the GQDs in water and DMSO were compared to **Fig. 4.2**.

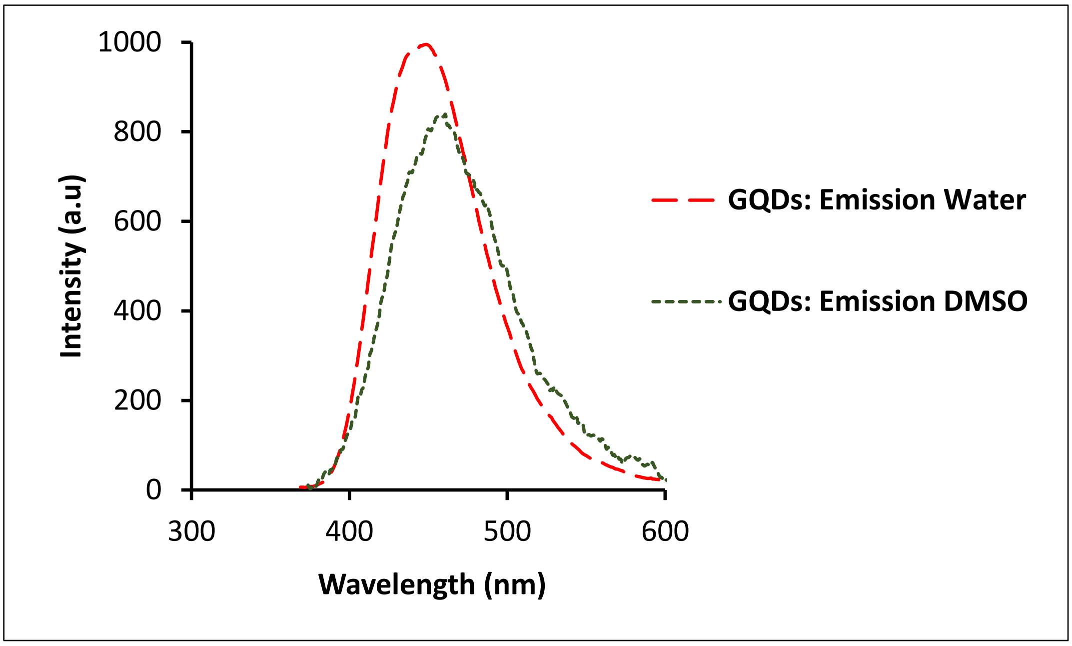

Figure 4.2. The UV-vis emission spectra of GQDs in DMSO and water where λ_{exc}: 355 nm.

The emission intensity of the GQDs is slightly reduced in DMSO in comparison to the emission intensity in water at same concentration and is also red-shifted from 453 nm in DMSO to 462 nm in water, **Fig. 4.2**. The emission spectra are similar for the GQDs and GQDs-biotin since they absorb close to each other and they both have a broad absorbance.

4.1.2. Fluorescence quantum yields and lifetimes

The fluorescence quantum yields (Φ_F) were determined for the Pc complexes, GQDs, GQDs-biotin and GQDs and/ or GQDs-biotin conjugates. The Φ_F of the complexes change upon structural modifications, including quaternization, conjugation to GQDs and GQDs-biotin. The Φ_F are reported in **Table 4.1**.

The Φ_F of complex **5** is lower compared to the corresponding complex **4** in DMSO, this may be due to the additional methyl groups upon quaternization to the heavy S and N atom, causing the heavy atomic effect enhancing ISC to the triplet state and consequently decreasing the

Φ_F. A similar trend was observed for **4**-GQDs and **5**-GQDs and for **6**-GQDs-biotin and **7**-GQDs-biotin. The effect of additional methyl groups upon quaternization on the Φ_F was, however, not observed for complex **6** and **7** and for the **6**-GQDs and **7**-GQDs conjugates. The Φ_F of GQDs-biotin is higher compared to the pristine GQDs. In water, the Φ_F is higher for GQDs, this may be due to better solubility compared to DMSO, where aggregates in DMSO may cause reduction in the Φ_F for GQDs, and no change was observed for GQDs-biotin. The Φ_F of the Pc complexes generally decreases upon conjugation to GQDs and/ or GQDs-biotin (no changes in some cases), **Table 4.1**. This may be attributed to the photoinduced electron transfer between the excited singlet state of the complexes and the carbon material in the conjugates [**170**]. The Φ_F of the GQDs and GQDs-biotin drastically decrease upon conjugation compared to the GQDs/ GQDs-biotin alone when excited where GQDs absorb, 355 nm.

The fluorescence lifetimes (τ_F) of the complexes and conjugates were determined, where the fluorescence decay curve of complex **1** is shown in **Fig. 4.3** as an example.

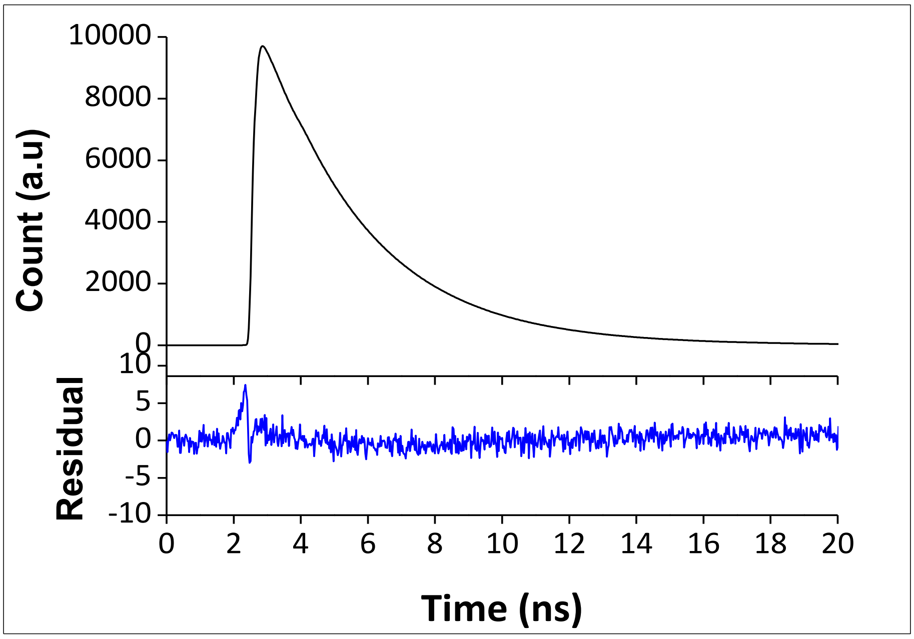

Figure. 4.3. The fluorescence decay curve of complex **1** in DMSO.

The τ_F decreases upon quaternization for complexes **4** and **5**, and complex **6** and **7**, corresponding to the Φ_F in the case of complex **4** and **5**. The τ_F of the GQDs increase upon conjugation to biotin, in GQDs-biotin in DMSO. The increase in the τ_F corresponds to the increase in the Φ_F. The τ_F of the Pc complexes decrease upon conjugation even though there were no changes in Φ_F in some cases, **Table 4.1**. The τ_F and Φ_F values are expected to change in unison. Increase or decrease in fluorescence lifetimes may depend on the geometry or distance between the metal and Pc molecule [**171**]. The τ_F for the GQDs and GQDs-biotin drastically decrease (≤ 0.1 ns) upon conjugation to Pc complexes. The decrease in the Φ_F and τ_F may be due to FRET or other inter and intramolecular processes.

Fluorescence resonance energy transfer (FRET) is based on the phenomenon of energy transfer between the emitting donor to the acceptor molecules [**172**]. In this case the GQDs as the donor and Pc as the acceptor in the conjugate. However, for FRET to occur there must be a spectral overlap between the emission spectra of the donor (in this case, GQDs) and the absorbance spectrum of the acceptor (Pc). There is little overlap between the spectra, **Fig 4.4**. Hence the decrease in Φ_F and $\boldsymbol{\tau}_F$ values of the GQDs, could be due to non-FRET processes such as changes in surface defects [**173**].

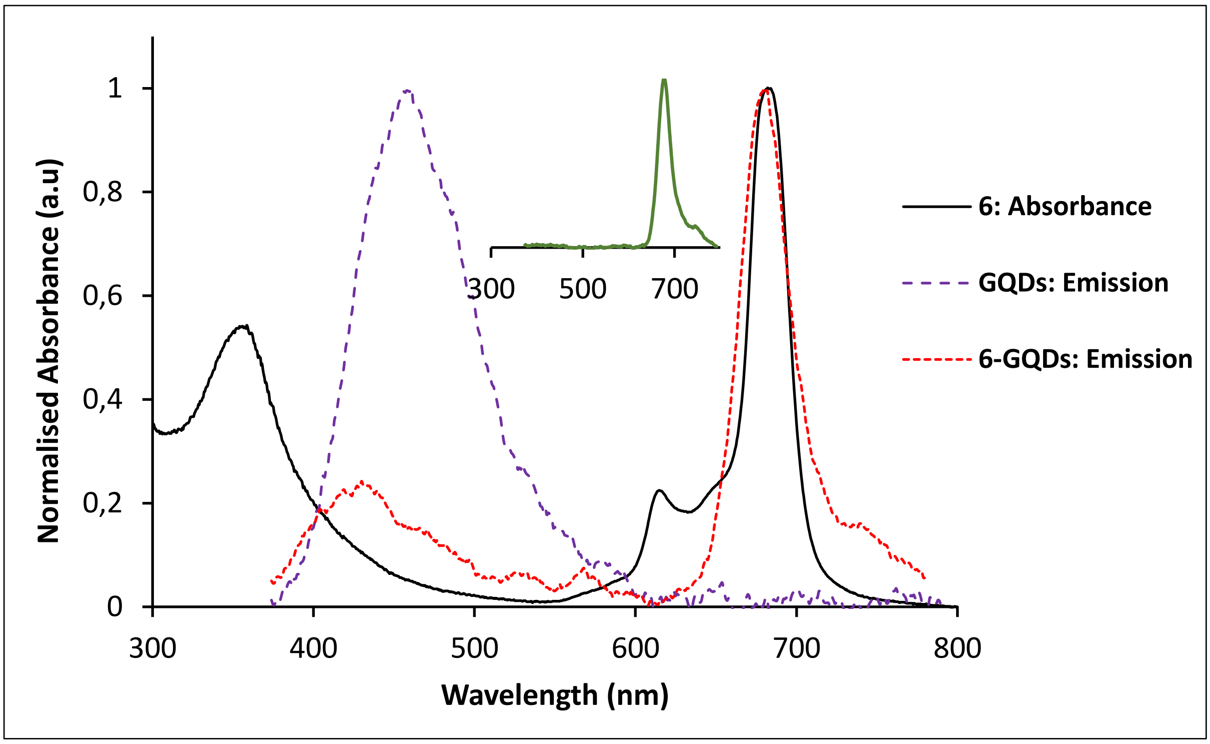

Figure 4.4. The UV-vis absorption spectrum of complex **6**, the emission spectrum of GQDs and the emission spectrum of **6**-GQDs, where λ_{exc} 355 nm in DMSO. *Insert*: Emission spectrum of complex **6** where λ_{exc} 355 nm in DMSO. Concentrations: complex **6** at 1.35 x 10^{-5} M.

The emission of the GQDs is reduced compared to the emission of complex **6** in the conjugate upon excitation at 355 nm, **Fig. 4.4**. When complex **6** alone is excited at 355 nm, emission in the NIR is observed. It is important to note that the B bands of the complexes are located where GQDs absorb, this is likely to affect the Φ_F values. Hence the stimulated emission and FRET cannot certainly be confirmed, and the values are therefore for comparative purpose only. The decrease in the Φ_F of GQDs in the conjugates may be due to the occurrence of several processes including photon induced electron transfer (PET), inter-charge transfer (ICT) which occurs between functional groups on the structures, or FRET among other processes [**172**].

4.1.3. Triplet quantum yields and lifetimes

The triplet quantum yields (Φ_T) and lifetimes (τ_T) are listed in **Table 4.1.** The transient and triplet decay curves of complex **7** are shown in **Fig. 4.5A** and **B**, respectively.

The transient curve shows a broad absorption band between 386 nm and 603 nm, a peak within this range is observed at 506 nm and attributed to the triplet-triplet state absorption (T_1-T_n) **Fig. 4.5A**. The negative peak was observed at 680 nm. The negative absorption can be attributed to the depletion or photobleaching of complex **7** in the grounds state [**174**]. A similar trend was observed for the all complexes for both the transient and absorption spectra.

Complex **1**, **2** and **5** have a high Φ_T. The Φ_T of complex **5** however, is not the highest even though its Φ_F is the lowest. This is unexpected since the structure of complexes **1** and **2,** unlike **5**, do not have the S and N atoms which may promote the population of the triplet state through the heavy atomic effect. The increase in the Φ_T is observed upon quaternization for complexes **4** and **5**, corresponding to the decrease in the Φ_F, since the two are competing processes. This is not observed for complex **6** and **7**. The Φ_T generally increases upon conjugation to GQDs. No change is observed in the Φ_T of **6**-GQDs-biotin compared to **6**-GQDs, and a decrease in the Φ_T for **7**-GQDs-biotin compared to **7**-GQDs is observed.

The triplet decay curves were fitted exponentially on ORIGIN® 8 Professional software to obtain the triplet lifetimes. The triplet decay curves obeyed second order kinetics, as shown in **Fig. 4.5B**. This trend is typical of MPc complexes at high concentration, due to triplet–triplet recombination [**175**] and was observed for all the complexes and respective conjugates. The triplet lifetimes of the complexes are summarized in **Table 4.1**. Shortening of triplet lifetimes is expected with increase in triplet quantum yields [**176**], this is not observed in this work. Lengthening of lifetimes upon conjugation was observed in most cases, except for **6**-GQDs and **7**-GQDs. This could be due to the protection of Pc afforded by GQDs in the case of conjugates. Complex **1** has the highest Φ_T and τ_T, while complexes **3** and **4** both have the lowest Φ_T and shortest τ_T. The τ_T lengthens upon quaternization for complexes **4** and **5** and complexes **6** and **7**. The lengthening of the τ_T for complexes **4** and **5** corresponds to the increase in the Φ_T.

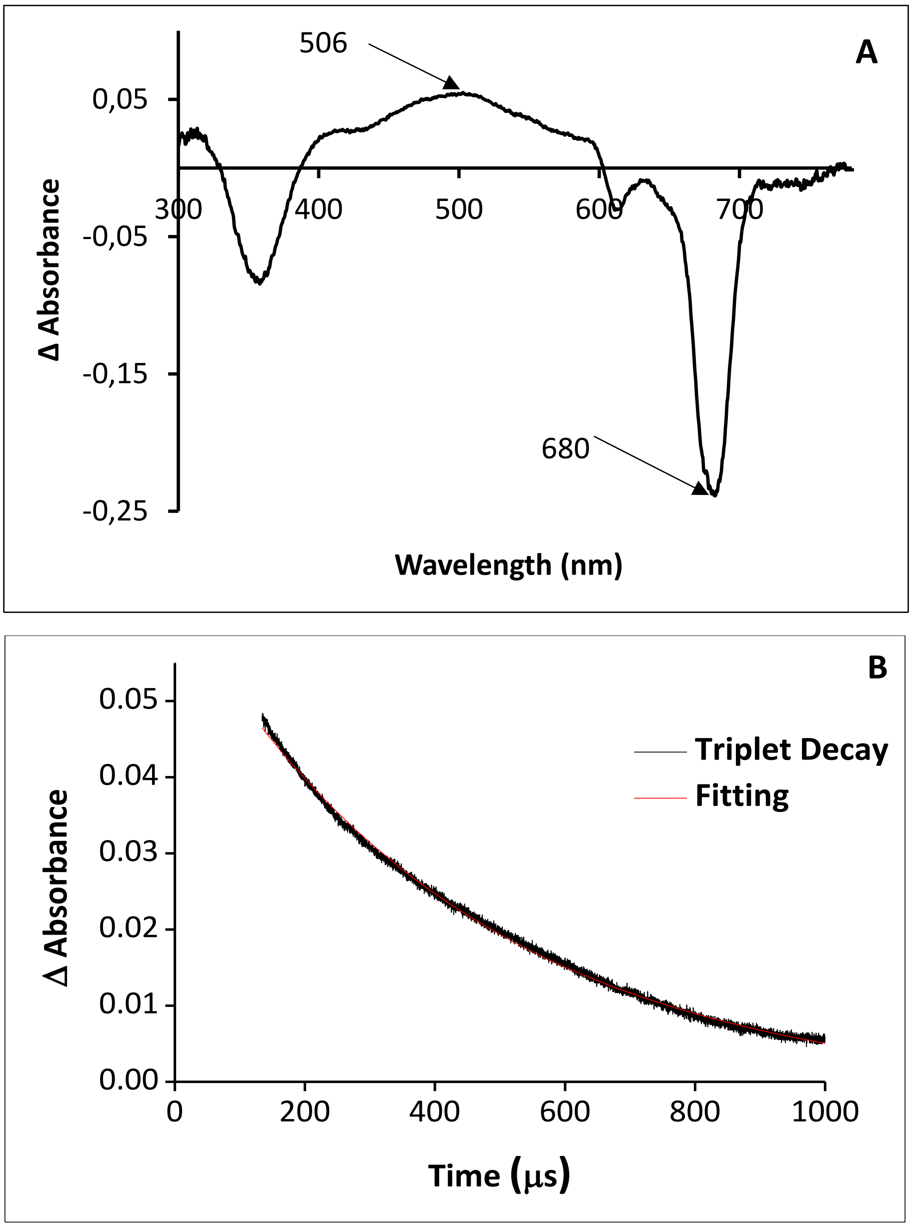

Figure 4.5. **A**) Transient curve and **B**) triplet absorption decay curve and fitting for complex **7** in DMSO.

4.2. Photochemical properties: Singlet oxygen quantum yields

The singlet oxygen quantum yields (Φ_Δ) were determined by the photodegradation of singlet oxygen quenchers. The degradation of DPBF in DMSO, **Fig. 4.6**, and ADMA in water, **Fig. 4.7** mediated by complex **7** are shown as examples.

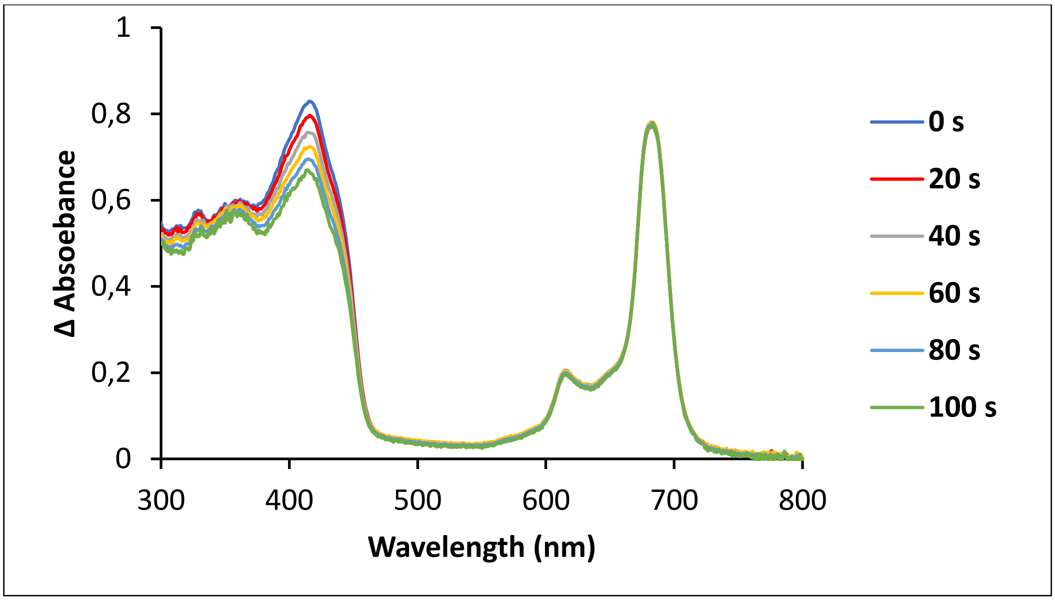

Figure 4.6. The singlet oxygen generation by complex **7** monitored by the degradation of DPBF over 100 s at 20 s time intervals in DMSO

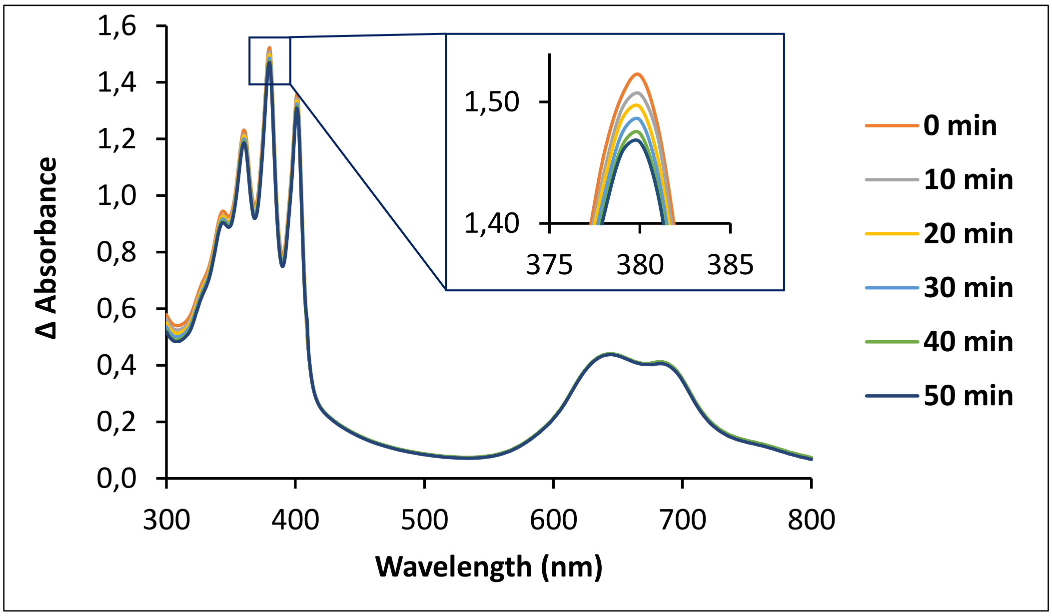

Figure 4.7. The singlet oxygen generation by complex **7** monitored by the degradation of ADMA over 50 min at 10 min time intervals in water.

The decrease in the absorbance of the DPBF (monitored at 417 nm) in DMSO and ADMA (monitored at 380 nm) in water, is indicative of photo-dependant singlet oxygen generation since the DPBF and ADMA are singlet oxygen scavengers. The DPBF and ADMA degrade upon reaction with the singlet oxygen, as shown in **Fig. 4.6** and **Fig. 4.7**, respectively. A summary of the Φ_Δ values for the complexes and conjugates are summarized in **Table 4.1**.

Φ_Δ are generated from Φ_T, hence where the latter is high, Φ_Δ is likely to be high. Complex **5** with a relatively high Φ_T however, has a low Φ_Δ. Complexes **4**, **6** and **7** have high Φ_Δ even though they do not have the highest Φ_T. The Φ_Δ decreases upon quaternization, this is observed for complexes **5** and **7**, even though there was an increase in the Φ_T for complex **5** (from complex **4**), and no change for complex **7** (from complex **6**).

The Φ_Δ decreases upon GQDs conjugation for the complexes. This decrease may be due the screening effect of the GQDs on the Pc, which may shield the transfer of energy to oxygen, and hence the reduction of the Φ_Δ [**177**]. A similar effect is observed for GQDs-biotin conjugates compared to the complexes alone except for complex **7**. There is a decrease in the Φ_Δ in water compared to DMSO, **Table 4.1**. The decrease in the Φ_Δ in water may be due to the quenching effect of water [**62**] and the low solubility of singlet oxygen in water [**178**].

4.3. Conclusion of chapter

The photophysical and photochemical properties defining the Φ_F, Φ_T and Φ_Δ were obtained for the Pc complexes and Pc-GQDs and Pc-GQDs-biotin conjugates in DMSO. The Φ_F of the Pc complexes decrease upon conjugation to GQDs and GQDs-biotin along with the τ_F. The Φ_F of the complexes decreases upon quaternization, as seen with complexes **4** and **5**, however, complex **6** and **7** remain unchanged. The Φ_T increases upon quaternization for complexes **4** and **5**, but not for complex **6** and **7**. The Φ_T generally increases upon conjugation to GQDs. The Φ_Δ of the Pc decreases upon conjugation for complexes **1-6**, however, an increase is observed for complex **7**. The Φ_Δ further decreases for **6**-GQDs-biotin and **7**-GQDs-biotin. However, the Φ_Δ of complex **7** and **7-**GQDs-biotin are similar. The high Pc concentrations used for singlet studies, where absorbance ~1.5 (a.u) may cause susceptibility to aggregation and consequently affecting the Φ_Δ.

CHAPTER FIVE

5. Cell studies

5.1. *In vitro* photodynamic therapy (PDT)

The PDT activities of the Pc complexes, Pc-GQDs and Pc-GQDs-biotin were evaluated on the MCF-7 cell lines *in vitro* (using 10^5 cells/ well in 96-well plates). The cells prior and post treatments were viewed under a microscope to visually asses the effects of the synergistic activity of light with the samples, **Fig. 5.1**.

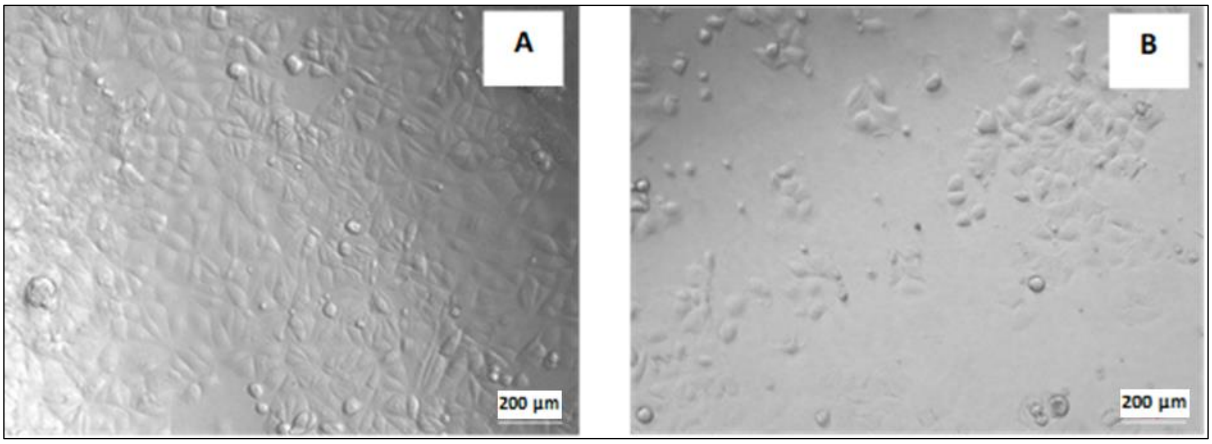

Figure 5.1. The cytograms of the MCF-7 cells on clear-bottom-96-well plates in 1% DMSO-cultured media inoculated with 100 µg/ mL of **5**-GQDs incubated at 37 ^oC at 5% CO_2, **A**) when incubated in the dark and **B**) irradiated for 5 min. Magnification: 10X, Scale bar: 200 µm.

The number of viable cells incubated in the dark, **Fig. 5.1A**, is higher in comparison to cells after PDT **Fig. 5.1B** in the presence of **5**-GQDs. Similarly, a reduction in cells was observed only for samples irradiated with light for PDT as shown in **Fig. 5.1B**, for all the Pcs complexes and GQDs/ GQDs-biotin conjugates.

To quantify viable cells after irradiation, the cells were treated with WST and the absorbances of the test samples were obtained and calculated as a percentage from the total cells in the 1% DMSO control sample. The cell viabilities are represented in the histograms, showing the dark toxicity studies, **Fig. 5.2** and PDT studies **Fig. 5.3**, mediated by **6**-GQDs, **7**-GQDs and **7**-GQDs-biotin, for example. There were no cytocidal effects observed for cells incubated in the dark for each of the studied complexes. In contrast, upon exposure to light, the number of viable cells reduced for all complexes/conjugates **Table 5.1**.

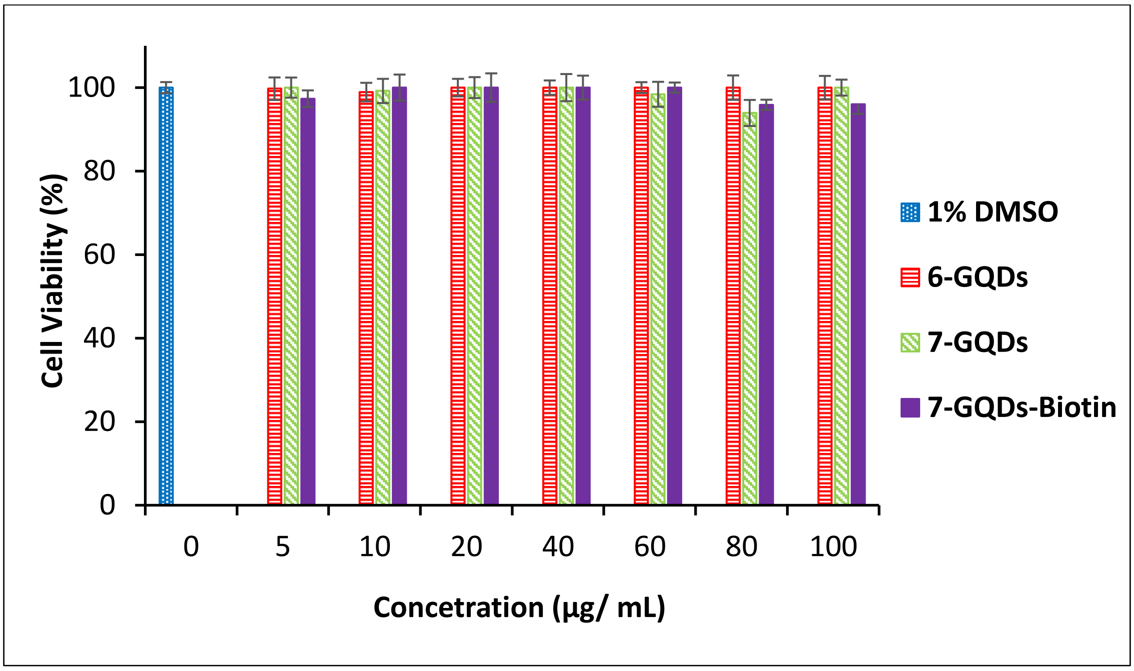

Figure 5.2. Histograms showing the MCF-7 cells cell viability (%) when incubated in the dark in the presence **6**-GQDs, **7**-GQDs and **7**-GQDs-biotin *in vitro*. Control = 1% DMSO in cultured media. n=3.

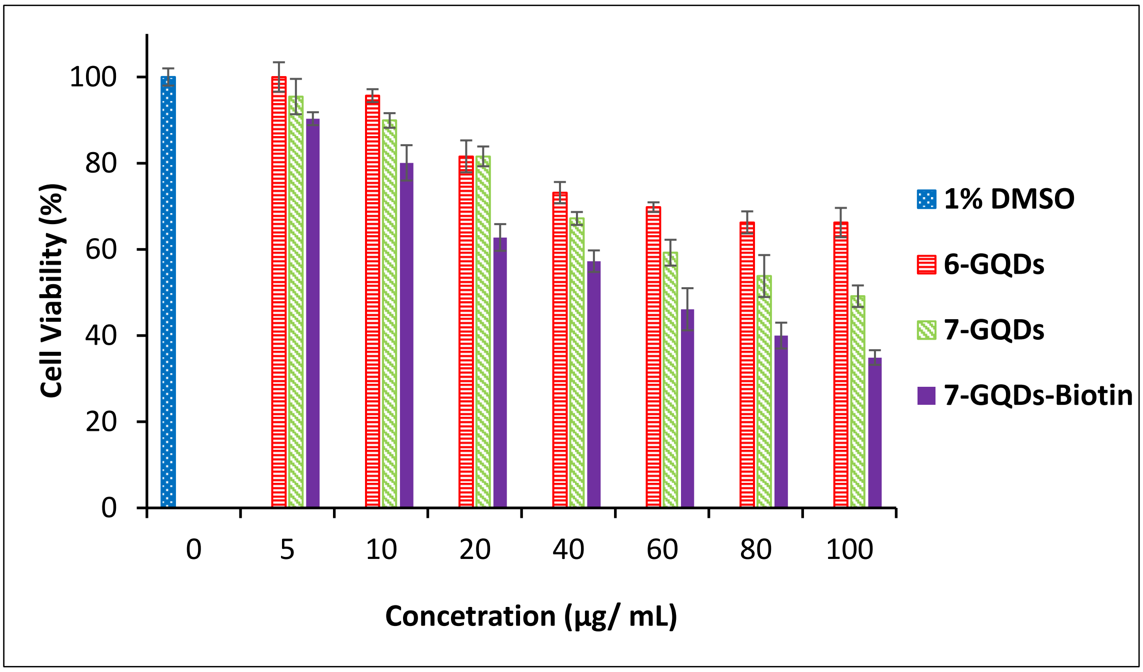

Figure 5.3. Histograms showing the MCF-7 cells cell viability (%) after PDT by **6**-GQDs, **7**-GQDs and **7**-GQDs-biotin *in vitro*. Control = 1% DMSO in cultured media. n=3.

For control samples, 1% DMSO, pristine GQDs and GQDs-biotin, no cytotoxic effect was observed upon irradiation. For GQDs and GQDs-biotin, no activity was expected since the light source was out of the range of absorbance for GQDs, hence no photo-activation to initiate cell death.

A summary on the activity of the complexes/conjugates, as a function of cell viability after PDT at the highest concentration used, 100 µg/ mL, is shown in **Table 5.1**.

Table 5.1. Summary of the Φ_Δ in DMSO and PDT activity of 100 µg/ mL the complexes and conjugates on MCF-7 *in vitro*, n=3.

Complex	**Φ_Δ**	**% Cell Viability**	**Conjugates**	**Φ_Δ**	**% Cell Viability**
1	0.50	43.4	**1**-GQDs	0.44	54.5
2	0.49	48.1	**2**-GQDs	0.40	52.2
3	0.5	49.7	**3**-GQDs	0.45	34.7
4	0.54	57.0	**4**-GQDs	0.50	43.4
5	0.35	32.4	**5**-GQDs	0.30	48.1
6	0.67	47.7	**6**-GQDs	0.60	66.2
			6-GQDs-biotin	0.47	40.8
7	0.53	44.1	**7**-GQDs	0.58	51.2
			7-GQDs-biotin	0.54	34.9

There are no obvious trends between the Φ_Δ and the PDT activity for both the complexes and the conjugates, **Table 5.1**. For example, there is an increase in cell viability (decrease in PDT activity) for **1**-GQDs, **2**-GQDs, **5**-GQDs, **6**-GQDs and **7**-GQDs compared to the complex alone, corresponding to decrease in Φ_Δ values. However, for **3**-GQDs and **4**-GQDs, there is a decrease in cell viability (increase in PDT activity) compared to the complexes alone, even though Φ_Δ values decreased upon conjugation. The cationic complexes were generally better performing compared to the corresponding non-charged complexes, including complex **4** compared to **5**, and complex **6** compared to **7**, as well as the conjugates **6**-GQDs compared to **7**-GQDs. This has previously been reported for Pcs [**94**] and other charged complexes for cancer treatment [**89,178**]. The net anionic membrane charge of cancer cells is believed to be susceptible to cationic drug complexes through electrostatic attraction. This may result in improved drug retainment and hence more available Pcs for therapy. The **4**-GQDs however, showed better PDT activity compared to the cationic **5**-GQDs.

The conjugates of GQDs-biotin showed higher PDT activities compared to the conjugates of GQDs alone, **Table 5.1**. This may be a result of improved cellular uptake since cancer cells are known to overexpress biotin receptors. Moreover, the DMEM used in this study had no biotin content, and therefore, there was no binding competition between the biotin on the GQDs to nutrient biotin. It should be noted that the cytocidal effect of the different photosensitizer is dependent on several factors including cell type, cellular uptake, and localization [**179,180**].

5.2. Cellular drug uptake

The cellular uptake of the complexes, GQDs, GQDs-biotin and conjugates were determined to predict the amounts of samples that were available in cells for PDT after incubation for 24 h.

The cellular uptake of the non-ionic complex **6**-GQDs and the cationic complex **7**-GQDs were determined and compared to evaluate the effect of charge on the uptake of the complexes. The cellular uptake of the **6**-GQDs and **7**-GQDs were then compared to the cellular uptake of the corresponding GQDs-biotin conjugates. The cellular uptake of pristine GQDs and GQDs-biotin were also obtained to evaluate the effect of biotin. The uptake curves of the complexes are shown for the **6**-GQDs, **7**-GQDs and **7**-GQDs-biotin **Fig. 5.4**.

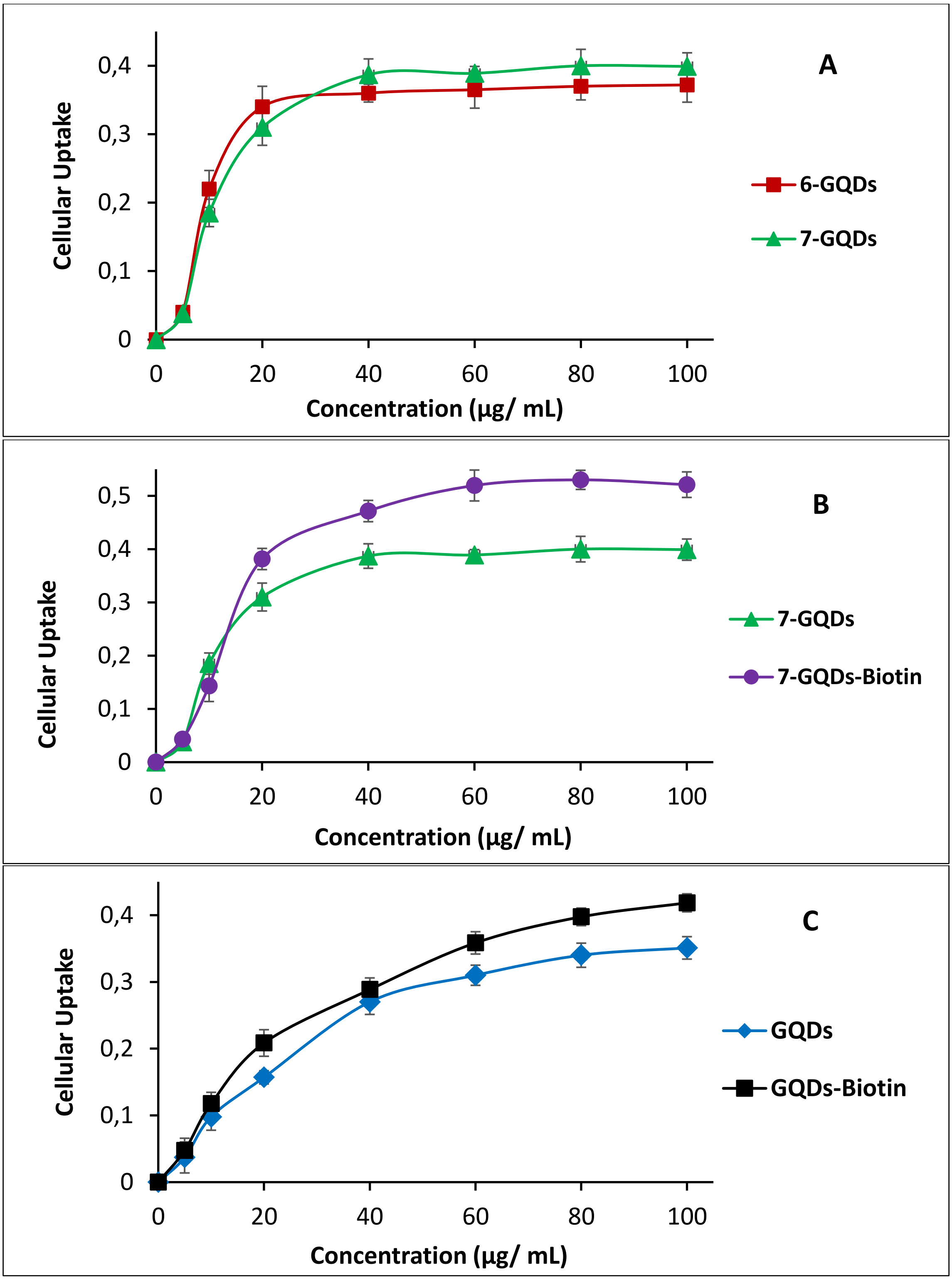

Figure 5.4. MCF-7 cellular uptake over 24 h as a function of fluorescence intensity, for **A**) **6**-GQDs and **7**-GQDs and **B**) **7**-GQDs and **7**-GQDs-biotin where λ_{exc} 680 nm, and **C**) GQDs and GQDs-biotin at λ_{exc} 360 nm.

The cellular uptake of the complexes, GQDs and the conjugates increases upon increase in the concentration.

The point at which the cellular uptake concentrations begin to plateau, for each of the Pc complexes (complexes **6** and **7**), their corresponding conjugates and the GQDs and GQDs-biotin, are summarized in **Table 5.2**.

Table 5.2. Summary of the maximum concentration uptake of the complexes, GQDs, GQDs-biotin and conjugates over 24 h.

When excited where Pcs absorb			
Complex	**Max concentration (µg/ mL)**	**Conjugate**	**Max concentration (µg/ mL)**
6	40 – 60	**6**-GQDs	20 – 40
		6-GQDs-biotin	40 – 60
7	40 – 60	**7**-GQDs	40 – 60
		7-GQDs-biotin	60 – 80
When excited where GQDs absorb			
GQDs	> 80		
GQDs-biotin	> 80		

There is an increase in the uptake upon introduction of cations in the complexes, and a further increase upon biotin conjugation observed for the Pcs-GQDs conjugates **Fig. 5.4A** and **Fig. 5.4B** respectively. This may further justify the improvement of PDT in that improved cellular uptake avails more cellular Pcs units for PDT. The pristine GQDs and GQDs-biotin uptake continue to increase above 80 µg/ mL **Fig. 5.4C**. GQDs-biotin however, showed an increase in the concentration uptake when compared to GQDs alone. This increase may be afforded by the presence of biotin on the GQDs which enhance the uptake of the particles through a receptor mediated transport system.

5.3. Conclusion of chapter

The studies showed that the Pcs complexes and the conjugates to GQDs and GQDs-biotin have no dark toxicity. The PDT activity of the Pcs complexes is higher compared to the GQDs conjugates (high number of viable cells). However, upon conjugation to GQDs-biotin, for complex **6** and **7**, the PDT activity increases (low number of viable cells).

The cellular uptake for the complexes increases upon introduction of cations, as seen for complexes **6** and **7**. A further increase is observed for complexes conjugated to GQDs-biotin, **7**-GQDs-biotin in comparison to complexes **7**-GQDs.

CHAPTER SIX

6. Side Work: Trifluoromethylthiolation reaction in flow

6.1. Solvent screening

The aim was to develop the trifluoromethylthiolation in flow for the preparation of SCF3-labbeled Pcs complexes as potential PET/ PDT theranostic as shown in **Scheme 6.1**.

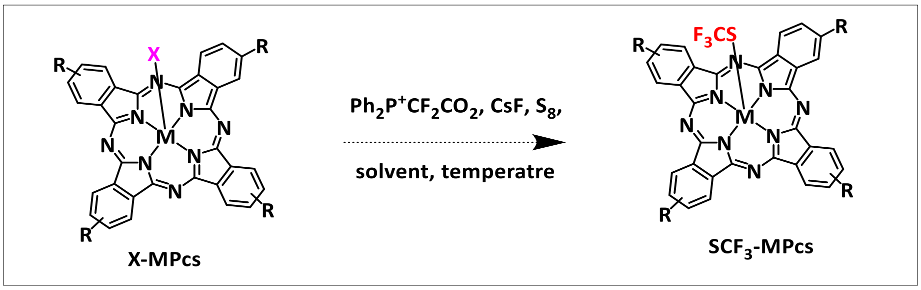

Scheme 6.1. Trifluoromethylthiolation of MPcs with electrophilic axial ligand.

The trifluoromethylthiolation reaction was reproduced as described in literature, **Scheme 6.2** [**149**]. Since not all reagents were completely soluble in DMF before and after the reaction was completed (at 70 ⁰C, over 5 min), several solvents were screened to determine a solvent system in which a homogenous liquid solution can be prepared for flow, **Table 6.2**.

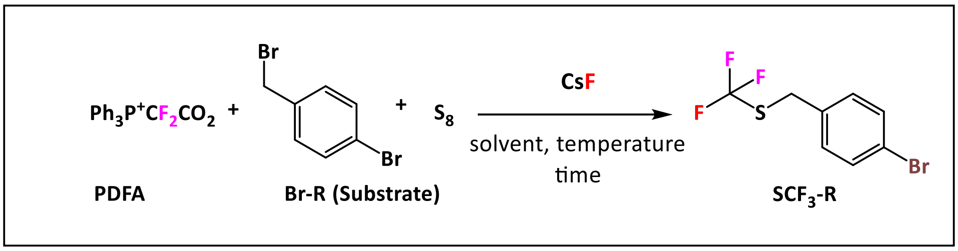

Scheme 6.2. Trifluoromethylthiolation reaction. PDFA: difluoromethylene phosphobetaine ($Ph_3P^+CF_2CO_2$).

The samples for determining a working solvent-system were prepared by adding each reagent (~10 mg) separately in an eppendorf tube for each solvent (1 mL) at room temperature (r.t) and when heated at 70 ⁰C stirring for 5 min to determine the reagents that remain unreacted. The mixtures were then checked to see if the reagents go into solution (Yes) or remain undissolved (No) or partially dissolved (Yes*) after 5 min in the respective solvent.

Table 6.1. Selection of solvents screened to dissolve reagents

Solvent	Reagents							
	PDFA		S_8		CsF		Substrate	
	r.t	70 °C	r.t	70 °C	r.t	70 °C	r.t	70 °C
DMF	Yes*	Yes	No	No	No	No	Yes	Yes
DMSO	Yes*	Yes	No	No	Yes*	Yes*	Yes	Yes
DMA	No	Yes	No	No	No	No	Yes	Yes
Toluene	No	Yes	Yes	Yes	No	No	Yes	Yes
DCM	Yes	-	Yes	-	No	-	Yes	-
$CHCl_3$	Yes	Yes	No	No	No	No	Yes	Yes
THF	Yes	Yes	Yes	Yes	No	No	Yes	Yes
MeCN	No	Yes	No	No	No	No	Yes	Yes

DMF: dimethylformamide, DMSO: dimethylsulfoxide, DMA: dimethylacetamide, DCM: dichloromethane, THF: tetrahydrofuran, MeCN: acetonitrile.

The DMF as used by Zheng [**149**] for the trifluoromethylthiolation reaction evidently does not dissolve the regents even at increased temperatures as shown in **Table 6.1**. The DMSO, toluene, DCM and THF were better compared to the other solvents. The solubility of the S_8 in toluene compared to DMF is shown in **Fig. 6.1** as an example of the method of solvent screening.

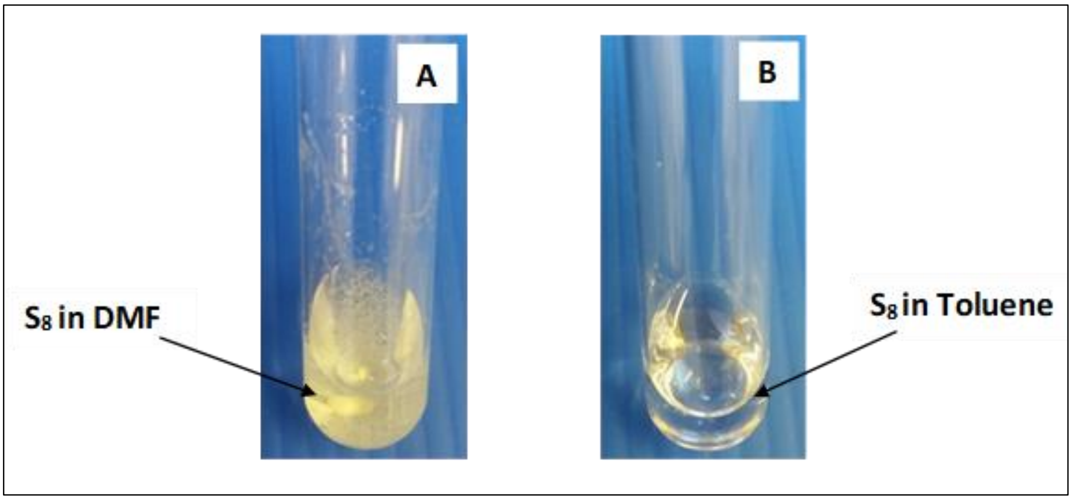

Figure 6.1. Solubility of the S_8 in DMF vs toluene at room temperature.

The trifluoromethylthiolation reaction was performed in the solvents that better dissolved the reagents, including DMSO and DCM, and solvent mixtures including DMF + toluene, DMSO + toluene and DMSO + DCM + toluene in comparison to DMF as in literature [**149**]. The reaction conditions were as described by Zheng *et al.* [**149**] in terms of the reagent molar ratio, time and temperature. For mixed solvents, toluene was used to dissolve S_8 and DCM for PDFA, in the case were DCM was used. The rest of the reagents were dissolved in DMSO. For each reaction with mixed solvents, the solutions were prepared separately then mixed immediately before the reaction vessel was immersed in a heat oil-bath.

For each reaction, the ^{1}H NMR spectrum was determined to evaluate the quality of each reaction. Considering the product yield percentage as well as presence of by-products. The peak of interest by ^{1}H NMR analysis occurs around 4.02 ppm [**149**], representing the hydrogens attached to the C directly linked to the S on the SCF_3 group (S-C-H_2-F_3).

From the ^{1}H NMR spectra **Fig. 6.2A** and **B**, all the reactions showed presence of the product peak expected at ~4.02 ppm. The DCM spectrum, however, showed many more peaks which are representative of contaminants, therefore, disqualifying DCM as a solvent for this application as it would require tedious purification processes. The reactions in DMF, DMF + toluene, DMSO and DMSO + toluene were relatively better, however, the DMF alone would not completely dissolve all the reagents and thus not ideal for flow reactions. The DMSO + toluene compared to the rest of the solvents was better in that the yield was relatively higher with reduced side-products peaks. Additionally, the mixed solvents; DMSO + toluene improved the solubility of the reagents. Therefore, making the mixed solvent a potential solvent system for the trifluoromethylthiolation reaction in a flow reactor.

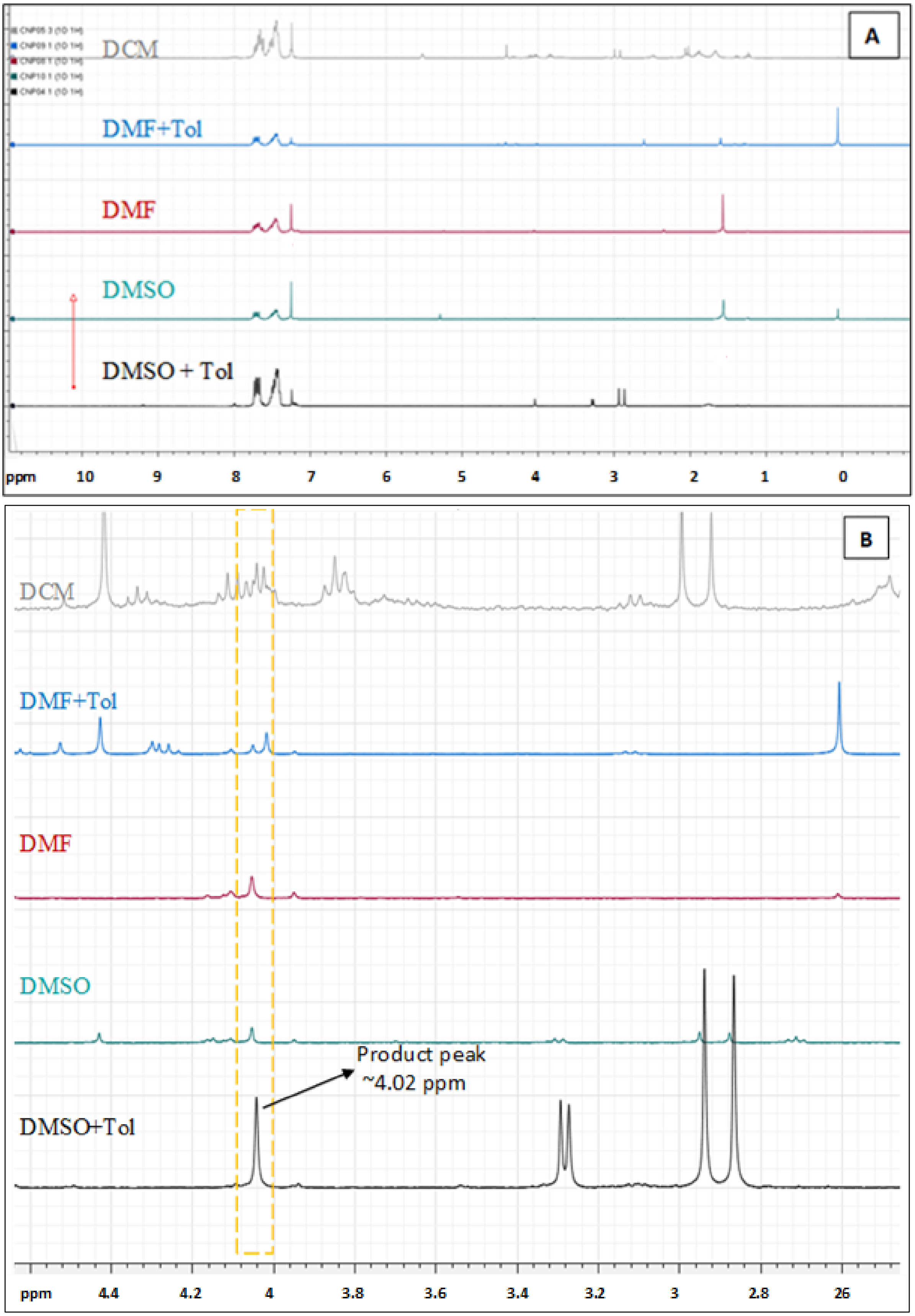

Figure 6.2: The **A**) full ^{1}H-NMR spectra and **B**) near product-region ^{1}H-NMR spectra of the trifluoromethylthiolation reaction in different solvents.

6.2. Optimization of the reaction conditions in batch

The reaction in DMSO + toluene was thereafter performed in varied conditions to assess how it can be improved for flow. The time and temperature of the reaction were varied, keeping the reagent ratios constant, **Table 6.2**.

Table 6.2. Batch reaction in mixed DMSO and toluene at different reaction conditions. Where the concentration ratio were 1:2:0.7:5 for substrate:PDFA:S_8:CsF.

Temperature (°C)	**Time (min)**	**Yield (%)**
60	5	23.0
70	5	68.0
70	60	77.4
80	5	86.6
90	5	90.0
90	10	89.1

From the ^{1}H NMR analysis, the trifluoromethylthiolation reaction in DMSO + toluene showed improvement when performed at 90 °C for 5 min, compared to lower temperatures, 60 °C, 70 °C and 80 °C, **Table 6.2**. Moreover, at 90 °C, when reaction time was increased to 10 min, the reaction efficiency neither improved nor deteriorates. Therefore, the temperature and time for the trifluoromethyl thiolation reaction in DMSO + toluene was kept at 90 °C for 5 min and tested in a flow reactor. However, noting that the reaction behaviour in batch may not necessarily be the same in flow, time and temperature were also slightly changed and tested in flow.

6.3. Flow reaction

The trifluoromethylthiolation reaction using the DMSO + toluene solvent-system was performed in flow using a 16 mL volume flow reactor. The reaction conditions were varied in terms of reagent concentration ratios, temperature, time and flow rate, **Table 6.3**.

Table 6.3. Flow reaction in mixed DMSO and toluene at different reaction conditions.

Concentration ratios Substrate: PDFA: S_8: CsF	Temperature (^oC)	Time (min)	Flow rate (mL/ min)	Yield (%)
1:2:0.7:5	90	5	3.2	>99.9
1:2:0.7:2.5	90	5	3.2	60.2
1:1.5:0.7:5	90	5	3.2	90
1:2:0.7:5	90	3.5	4.6	40.5
1:2:0.7:5	70	5	3.2	24.15

The reaction at 90 ^oC in flow still maintained a high yield, of >99.9 % when the reagent concentration ratio was 1:2:0.7:5. The reduction of PDFA molar equivalent from 2 to 1.5 impressively maintained a high yield of 90 %. Further variations in the reaction conditions included reduction in the concentration of CsF from a molar equivalent to the substrate of 5 to 2.5 which resulted in the reduction of the product yield to 60.2 %. Reducing the reaction time from 5 min to 3.5 min, and reducing the reaction temperature to 70 ^oC, also reduced product yield percentage down to 40.5% and 24 % respectively.

The ^1H NMR of crude product from the batch reaction (reaction conditions, concentration ratios: 1:2:0.7:5, temperature: 90 ^oC, time: 5 min in DMSO + toluene) was compared to the ^1H NMR of the crude product from the flow reaction, **Fig. 6.3A**. The reaction performed in flow showed reduced side products in comparison with the reaction mixture from a batch reaction. The ^{19}F NMR was obtained and confirmed presence of product, at ~-41.5 ppm **Fig. 6.3B** [**149**].

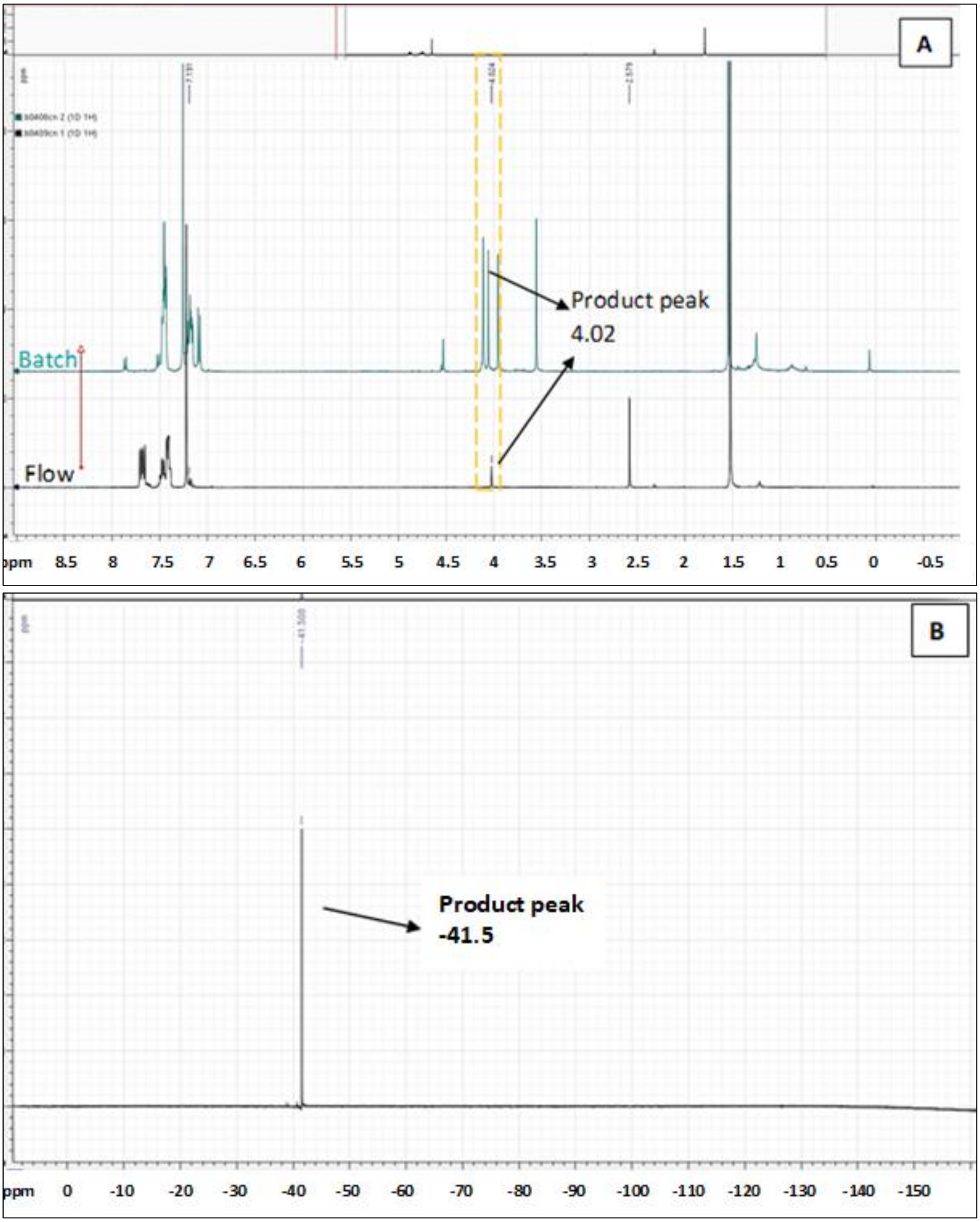

Figure 6.3. The **A**) ^{1}H NMR spectra of the trifluoromethylthiolation reaction mixture in batch and in flow, at 90 °C for 5 min in DMSO + toluene. **B**) ^{19}F NMR spectrum of the reaction in flow at 90 °C for 5 min in DMSO + toluene.

The formation of side-products was evident in the reaction mixtures (at 90 ^{0}C, 5 min) in batch, however, much lower in flow **Fig. 6.3A**. The attempt to predict which compounds were formed as side-products was done using a method of reagent-elimination, where the reaction with all the reaction conditions were kept the same however one or two reagents would be excluded in the reaction. The results were analysed by ^{1}H NMR, **Fig. 6.4**.

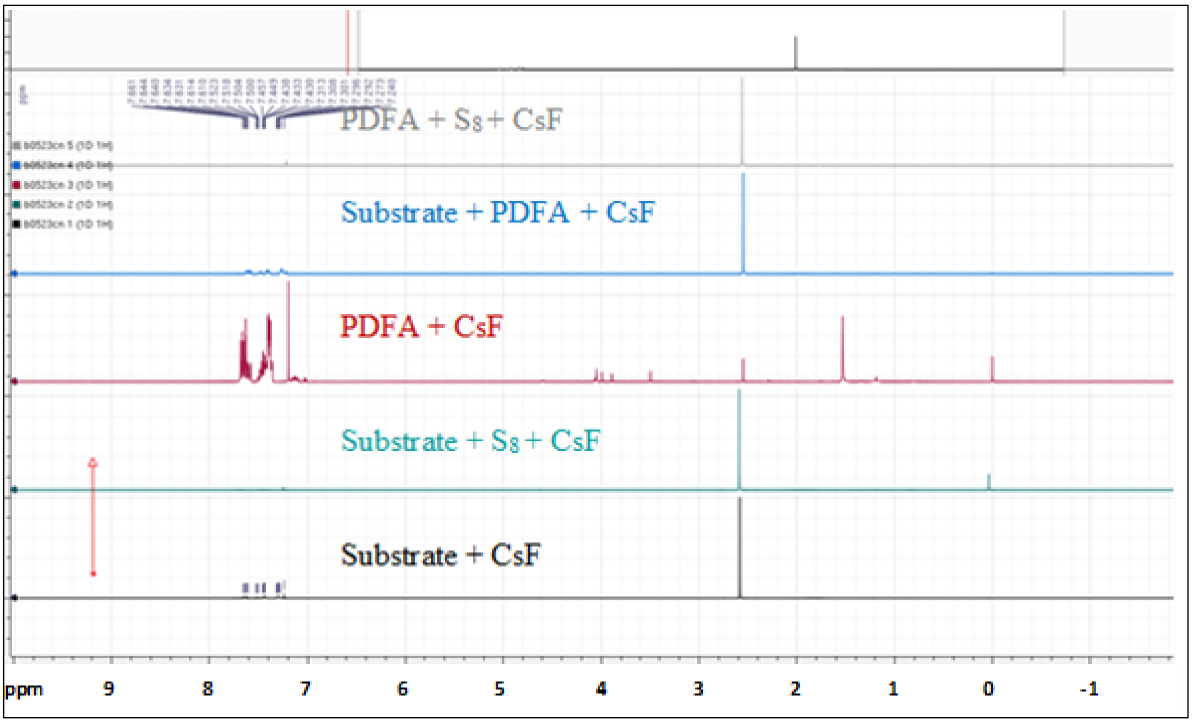

Figure 6.4. The ^{1}H NMR spectra of reaction at 90 °C for 5 minutes in DMSO + toluene with some reagents

From the ^{1}H NMR spectra of the reaction mixtures, the reaction of PDFA and CsF, surprisingly showed a peak like that of the protons of the C in the - SCF_3 group, **Fig. 6.4**. Therefore, it is worthy of consideration to perform further characterization such as ^{19}F NMR for this reaction and additional characterization techniques such as infrared spectroscopy, mass spectrometry or elemental analysis to confirm synthesis of desired product. The PDFA + CsF reaction also had more proton peaks that any other reaction. However, generally, the mixtures did not show any reaction products.

The SCF_3-Pcs, as shown in **Fig**. **6.1** was not obtained due to time constraints, and it is therefore part of the future work.

6.4. Conclusion of chapter

The reagents used in the trifluoromethylthiolation reaction were soluble in the DMSO + toluene solvent system. The reaction showed better performance in comparison to other solvent systems at 90 ^{o}C for 5 min, using reagent ratios described in literature [**149**].

The trifluoromethylthiolation reaction in flow using the DMSO + toluene at 90 ^{o}C for 5 min solvent system was relatively purer compared to the reaction performed in flow. The target products were confirmed by ^{1}H NMR and ^{19}F NMR.

CHAPTER SEVEN

7. General conclusion and future work

7.1. Conclusion

The photo-physicochemical properties and *in vitro* photodynamic activity of a series of Zn(II)Pcs derivatives and how these properties may be affected upon conjugation to GDQs and GQDs-biotin by π-π interactions, was investigated on human breast cancer MCF-7 cell lines.

A decrease in the Φ_F (insignificant in some cases) and the consequent increase in the Φ_T was observed for the conjugates. The Φ_Δ however, was reduced for the conjugates compared to the non-conjugated complexes. This was suspected to be caused by the screening effect from the GQDs, inhibiting facile energy transfer to the oxygen from the triplet state. The conjugates did however demonstrate PDT activity on the human breast cancer MCF-7 cell lines upon irradiation. The conjugation of the Pcs complexes to pristine GQDs (without biotin) did not show improvement in the photophysical parameters nor the *in vitro* PDT activity on MCF-7 cell lines. However, upon functionalization of GQDs with biotin, the PDT activity improves due to improved drug uptake in the Pcs-GQDs-Biotin conjugates.

In addition to assisted uptake using biotin, the cationic complex **7** and **7**-conjugates showed improved PDT activity compared to the non-ionic complex **6**. This is also believed to be due to the enhanced uptake of the cationic complexes. Overall, the combination of cancer drug-uptake methods, viz GQDs, cationic charges and biotin transport, help improve the therapeutic efficacy of Pcs during PDT *in vitro* by improving the concentration of Pcs penetrating the cells.

7.2. Futures work

a) To synthesize Pcs that may be linked both covalently, possibly through amide bond, and non-covalently, through π-π bonds, and compare the PDT activity *in vitro.*

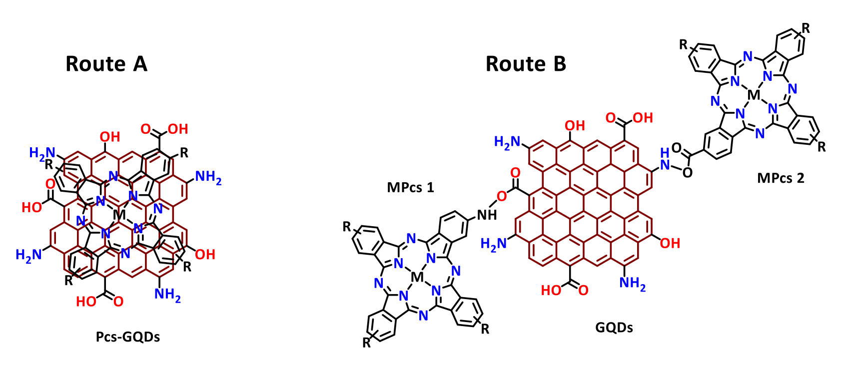

Figure 7.1. Methods of conjugating Pcs to GQDs; Route A: through π-π bonds and Route B: through covalent linkages, using amide bond as an example.

The Pcs linked covalently to the GQDs may be amino-substituted MPcs (MPcs 1) or carboxy-substituted MPcs (MPcs 2), which may be linked via the carboxy or amino groups on the GQDs, respectively.

b) To develop the trifluoromethylthiolation of Pcs reaction to prepare a potential PET/ PDT theranostic as shown in **Scheme 7.1**.

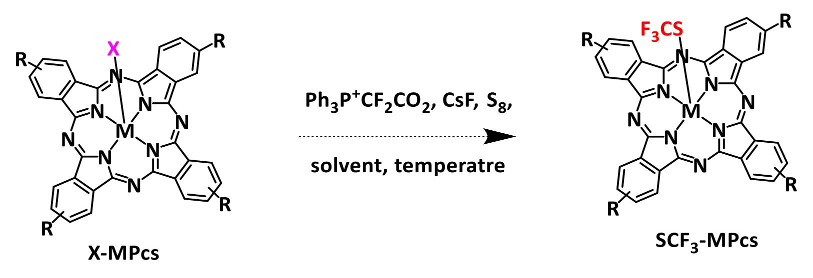

Scheme 7.1. Trifluoromethylthiolation of MPcs with electrophilic axial ligand.

Study the structural properties, photo-physicochemical properties, PDT activity of the SCF_3-Pcs and the effect of the SCF_3 on the cellular uptake of the Pcs.

1. Moorthi. C.; Manavalan. R.; Kathiresan. K. *J. Pharm. Pharm. Sci.* **2011**, 14: 67-77.
2. Casanovas, O. *Nature* **2012**, 484: 44-46.
3. Agostinis, P.; Berg, K.; Cengel, K. A.; Foster, T. H.; Girotti, A. W.; Gollnick, S. O.; Hahn, S. M.; Hamblin, M. R.; Juzeniene, A.; Kessel, D.; Korbelik, M.; Moan, J.; Mroz, P.; Nowis, D.; Piette, J.; Wilson, B. C.; Golab, J. *CA Cancer J. Clin.* **2011**, 61: 250-281.
4. Miller, J. D.; Baron, E. D.; Scull, H.; Hsia, A.; Berlin, J. C.; McCormick, T.; Colussi, V.; Kenney, M. E.; Cooper, K. D.; Oleinick, N. L. *Toxicol. Appl. Pharm.* **2007**, 224: 290-299.
5. Mfouo-Tynga, I.; Abrahamse, H. *Int. J. Mol. Sci.* **2015**, 16: 10228-10241.
6. Triesscheijn, M.; Baas, P.; Schelliens, J. H. M.; Stewart, F. *Oncologist* **2006**, 11: 1034-1044.
7. Robertson, C. A.; Hawkins, Evans, D.; Abrahams, H. *J. Photochem. Photobiol. B* **2009**, 96: 1-8.
8. Maloth, K. N.; Velpula, N.; Kodangal, S.; Sngmesh, M.; Vellamchetla, K.; Ugrappa, S.; Meka, N. *J. Las. Med. Sci.* **2016**, 7: 30-36.
9. Sharman, W. M.; Allen, C. M.; van Lier, J. E. *Drug Discov. Today* **1999**, 4: 507-517.
10. Macdonald, I. J.; Dougherty, T. J. *J. Porphyrin Phthalocyanines* **2001**, 5: 105-109.
11. Dai, T.; Fuchs, B. B.; Coleman, J. J.; Prates, R. A.; Astrakas, C.; St. Denis, T. G.; Ribeiro, M. S.; Mylonakis, E.; Hamblin, M. R.; Tegos, G. P. *Front. Microbiol.* **2012**, 3: 1- 16.
12. Allison, R. R.; Downie, G. H.; Cuenca, R.; Hu, X-H.; Childs, C. J. H.; Sibata. C. H. *Photodiagnosis Photodyn. Ther.* **2004**, 1: 27-42.
13. Kudinova, N. V.; Berezov, T. T. *Biomed. Khim.* **2009**, 55: 558-569.
14. Mehraban, N.; Freeman, H. S. *Materials* **2015**, 8: 4421-4456.
15. Zhang, J.; Jiang, C.; Longo, J. P. F.; Azevedo, R. B.; Zhang, H.; Muehlmann, L. A. *Acta. Pharm. Sin. B* **2018**, 8: 137-146.
16. Levy, J. G. *Semin. Oncol.* **1994**, 6: 4-10.
17. Nyokong, T. *Pure Appl. Chem.* **2011**, 83: 1763-1779.
18. Wang, A.; Long, L.; Zhang, C. *J. Incl. Phen. Macrocycl. Chem.* **2011**, 71: 1-24.
19. Abrahamse, H.; Hamblin, M. R. *Biochem. J.* **2016**, 473: 347-364.
20. Mehraban, N.;Freeman, H. S. *Materials* **2015**, 8: 4421-4456.
21. Kou, J.; Dou, D.; Yang, L. *Oncotarget* **2017**, 8: 81591-81603.
22. Lukyanets, E. A. *J. Porphyrin Phthalocyanines* **1999**, 3: 424-432.

23. Nyokong T.; Gledhill I. *AIP Conf. Proc.* **2013**, 1517: 49-52.

24. Ng, D. K. P. *Future Med. Chem.* **2014**, 6: 1991-1993.

25. Braun, A.; Tcherniac, J. Ber. Dtsch. Chem. Ges. **1907**, 40: 2709-2714.

26. Arslan, S. *J. Life Sci.* **2016**, 6: 188-197.

27. Kuzyniak, W.; Schmidt, J.; Glac, W.; Berkholz, J.; Steinemann, G.; Hoffmann, B.; Ermilov, E. A.; Gürek, A. G.; Ahsen, V.; Nitzsche, B.; Höpfner, M. *Int. J. Oncol.* **2017**, 50: 953-963.

28. Dodsworth, E. S.; Lever, A. B. P.; Seymour, P.; Leznoff, C. C. *J. Phys. Chem.* **1985**, 89: 5698-5705.

29. Bilgicli, A. T.; Tekin, Y.; Alici, E. H.; Yaraşir, M. N.; Arabaci, G.; Kandaz, M. *J. Coord. Chem.* **2015**, 68: 4102-4116.

30. Dahlen, M. A. *J. Ind. Eng. Chem.* **1939**, 31: 839-847.

31. Staicu, A.; Pascu, A.; Nuta, A.; Sorescu, A.; Rditoiu, V.; Pascu, M. L. *Rom. Rep. Phys.* **2013**, 65: 1032-1051.

32. Nombona, N.; Chidawanyika, W.; Nyokong, T. *Polyhedron* **2010**, 30: 654-659.

33. Gregory, P. *J. Porphyrin Phthalocyanines* **2000**, 4: 432-437.

34. Kudrevich, S. V.; Ali, H.; van Lier, J. E. *J. Chem. Soc. Perkin Trans.* **1994**, 1: 2767-2774.

35. Kobayashi, N.; Kondo, R.; Nakajima, S.; Osa, T. *J. Am. Chem. Soc.* **1990**, 112: 9640-9641.

36. Torres, T. *J. Porphyrins Phthalocyanines.* **2000**, 4: 325-330.

37. Durmuş, M.; Nyokong, T. *Photochem. Photobiol.* **2007**, 6: 659-668.

38. Nemykin, V. N.; Lukyanets, E. A. *ARKIVOC* **2010**, 1: 136-208.

39. Atilla, D.; Gürek, AG.; Basova, T. V.; Kiselev, V. G.; Hassan, A.; Sheludyakova, L. A.; Ahsen, V. *Dyes Pigm.* **2011**, 88: 280-289.

40. Edwards, L.; Gouterman, M. *J. Mol. Spectrosc.* **1970**, 33: 292-310.

41. Alzeer, J.; Roth, P. J. C.; Leudtke, N. W. *Chem. Commun.* **2009**, 0: 1970-1971.

42. Gouterman, M.; Waniere, G. H.; Synder, L. C.; *J. Mol. Spectrosc.* **1963**, 11, 108-127.

43. Mack, J.; Stillman, M. J. *J. Am. Chem. Soc.* **1994**, 116: 1292-1034.

44. Mack, J.; Stillman, M. J. *Inorg. Chem.* **1997**, 36: 413-425.

45. Nesterova, I. V.; Verdree, V. T.; Pakhomov, S.; Strickler, K. L.; Allen, M. W.; Hammer, R. P.; Soper, S. A. *Bioconjug. Chem.* **2007**, 18: 2159-2168.

46. Sakamoto, K.; Ohno-Okumura, E. *Materials* **2009**, 2: 1127-1179.

47. Sakamoto, K.; Ohno-Okomura, E.; Kato, T.; Soga, H. *J. Porphyrin Phthalocyanines* **2010**, 14: 47-54.

48. Huang, G.; Li, J.; Cong, F.; Li, C.; Chu, X.; Meng, Y.; Du, G.; Du, X. *Molecules* **2013**, 18: 4628-4639.

49. Ormond, A. B.; Freeman, H. S. *Materials* **2013**, 6: 817-840.

50. Sternberg, E. D.; Dolphin, D. *Tetrahedron* **1998**, 54: 4151-4202.

51. Ramos, A. A.; Nascimento, F. B.; de Souza, T. F. M.; Omori, A. T.; Manieri, T. M.; Cerchiazo, G.; Ribeiro, A. O. *Molecules* **2015**; 20: 13575-13590.

52. Mthethwa, T. P.; Tunce,l S.; Durmuş, M.; Nyokong, T. *Dalton Trans.* **2013**, 42: 4922-4930.

53. Tayfuroğlu, O.; Kiliçarslan, F. A.; Atmaca, G. Y.; Erdoğmuş, A. *J. Porphyrin Phthalocyanines* **2018**, 22: 1-16.

54. Fery-Forgues, S.; Lavabre, D. J. *J. Chem. Educ.* **1999**, 76: 1260-1264.

55. Ogbodu. R. O.; Nyokong, T. *Spectrochim. Acta A Mol. Biomol. Spectrosc.* **2015**, 151: 174-183.

56. Maree, S. E.; Phillips, D.; Nyokong, T. *J. Porphyrin Phthalocyanines* **2002**, 6: 17-25.

57. Wang, X. F.; Uchida, T.; Minami, S. *Appl. Spectros.* **1991**, 45: 560-565.

58. Antunes, E. M.; Nyokong, T. *Met. Based. Drugs.* **2008**, 2008: 1-9.

59. Managa, M.; Idowu, M.; Beukes, E.; Nyokong, T. *Spectrochim. Acta A Mol. Biomol. Spectrosc.* **2014**, 125: 147-153.

60. Ogbodu, R. O.; Antunes, E.; Nyokong, T. *Polyhedron* **2013**, 59-67.

61. Bachilo, S. M.; Weisman, R. B. *J. Phys. Chem. A* **2000**, 104: 7711-7714.

62. Ogunsipe, A.; Chen, J-Y.; Nyokong, T. *New. J. Chem.* **2004**, 28: 822-827.

63. Brannon, J. H.; Magde, D. *J. Am. Chem. Soc.* **1980**, 102: 62-65.

64. Spiller, W.; Kliesch, H.; Wöhrle, D.; Hackbarth, S.; Röder, B.; Schnurpfeil, G. *J. Porphyrin Phthalocyanines* **1999**, 2: 145-158.

65. Nwahara, N.; Britton, J.; Nyokong, T. *J. Coord. Chem.* **2017**, 70: 1601-1616.

66. Niedre, M.; Patterson, M. S.; Wilson, B. C. *Photochem. Photobiol.* **2002**, 75: 382-391.

67. Wilkinson, F.; Helman, W. P. P.; Ross, A. B. J. *Phys. Chem. Ref. Data.* **1993**, 22: 113-262.

68. Al-Sohaimi, B. R.; Pişkin, M.; Ghanem, B. S.; Al-Raqa, S. Y.; Durmuş, M. *Tetrahedron Lett.* **2016**, 57: 300-304.

69. Chernonosov, A. A.; Ermilov, E. A.; Röder, B.; Solovyova, L. I.; Federova, O. S. *Bioinorg. Chem. Appl.* **2014**, 2014: 1-7.
70. Furuyama, T.; Satoh, K.; Kushiya, T.; Kobayashi, N. *J. Am. Chem. Soc.* **2014**, 136: 765-776.
71. Hammer, R. P.; Owens, C. V.; Hwang, S-H.; Sayes, C. M.; Soper, S. A. *Bioconjugate Chem.* **2002**, 13: 1244-1252.
72. Matlou, G. G.; Oluwole, D. O.; Prinsloo, E.; Nyokong, T. *J. Photochem. Photoiol. B* **2018**, 186: 216-224.
73. Liu, Q.; Pang, M.; Tan, S.; Wang, J.; Chen, Q.; Wang, K.; Wu, W.; Hong, Z. *J. Cancer* **2018**, 9: 310-320.
74. Stuchinskaya, T.; Moreno, M.; Cook, M. J.; Edwards, D. R.; Russell, D. A. *Photochem. Photobiol. Sci.* **2011**, 10: 822-831.
75. Taquet, J-P.; Frochot, C.; Manneville, V.; Barberi-Heyob, M. *Curr. Med. Chem.* **2007**, 14: 1673-1687.
76. Alberto, M. E.; De Simone, B. C.; Mazzone, G.; Sicillia, E.; Russo, N. *Phys. Chem. Chem. Phys.* **2015**, 17: 2359-23601.
77. Nyokong, T.; Antunes, E. *Coord. Chem. Rev.* **2013**, 257: 2401-2418.
78. Chen, X.; Li, Y.; Wang, A.; Zhou, L.; Lu, S.; Zhou, J.; Lin, Y.; Wei, S. *Dyes Pigm.* **2015**, 114: 93-104.
79. Tuhl, A.; Makhseed, S.; Zimcik, P.; Al-Awadi, N.; Novakova, V.; Samuel, J. *J. Porphyrin Phthalocyanines* **2012**, 16: 817-825.
80. Ramos, A. A.; Nascimento, F. B.; de Souza, T. F. M.; Omori, A. T.; Manieri, T. M.; Cerchiaro, G.; Ribeiro, A. O. *Molecules* **2015**, 20: 13575-13590.
81. Lyubimtsev, A.; Iqbal, Z.; Crucius, G.; Syrbu, S.; Taraymovich, E. S.; Ziegler, T.; Hanack, M. *J. Porphyrin Phthalocyanines* **2011**, 15: 39-46.
82. Ranta, J.; Kumulainen, T.; Lemmetyinen, H.; Efimov, A. *J. Org. Chem.* **2010**, 75: 5178-5194.
83. Bayar, Ş.; Dinçer, H. A.; Gonca, E. *Dyes Pigm.* **2009**, 80: 156-162.
84. Shankar, R.; Jha, N. K. *Indian J. Chem.* **1993**, 32: 1029-1033.
85. Biyiklioğlu, Z.; Aktaş, A. *Color Technol.* **2013**, 129: 425-430.
86. Çakir, D.; Çakir, V.; Biyiklioğlu, Z.; Durmuş, M.; Kantekin, H. J. *Organomet. Chem*. **2013**, 745-746: 423-431.

87. Li, H.; Jensen, T. J.; Fronczek, F. R.; Vincente, M. G. H. *J. Med. Chem.* **2008**, 51: 502-511.

88. Makarov, D. A.; Yuzhakova, O. A.; Silvka, L. K.; Kuznetsova, N. A.; Negrimovsky, V. M.; Kaliya, O. L.; Lukyanets, E. A. *J. Porphyrins Phthalocyanines* **2007**, 11: 586-595.

89. De, M.; Ghosh, S.; Sen, T.; Shadab, M.; Banerjee, I.; Basu, S.; Ali, N. *Mol. Ther. Nucleic Acids* **2018**, 10: 9-27.

90. Jobin, M-L.; Bonnafous, P.; Temsamani, H.; Dole, F.; Grélard, A.; Dufourc, E. J.; Alves, I. D. *Biochimica. et Biophysica. Acta* **2013**, 1828: 1257-1470.

91. Ongarora, B. G.; Hu, X.; Verberne-Sutton, S. D.; Garno, J. C.; Vicente, M. G. H. *Theranostics* **2012**, 2: 850-870.

92. He H.; Li D-W.; Yang L-W.; Fu L.; Zhu X-J.; Wong W-K.; Jiang F-L.; Liu Y. *Sci. Rep.* **2015**, 5: 1-10. DOI: 10.1038/srep13543.

93. Senapati, S.; Mahanta, A. K.; Kumar, S.; Maiti, P. *Signal Transduct. Target. Ther.* **2018**, 3: 1-19.

94. Matshitse, R.; Nwaji, N.; Managa, M.; Prinsloo, E.; Nyokong, T. *J. Photochem. Photobiol. A* **2018**, 367: 253-260.

95. Alpugan, S.; Topkaya, D.; Atilla, D.; Ahsen, V. *J. Porphyrins Phthalocyanines* **2017**, 21: 887-892.

96. Gracía, C. P.; Chambrier, I.; Cook, M. J.; Haines, A. H.; Field, R. A.; Russell, D. A. *J. Colloid Interface Sci.* **2018**, 512: 248-259.

97. Zhang, Y.; Lovell, J. F. *Wiley, Interdiscip. Rev. Nanomed. Nanobiotechnol.* **2017**, 9: 1-24.

98. Singh, M.; Singh, S. K. *Anticancer Agents Med. Chem.* **2014**; 14: 127-146.

99. Chen, S. X.; Du, S. Y.; Wang, Y-T.; Zhao, H. C.; Zhang, Y. L.; Yao, L. *Tumor Biol.* **2016**, 37: 323-329.

100. Çolak, S.; Durmuş, M.; Yildiz, S. Z. *J. Photochem. Photobiol. A* **2016**, 324: 125-134.

101. Albanese, A.; Tang, P. S.; Chan, W. C. *Annu. Rev. Biomed. Eng.* **2012**, 14: 1-16.

102. Singh, R.; Lillard, Jr. J. W. *Exp. Mol. Pathol.* **2009**, 86: 215-223.

103. Tran, S.; DeGiovanni, P-J.; Piel, B.; Rai, P. *Clin. Trans. Med.* **2017**, 6: 1-21.

104. Xin, Y.; Yin M.; Zhao, L.; Meng, F.; Luo, L. *Cancer Biol. Med.* **2017**, 14: 228-241.

105. Zhao, H.; Li, Y.; Wei, D.; Luo, H. *J. Immunol. Res.* **2018**, 2018: 1-13.

106. Camerin, M.; Moreno, M.; Marín, M. J.; Schofield, C. L.; Chambrier, I.; Cook, M. J.; Coppellotti, O.; Jori, G.; Russell, D. A. *Photochem Photobiol. Sci.* **2016**, 15: 618-625.
107. Mfouo-Tynga, I.; Houreld, N. N.; Abrahamse, H. *Biomed. J.* **2018**, 41: 254-264.
108. Kuruppuarachchi, M.; Savoie, H.; Lowry, A.; Alonso, C.; Boyle, R. W. *Mol. Pharm.* **2011**, 8: 920-931.
109. Broekgaarden, M.; Weijer, R.; van Wijk, A. C.; Cox, R. C.; Egmond, M. R.; Hoebe, R.; van Gulik, T. M.; Heger, M. *J. Biomed. Nanotechnol.* **2017**, 13: 204-220.
110. Iannazzo, D.; Pistone, A.; Salamò, M.; Galvagno, S.; Romeo, R.; Giofré, S. V.; Branca, C.; Visalli, G.; Pietro, A. D. *Int. J. Pharm.* **2017**, 518: 185-192.
111. Dong, H.; Dai, W.; Ju, W.; Lu H.; Wang, S.; Xu, L.; Zhou, S-F.; Zhang, Y.; Zhang, X. *Appl. Mater. Interfaces* **2015**, 7: 11015-11023.
112. Dube, E.; Oluwole, D. O.; Prinsloo, E.; Nyokong, T. *New J. Chem.* **2018**, 42: 10214-10225.
113. Dong, J.; Wang, K.; Sun, L.; Yang, M.; Chen, H.; Wang, Y.; Sun, J.; Dong, *L. Sensor. Actuat. B Chem.* **2018**, 256: 616-623.
114. Tong, X.; Wei, Q.; Zhan, X.; Zhang, G.; Sun, S. *Catalysis* **2017**, 7: 1-26.
115. Song, S. H.; Jang, M-H.; Chung, J.; Jin, S. H.; Kim, B. H.; Hur, S-H.; Yoo, S.; Cho, Y-H.; Jeon, S. *Adv. Opt. Mater.* **2014**, 2: 1016-1023.
116. Yeh, T-F.; Teng, C-Y.; Chen, S-J.; Teng, H. *Adv. Mater.* **2014**, 26: 3297-3303.
117. Shinde, D. B.; Pillai, V. K. Chem, *A Eur. J.* **2012**, 18: 12522-12528.
118. Iannazzo, D.; Ziccarelli, I.; Pistone, *A. J. Mater. Chem. B* **2017**, 5: 6471-6489.
119. Naik, J. P.; Sutradhar, P.; Saha, M. *J. Nanostructure. Chem.* **2017**, 7: 85-89.
120. Gu, J.; Hu, M. J.; Guo, Q. Q.; Ding, Z. F.; Sun, X. L.; Yang J. *RSC Adv.* **2014**, 4: 50141-50144.
121. Choyke, P. L.; Kobayashi, H. *Abdom. Imaging* **2006**, 31: 224-231.
122. Achadu, O.J.; Uddin, I.; Nyokong, T. *J. Photochem. Photobiol. A* **2016**, 317: 12-25.
123. Oluwole, D. O.; Nwaji, N.; Nene, L. C.; Mokone, L.; Dube, E.; Nyokong, T. *New J. Chem.* **2018**, 42: 10124-10133.
124. Centane, S.; Achadu, O. J.; Nyokong, T. *Electroanalysis* **2017**, 29: 2470-2482.
125. Achadu, O. J.; Nyokong, T. *New J. Chem.* **2017**, 41: 1447-1458.
126. Mafukidze, D. M.; Nyokong, T. *J Coord. Chem.* **2017**, 70: 3598-3618.

127. Achadu, O. J.; Nyokong, T. *Spectrochim. Acta A Mol. Biomol.* **2017**, 174: 339-347.

128. Matshitse, R.; Nyokong, T. *J. Fluoresc.* **2018**, 28: 827-838.

129. Nwahara, N.; Nkhahle, R.; Ngoy, B. P.; Mack, J.; Nyokong, T. *New J. Chem.* **2018**, 42: 6051-6061.

130. Fomo, G.; Achadu, O. J.; Nyokong, T. *J. Mater. Sci.* **2018**, 53: 538-548.

131. Achadu, O. J.; Nyokong, T. *New J. Chem.* **2016**, 40: 8727-8736.

132. Wang, X.; Sun, X.; Lao, J.; He, H.; Cheng, T.; Wang, M.; Wang, S.; Huang, F. *Colloids Surf. B Biointerfaces* **2014**, 122: 638-644.

133. Ding, H.; Zhang, F.; Zhao, C.; Lv, Y.; Ma, G.; Wei, W.; Tian, Z. *Appl. Mater. Interfaces* **2017**, 9: 27396-27401.

134. Qiu, J.; Zhang, R.; Li, J.; Sang, Y.; Tang, W.; Gil, P. R.; Liu, H. *Int. J. Nanomedicine* **2015**, 10: 6709-6724.

135. Ko, N. R.; Nafiujjaman, M.; Le, J. S.; Lim, H-N.; Lee, Y-K.; Kwon, I. K. *RSC Adv.* **2017**, 7: 11420-11427.

136. Nasrollahi, F.; Koh, Y. R.; Chen, P.; Varshosaz, J.; Khodadadi, A. A.; Lim, S. *Mater. Sci. Eng. C.* **2019**, 94: 247-257.

137. Nigam, P.; Waghmode, S.; Louis, M.; Wangnoo, S.; Chavan, P.; Sarkar, D. *J. Mater. Chem. B* **2014**, 2: 3190-3195.

138. Chen, S.; Zhao, X.; Chen, J.; Chen, J.; Kuznetsova, L.; Wong, S. S.; Ojima, I. *Bioconjug. Chem.* **2010**, 21: 979-987.

139. Yang, W.; Cheng, Y.; Xu, T.; Wang, X.; Wen, L-P. *Eur. J. Med. Chem.* **2009**, 44: 862-868.

140. Ren, W. X.; Han, J.; Uhm, S.; Jang, Y. J.; Kang, C.; Kim, J-H.; Kim, S. *Chem. Commun.* **2015**, 51: 10403-10418.

141. Strzelczyk, P.; Plażuk, D.; Zakrzewski, J.; Bujacz ,G. *Molecules* **2016**, 21: 1-11.

142. Iida, N.; Tanaka, K.; Tokunaga, E.; Takahashi, H.; Shibata, N. *ChemistryOpen* **2015**, 4: 102-106.

143. Forteath, S.; Antunes, E.; Chidawanyika, W.; Nyolong ,T. *J. Lumin.* **2012**, 132: 2318-2324.

144. Ağirtaş, M. S.; Yildiko, U. *J. Coord. Chem.* **2008**, 61: 2781-2786.

145. Volpi, S.; Ali, J. M.; Tasker, A.; Peryt, A.; Aresu, G.; Coonar, A. *Ann. Transl. Med.* **2018**, 6: 10-9.

146. Almubarak, M.; Osman, S.; Marano, G.; Abraham, J. *Oncology* **2009**, 23: 255-261.

147. Mieli, E.; Spinelli, G. P.; Tomao, F.; Zullo, A.; De Marinis, F.; Pascuiti, G.; Rossi, L.; Zoratto, F.; Tomao, S. *J. Exp. Clin. Canc. Res.* **2008**, 27: 1-10.

148. Xi, C-C.; Chen, Z-M.; Zhang, S-Y.; Tu, Y-Q. *Org. Lett.* **2018**, 20: 4227-4230.

149. Zheng, J.; Wang, L.; Lin, J.; Xiao, J.; Liang, S. H. *Angew. Chem. Int. Ed.* **2015**, 54: 13236-13240.

150. Plutschack, M. B.; Pieber, B.; Gilmore, K.; Seeberger, P. H. *Chem. Rev.* **2017**, 1127: 11796-11893.

151. Hartman, R. L.; McMullen, J. P.; Jensen, K. F. *Angew. Chem. Int. Ed.* **2011**, 50: 7502-7519.

152. Yildiz, M.; Beeby, A.; MacRobert, A. J.; Simpson M. S. C.; Svensen, R. K.; Phillips, D. *J. Photochem. Photobiol. B* **1991**, 9: 87-95.

153. Yahyazadeh, A.; Azimi, V. *Elixir Intern. J. Appl. Chem.* **2012**, 49: 9991-9993.

154. Eastmond, G. C.; Page, P. C. B.; Paprotny, J.; Richards, R. E.; Shaunak, R. *Polymer* **1994**, 35: 4215–4227.

155. Wang, C.; Xu, Z.; Zhang, C. *ChemNanoMat* **2015**, 1: 122-127.

156. Brouwer, A. M. *Pure Appl. Chem.* **2011**, 83: 2213-2228.

157. Tran-Thi, T. H.; Desforge, C.; Thiec, C. *J. Phys. Chem.* **1989**, 93: 1226-1233.

158. Kuznetsova, N. A.; Gretsova, N. S.; Yuzhakova, O. A.; Negrimovskii, V. M.; Kaliya, O. L.; Luk'yanets, E. A. *Russ.J. G. Chem.* **2001**, 71: 36-41.

159. Ogunsipe, A.; Nyokong, T. *J. Photochem. Photobiol. A.* **2005**, 173: 211-220.

160. Nwaji, N.; Bankole, O. M.; Britton, J.; Nyokong, T. *J. Porphyr. Phthalocyanines* **2017**, 21: 263-272.

161. Nyokong, T. *Struct. Bond* **2010** 135: 44-88.

162. Stillman, M.J.; Nyokong, T. In: Eds. C. C. Leznoff, A. B. P. Lever, Phthalocyanines: Properties and applications. New York: VCH Publishers, 1989 Ch 3.

163. Gürel, E.; Pişkin, M.; Altun, S.; Odabaş, Z.; Durmuş, M. *Dalton Trans.* **2015**, 44: 6202-6211.

164. Masilela, N.; Nyokong, T. *Dyes Pigm.* **2010**, 84: 242-248.

165. Qu, D.; Zheng, M.; Li, J.; Xie, Z.; Sun, Z. *Light Sci. Appl.* **2015**, 4: 1-8.

166. Li, L.; Zhao, J. F.; Won, N.; Jin, H.; Kim, S.; Chen, J. Y. *Nanoscale Res. Lett.* **2012**, 7: 386–393.

167. Kudin, K. N.; Ozbas, B.; Schniepp, H. C.; Prud'homme, R. K.; Aksay, I. A.; Car, R. *Nano Letters* **2008**; 8: 36-41.

168. Li, Z.; He, C.; Wang, Z.; Gao, Y.; Dong, Y.; Zhao, C.; Chen, Z.; Wu, Y.; Song, W. *Photochem. Photobiol. Sci.* **2016**, 15: 910–919.

169. Moeno, S.; Nyokong, T. *J. Photochem. Photobiol. A* **2010**, 215: 196–204.

170. Masih, D.; Aly, S. M.; Usman, A.; Alarousu, E.; Mohammed, O. F. Phys. *Chem. Chem. Phys.* **2015**, 17: 9015-9019.

171. Lakowicz, J. R.; Shen, Y.; D'Auria, S.; Malicka, J.; Fang, J.; Gryczynski, Z.; Gryczynski, I. *Anal. Biochem.* **2002**, 301: 261–277.

172. Berney, C.; Danuser, G. *Biophys. J.* **2003**, 84: 3992-4010.

173. Adarsh, K. S.; Singh, M. K.; Shivkumar, M. A.; Rabinal, M. K.; Jagatap, B. N.; Mulimani, B. G.; Savadatti, M. I.; Inamdar, S. R. *J. Fluoresc.* **2015**, 160: 216-222.

174. Erol, Z. N.; Atienzar, P.; Arslanoğlu, Y.; Hamuryudan, E.; García, H. *RSC Adv.* **2015**, 5: 55901-55908.

175. Debacker, M. G.; Deleplanque, O.; Van Vlierberge, B.; Sauvage, F. X. *Laser Chem.* **1988**, 8: 1-11.

176. Darwent, R.; Douglas, P.; Harriman, A.; Porter, G.; Richoux, M. C. *Coord. Chem. Rev.* **1982**, 44: 83–1126.

177. Sagun, E. I.; Zenkevich, E. I.; Knyukshto, V. N.; Shulga, A. M.; Starukhin, D. A.; von Borczyskowski, C. *J. Chem. Phys.* **2002**, 275: 211-230.

178. Göl, C.; Durmuş, M. *Synth. Met.* **2012**, 162: 605-613.

179. Castano, A. P.; Demidova, T. N.; Hamblin, M. R. *Photodiagnosis Photodyn. Ther.* **2004**, 1: 279-293.

180. Lukšiené, Ž. *Medicina* **2003**, 39: 1137-1150.